Climate and sea level controlled sedimentation processes in two submarine canyons off NW-Africa

Dissertation

zur Erlangung des Doktorgrades am Fachbereich Geowissenschaften der Universität Bremen

vorgelegt von

Roberto Pierau

Bremen, September 2008

Tag des Kolloquiums:

14.11.2008

Gutachter:

Prof. Dr. Rüdiger Henrich
Prof. Dr. Sebastian Krastel

Prüfer:

Prof. Dr. Heinrich Villinger
Prof. Dr. Hans-Joachim Kuss

Abstract

This study focuses on the trigger mechanisms of gravity-driven sediment transport in two submarine canyons at the passive continental margin off NW-Africa during the past 240 kyr. The sedimentary records allow to determine the turbidite emplacement times based on high resolution age models. The sediment textures of the turbidites were studied by using X-ray radiographies. The sedimentary properties like the terrigenous silt size distribution and XRF-core scanning element data allow to identify the variability of the aeolian dust input in the hemipelagic sediments. These variations can be used to reconstruct the climatic conditions in the hinterland which strongly influence the sediment supply on the shelf. In addition a clay mineral assemblage was used to reconstruct the fluvial input of the West-African rivers.

The trigger mechanisms of gravity-driven sediment transport in submarine canyons during sea level changes has been reported from many regions. However, the relationship of sea level changes and short-term climatic events with turbidite deposition is poorly documented. The turbidite history of the Dakar Canyon during the late Quaternary was reconstructed using gravity cores directly recovered from the canyon axis. The highest frequency of turbidite deposition is restricted to the last two major climatic terminations when remobilisation of sediments from the shelf was triggered by eustatic sea level rise. Coarse terrigenous silt size data and high Ti/Ca ratios reflect an overall increased dust supply during the last two peak glacials resulting in the formation of extensive sand seas covering the exposed shelf. The interglacials were characterised by less intensive wind stress. However, sporadic turbidite events coincide with the timing of Heinrich events in the North Atlantic. During these times continental climate has changed rapidly towards increased aridity and enhanced wind strength. This in turn led to a higher dust supply which has fed turbidity currents.

The turbidite being deposited during the two main periods of activity consist of sandy to silty sediments. Detailed grain size analyses were used to reconstruct the sedimentary characteristics of these turbidity currents. With increasing distance to the source area a downslope sorting trend in the grain size distribution towards finer grain sizes was observed. A much higher frequency in turbidite activity is recorded during the previous peak glacial in contrast to the last peak glacial. This suggests a higher sediment budget in the source area. The correlation of turbidites is based on their stratigraphic position. A single turbidite can exactly be dated at all core locations in the thalweg. Based on the sedimentological analysis of the turbidites this study provides a schematic model for the sedimentation processes in the Dakar Canyon.

The turbidite activity of the Dakar Canyon was then compared to the neighbouring submarine Diola Canyon. Both canyon systems are affected by the seasonal shifts of the Intertropical Convergence Zone. However, the southern Diola Canyon is further influenced by the discharge of the West African rivers. During the late Quaternary a mixture of fluvial derived material and aeolian dust was deposited at the exposed southern Senegalese shelf. Frequent turbidite deposition in the Diola Canyon is recorded during minor sea level rises which forced the remobilisation of this sediment mixture. Furthermore, the post glacial sea level rise removed the remaining sediment deposits from the now flooded shelf region.

The results of this PhD study highlight the influence of sea level rise and the subsequent remobilisation of shelf sediments as well as short-lasting climatic changes which act as main factors controlling the sediment flux in the investigated canyon systems.

Zusammenfassung

Die vorliegende Studie beschäftigt sich mit den Auslösemechanismen von gravitativ gesteuerten Sedimentationsprozessen in submarinen Canyonsystemen am passiven Kontinentalhang vor NW-Afrika während der letzten 240.000 Jahre. Anhand von Sedimentkernen aus den Canyons wurde die zeitliche Ablagerung von Turbiditen rekonstruiert. Das Alter der Kerne wurde mit Hilfe von Sauerstoffisotopenmessungen und der Korrelation mit der SPECMAP-Kurve bestimmt. Die Analyse der Zusammensetzung der „Hintergrundsedimente“ wie der Anteil der terrigenen Siltfraktion sowie der Verteilung der chemischen Elemente erlaubt die Abschätzung des Eintrags von Staub in den Ozean. Die Unterschiede in der Zusammensetzung der Sedimente werden benutzt um die Klimabedingungen im Hinterland zu rekonstruieren. Das Verständnis der klimatischen Bedingungen ist wichtig, da diese die Kontrollfaktoren für den Sedimenteintrag darstellen. Die Textur der Turbidite wurde anhand von Radiographien untersucht um eine genaue Abgrenzung zwischen umgelagerten Sedimenten und der regulären hemipelagischen Sedimentation machen zu können. Zusätzlich wurden tonmineralogische Untersuchungen durchgeführt, um den Eintrag von Flussfracht aus dem Hinterland zu charakterisieren.

Die Steuerprozesse von gravitativen Sedimentbewegungen in submarinen Canyons während Änderungen des Meeresspiegels sind aus diversen Gebieten der Erde bekannt. Allerdings ist über die Verbindung zwischen Meerspiegelschwankungen und kurzzeitigen Klimaänderungen im Zusammenhang mit der Ablagerung von Turbiditen wenig bekannt. Die zeitliche Abfolge von Turbiditen im Dakar Canyon während des späten Quartärs wurde anhand von Schwerelotkernen, die direkt aus dem Talweg entnommen wurden, rekonstruiert. Die höchste Turbiditaktivität ist an die beiden letzten Glaziale gebunden. Dazu wurde Material, welches auf dem Schelf abgelagert wurde, durch den sukzessiven Anstieg des Meeresspiegels aufgearbeitet und hangabwärts als Trübestrom transportiert. Gröbere Anteile von terrigenem Silt und höhere Ti/Ca Verhältnisse deuten auf einen ausgeprägteren Staubeintrag während der letzten beiden Glaziale hin. Generell waren die Glaziale durch stärkere Winde geprägt. Dies führte zur Entstehung von ausgedehnten Dünenfeldern auf dem trockengefallenen Schelf. Sporadisch auftretende Turbidite im Dakar Canyon fallen zeitlich mit Heinrich Ereignissen im Nordatlantik zusammen. Während dieser Ereignisse änderte sich das Klima auf dem afrikanischen Kontinent sehr schnell und Anzeichen für einen verstärkten Staubeintrag sind in den Hintergrundsedimenten zu finden. Trockenheit und verstärkte Winde sind verantwortlich

für den zunehmenden Eintrag von Staub welcher das Ausgangsmaterial für die in dieser Zeit abgelagerten Turbidite bildet.

Die Turbidite, die während der beiden Hauptaktivitätsphasen im Dakar Canyon abgelagert wurden bestehen aus sandig-siltigen Sedimente. Anhand von detaillierten Korngrößenuntersuchungen konnte der sedimentologische Charakter dieser Trübeströme rekonstruiert werden. Mit zunehmender Entfernung zum Quellgebiet setzt eine Sortierung innerhalb der Trübeströme zu feineren Korngrößen ein. Während des vorletzten Glazials wurde im Gegensatz zum letzten Glazial eine deutlich höhere Anzahl von Turbiditen abgelagert. Diese Beobachtung lässt auf ein deutlich größeres Sedimentreservoir im Quellgebiet schließen. Die Korrelation der Turbidite entlang der Canyonachse erfolgte über ihre stratigraphische Einordnung. Ein einzelner Turbidit im Dakar Canyon konnte mittels Radiokarbondatierung zeitlich genau bestimmt werden. Anhand der sedimentologischen Untersuchungen der Turbidite konnte ein schematisches Modell der Sedimentationsprozesse im Dakar Canyon erstellt werden. Dieses Modell trägt zum besseren Verständnis über den Aufbau von Turbiditeablagerungen in submarinen Canyonsystemen bei.

Abschließend wurde die Turbiditaktivität im Dakar Canyon mit dem in unmittelbarer Nachbarschaft gelegenen Diola Canyon verglichen. Beide Canyonsysteme werden durch die saisonalen Verlagerungen der Intertropischen Konvergenzzone beeinflusst. Allerdings wird die Sedimentation im südlich gelegenen Diola Canyon stärker vom Eintrag der westafrikanischen Flüsse geprägt. Während des späten Quartärs wurde eine Mixtur aus fluviatilen Material und Wüstenstaub auf dem freiliegenden Schelf abgelagert. Häufige Turbiditereignisse traten im Diola Canyon während kleinerer Anstiege des Meeresspiegels auf, während derer das auf dem Schelf befindliche Material aufgearbeitet und remobilisiert wurde. Während des postglazialen Meeresspiegelanstiegs wurden lediglich die übrig gebliebenen Sedimente aufgearbeitet.

Die Ergebnisse dieser Arbeit heben den Einfluss von Meeresspiegelschwankungen und die damit verbundene Aufarbeitung der Schelfsedimente sowie den Einfluss von kurzzeitigen Klimaänderungen als Steuermechanismen des Sedimentationsgeschehens in den untersuchten Canyonsystemen hervor.

Table of contents

1 Introduction

1.1 Terminology and definition of deep water channels and gravity-driven sediment transport: a brief overview

People dealing with deep water channels are faced by a wide array of terms and therefore I attempt to provide simple definitions for the terms used in this study.

The term *canyon* is an equivalent to the land valley meaning "a deep, relatively narrow valley with high and steep slopes" which seems reasonable to use as similar definition for *submarine canyons* (Shepard, 1972). These canyons can be found at all active and passive continental margins of the earth. Submarine canyons often gradually merge downslope into *channels* and are characterised by V- and U-shaped pattern in cross sections (Fig. 1) with or without depositional margins (Mayall et al., 2006; Wynn et al., 2007). The head area of submarine canyons is often characterised by a feeder system of narrow tributaries which are directly connected to the shelf. Further downslope the canyon morphology changes into a more U-shaped pattern with decreasing incision depths. However, a clear differentiation between canyons and channels does not exist (Wynn et al., 2007). Wide channel floors are often incised by a inner channel called the *thalweg*. Furthermore, a lot of morphologic features of submarine canyons like terraces and steep side walls can be observed in seismic or hydroacoustic cross sections (Fig 1A). High amplitude reflectors are common at the channel floor and representing the infill of coarse grained material.

Channels and their flanking depositional margins (*levees*, Fig. 1B) are commonly referred to as *channel-levee-systems* which build many major submarine fans (Flood and Damuth, 1987). Submarine fans, consisting of clastic material, are often radial formed, and were fed by gravity flows including *slumps*, *debris flows* and *turbidity currents* (Mutti and Normark, 1991). The term slump refers to a mass that moves downslope on a glide plane and shows no internal deformation (Fig. 2). Debris flows are incoherent sediment masses which are transported downslope via laminar flow and may evolve into turbidity currents (McHugh et al., 2002). Reading and Richards (1994) subdivided different types of submarine fan systems according to their grain size composition. Sand-rich submarine fans (>70% sand content) are common along active continental margins whereas mud-rich fans (< 30 % sand content) were found at passive margins.

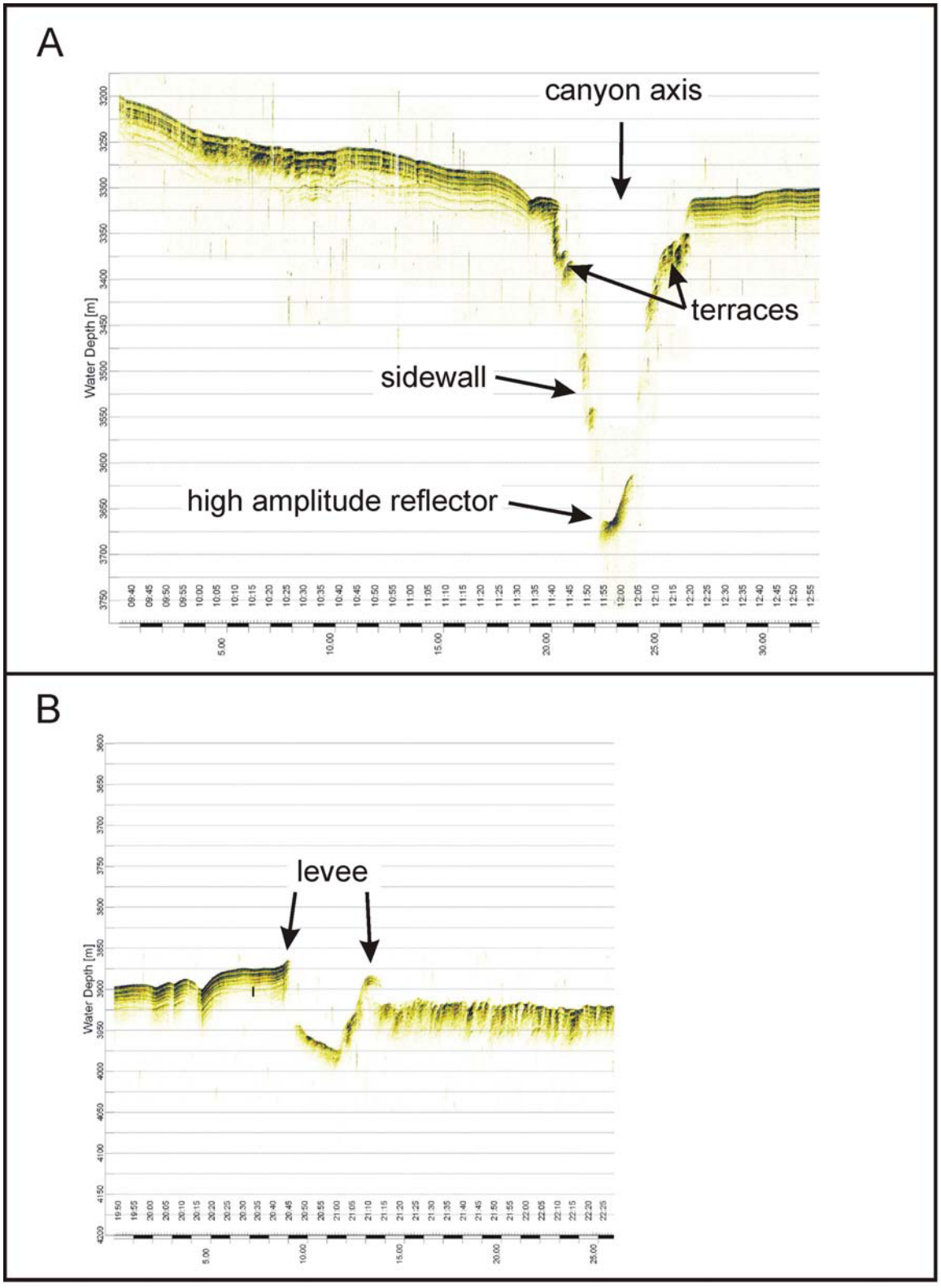

Figure 1: Sediment echosounder profiles crossing the Dakar Canyon. A) Typical V-shaped pattern of a submarine canyon including other morphologic features like terraces and steep sidewalls. The high amplitude reflectors at the canyon bottom indicate the infill of coarse material. B) U-shaped canyon structure with well developed levees.

Shanmugam (2002) defines turbidity currents as turbulent flows in which turbulence is the principle sediment-support mechanism operating under a wide range of velocity conditions. Deposits of turbidity currents (*turbidites*, Fig. 3) can be recognised by a sharp basal contact, fining-upward grain size grading and the development of BOUMA-units (Bouma, 1962). Several processes, such as earthquakes, sea level changes, and rapid sediment loading might cause sediment instabilities which in turn can trigger turbidity currents.

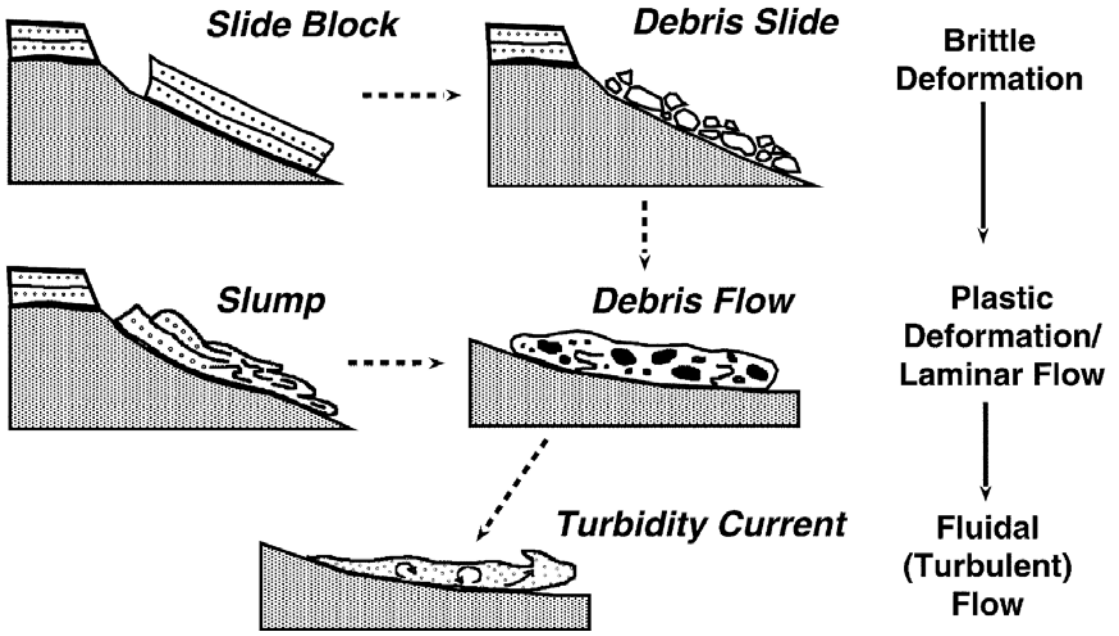

Figure 2: Schematic sketch showing types of gravity-driven sediment transport (after McHugh et al., 2002).

1.2 The economic and scientific relevance of submarine canyon systems

Submarine canyon systems are not only of academic interest. The study of gravity-driven sediment transport in the deep sea progressed rapidly since the 1950s (Masson et al., 1996). The analysis of underwater cable breaks caused by turbidity currents was the initiation for the understanding of downslope sediment transport. Furthermore, slope instabilities and the resultant sediment flows can destroy submarine telecommunication as well as marine infrastructure and in some cases can generate tsunamis.

Submarine canyons are major pathways for significant volumes of gravity-driven sediment transport in which sediments from shallow marine environments are transported over long

distance into the deep sea. On the other hand, submarine canyons are also important repositories for terrestrial derived clastic sediments and thus play a major role as hydrocarbon reservoirs (Emery and Myers, 1996; Weimer and Slatt, 1999; Stow and Mayall, 2000). Therefore, outcrops of fossil submarine canyon systems were studied to reconstruct reservoirs and provide essential inputs for 3D geological models that were used for further predictions of the reservoir behaviour (Eschard et al., 2003; Satur et al., 2005). Modern canyon systems can be used as analogues for ancient deep-water clastic systems, and therefore detailed investigations of modern systems provide valuable information about structure, architecture and evolutionary trends in sedimentary regimes in canyon systems.

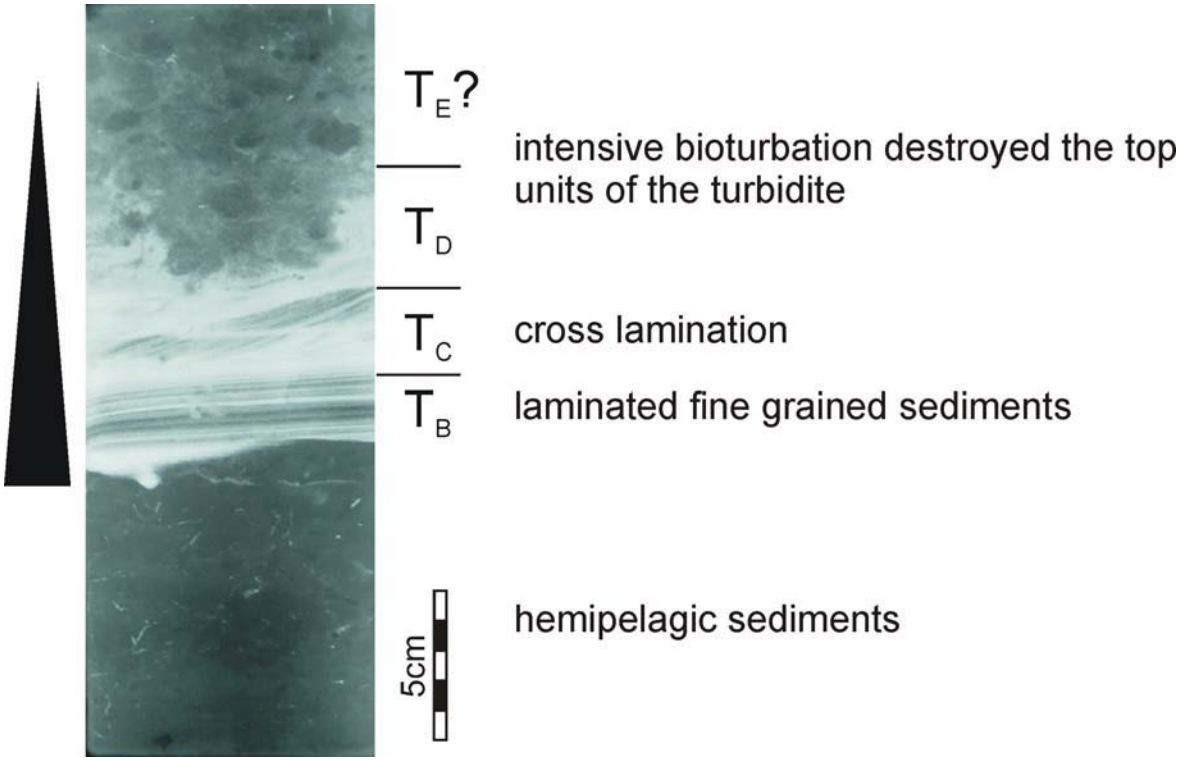

Figure 3: X-ray radiography (negative) of an incomplete BOUMA-Sequence (base cut-out sequence) of core GeoB9612-3. However, the most prominent features of a turbidite are represented. A sharp basal contact and fining-upward grain-size sorting are developed. The top is destroyed due to intensive bioturbation.

A lot of studies are published in the last decades dealing with submarine canyons. Gravity cores recovered in submarine canyons can be used to reconstruct the terrigenous sediment supply from the continent to the ocean (Normark et al., 1998; Prins et al., 2000; Weber et al., 2003; Mullenbach et al., 2004; Talling et al., 2007). In regions with strong tectonic activity like Japan, South Chile or Greece, turbidite deposits can be used as a quantitative

recorder of the frequency and periodicity of paleo-earthquakes (Klein, 1985; Hasiotis et al., 2005; Blumberg et al., 2008). Furthermore, analyses of the emplacement times of turbidites can be used to reconstruct the paleo-environmental conditions. Toucanne et al. (2008) document the evolution of the turbidite system a the Celtic-Amorican margin which was forced by meltwater releases from the European Ice sheets. Also climatic changes and sea level history can be documented by turbidity currents in submarine canyons (Prins and Postma, 2000; Pierau et al., in review-a).

1.3 Overview of sedimentation processes at the NW-African continental margin

The passive continental margin off Northwest Africa is strongly affected by gravity-driven sedimentation processes (Weaver et al., 2000). The major gravity-driven processes are debris flows, sediment slides and turbidity currents due to low terrigenous input and local upwelling (fig. 4). Very little fluvial sediment reaches the margin and the local upwelling give rise to high accumulation rates along the upper slope (Weaver et al., 2000). Well known large debris flows and slide complexes are the Saharan Debris Flow, the Mauritania Slide Complex and the recently discovered Dakar Slide in the study area (Masson et al., 1996; Krastel S. and cruise participants, 2006; Antobreh and Krastel, 2007; Henrich et al., 2008).

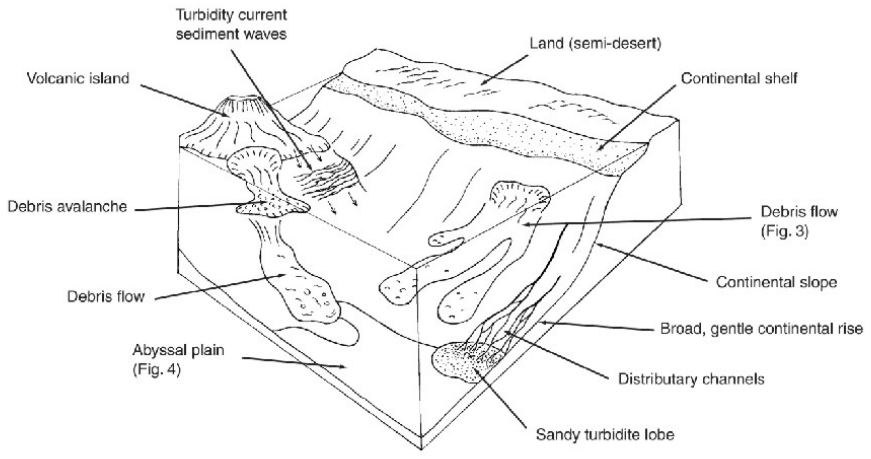

Figure 4: Schematic diagram of the idealised sedimentation features on the NW-African margin (after Weaver et al., 2000).

An overview of the sedimentation processes along the NW-African continental margin and some morphologic features of the deep-sea basin are given in figure 5. These mass wasting features transport significant volumes of sediment over long distances from the shelf into deep sea basins (Talling et al., 2007). In addition, numerous canyons along the passive northeast Atlantic continental margin are associated with turbidite activity like the Agadir Canyon, Cape Timiris Canyon, Cayar Canyon as well as some canyon systems south of the study area (Dietz et al., 1968; Dietz and Knebel, 1971; Babonneau et al., 2002; Wynn et al., 2002; Antobreh and Krastel, 2006; Zühlsdorff et al., 2007b). The principal controlling factors of the sedimentation processes off NW-Africa are the relief and climate of the hinterland, the width of the shelf, the inclination of the continental slope, upwelling and sea level changes (Seibold and Fütterer, 1982).

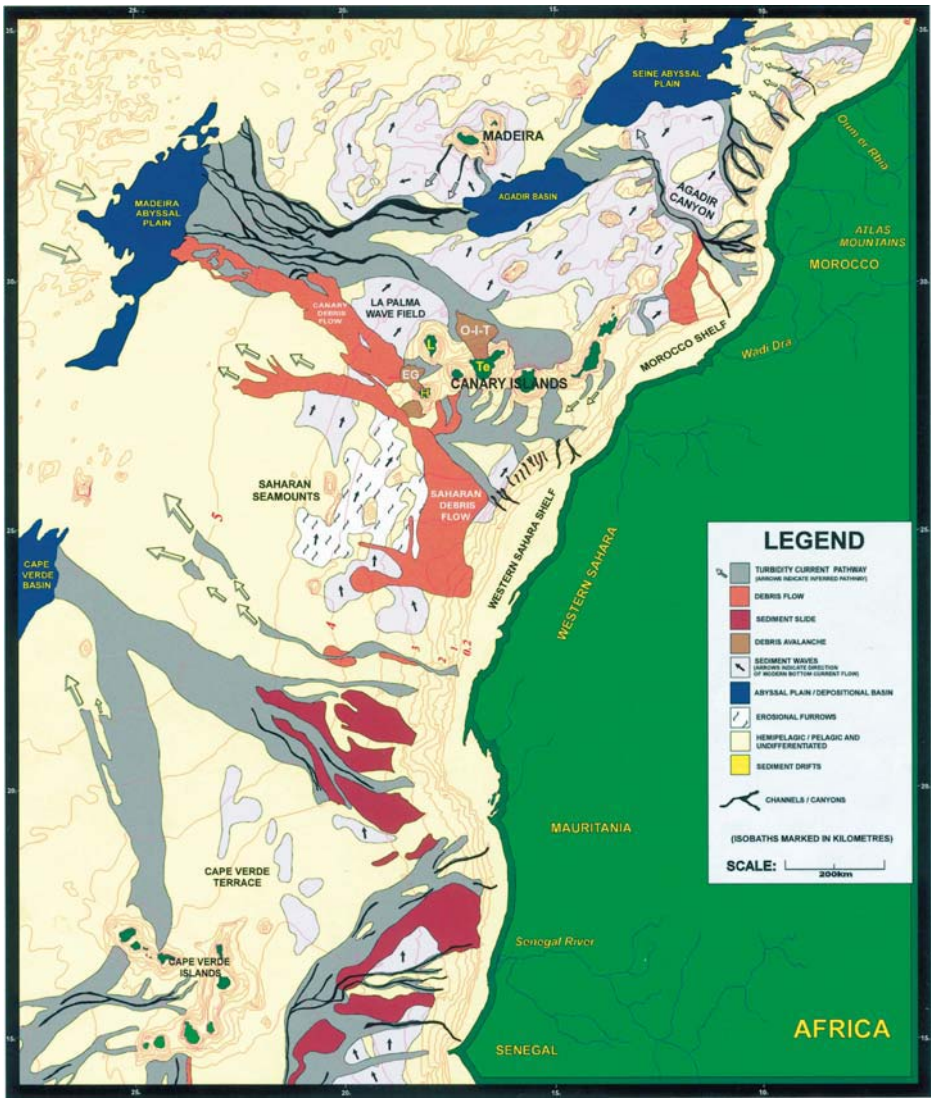

Figure 5: Sediment processes along the NW-African margin (after Wynn et al., 2000)

1.4 Oceanographic and climatic setting in the study area

The cool south-westward flowing Canary Current is the major surface current along the NW-African continental margin (Mittelstaedt, 1991). The surface currents in the subtropical North Atlantic south of 20°N are dominated by the wind driven subtropical gyre, the Guinea Dome (Stramma et al., 2005). During boreal winter a southward directed surface current flows along the coast of Mauritania and Senegal (Stramma and Schott, 1999). Instead, during summer the study area is influenced by the northward flowing Mauritania Current. These surface currents are underlain by the northward-flowing South Atlantic Central Water between 150 - 400 m, and in water depths down at about 700 m by the southward-flowing North Atlantic Central Water (Lonsdale, 1982; Mittelstaedt, 1991; Hagen, 2001). Deep-water currents are represented by south-flowing North Atlantic Deep Water (NADW) at depths between 2000 – 3800 m and the north-flowing Antarctic Bottom Water below a water depth of 3800 m (Wynn et al., 2000). Bottom current velocities are thought to be fairly weak at the present day. Coastal upwelling varies seasonally and spatially along the margin and is controlled by the NE trade winds due to the migration of the Intertropical Convergence Zone (ITCZ). The strongest upwelling off NW-Africa occurs during summer and early autumn when the trade winds reach their peak velocity (Mittelstaedt, 1991; Van Camp et al., 1991). South of 20°N upwelling occurs only during short periods in winter and spring.

The seasonal migration of the ITCZ is the most important atmospheric feature over Northwest Africa (Nicholson, 2000). During boreal summer the ITCZ shifts northward and NW-Africa is influenced by the low level humid SW monsoon flow south of the ITCZ (fig. 6). During winter when the ITCZ migrates southward, the NE trade winds dominate the study area. The trade winds and the overlying Saharan Air Layer (SAL) are the prevailing wind systems of NW Africa and are responsible for transport of dust across the Northwest African continent to the Atlantic Ocean (Sarnthein et al., 1982; Swap et al., 1996; Nicholson, 2000). Large dust plumes play a major role in terrigenous sediment supply along the Northwest African continental margin (Koopmann, 1981; Holz et al., 2004; Stuut et al., 2005). The SAL uplifts dust at heights to about 3 km and carries dust to the proximal part of the Atlantic Ocean, but the largest amount of dust is transported by the NE trade winds (Swap et al., 1996) to the adjacent ocean. A special kind of the NE trade winds is the Harmattan which also picks up high amounts of dust (Tiessen et al., 1991; Prospero and Lamb, 2003).

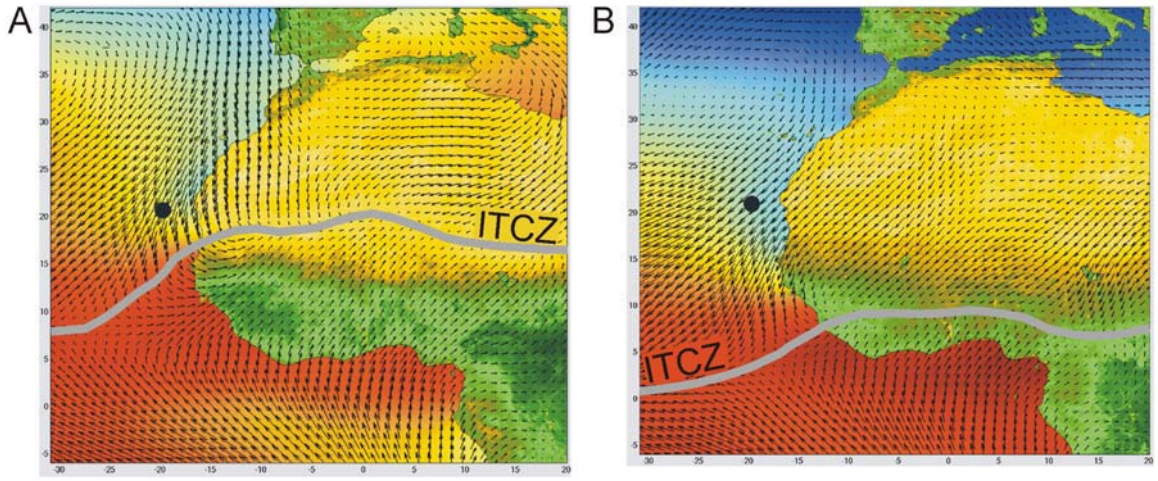

Figure 6: Map of the present-day climate conditions of NW-Africa, modified after Adkins et al., 2006. The grey line represents the position of the ITCZ. Black arrows showing the wind direction and wind speed. The vegetation is given in green colours and sea surface temperatures are represents by blue (cold) and red (warm). A) Summer conditions (JJA) when the ITCZ move at its northern position. B) Winter conditions (DJF).

Fluvial supply is restricted to a few small rivers draining onto the shelf, whereas in the southern part of the study area river discharge becomes more important. The majority of the sediment load of these rivers is trapped in estuaries along the inner shelf (McMaster and Lachance, 1969). Therefore, surface sediments of the Senegalese Shelf are dominated by aeolian derived quartz sands whereas higher amounts of fluvial derived silt and clay can be found at the shelf between The Gambia and Geba River (McMaster and Lachance, 1969; Debenay and Redois, 1997). These sands are generally wind-derived and originate from paleo-dunes ("Ogolian erg") whose remnants are still preserved on the shelf south of Cape Verde (Barusseau et al., 1988). These paleo-dunes formed during the Last Glacial Maximum (LGM), when active desert dunes migrated seawards over the exposed shelves in response to overall increased wind strengths (Matthewson et al., 1995; Rognon and Coudé-Gaussen, 1996; Martinez et al., 1999). The NW-African margin is bordered by a generally flat, 40 - 100 km wide shelf (Wynn et al., 2000). The Senegalese shelf varies in width between 20 - 150 km and reaches its maximum expansion in the southern part of the investigated area (Debenay and Redois, 1997; Hagen, 2001). The mean depth of the shelf break south of 15°N is located in water depths of 100 - 150 m associated with a continental slope with typical slope angles from 1° - 6° (McMaster and Lachance, 1969; Wynn et al., 2000).

1.5 Late Quaternary climatic variations off NW-Africa

The present day climatic conditions of the NW-African continent are reflected in the different vegetation zones. The relative humid Mediterranean vegetation zone in the north is separated by the Saharan desert from the subtropical NW-African monsoon belt (Nicholson, 2000; Hooghiemstra et al., 2006). The Mediterranean climatic zone is generally dry during the boreal summer and precipitation occurs during the winter when westerly cyclones influence the area. However, the Sub-Saharan-Sahel zone is strongly influenced by the monsoonal inflow of moisture laden air from the adjacent Atlantic Ocean. Kuhlmann et al. (2004) suggest that the transition between the influence of the North Atlantic climate system and the West-African monsoonal system was located between 27° - 30°N during the Holocene. Furthermore, Pierau et al. (subm.) postulate that the transition zone of arid/semiarid to humid climatic conditions during the Last Glacial Maximum (LGM) in NW-Africa could be located south of the Dakar Canyon at around 13°N.

The climatic variations of NW-Africa and the resulting hydrological balance over geological time scales is recorded in marine and terrestrial archives (Sarnthein et al., 1982; deMenocal et al., 1993; Tiedemann et al., 1994; Matthewson et al., 1995; Gasse, 2000; Holz et al., 2007). The variation of the aeolian dust load in marine sediment allows to estimates drier periods. Dust load increases when dry climatic conditions reduce the vegetation cover and deflation by wind erodes the exposed soil surfaces. Furthermore, lake level fluctuations in NW-Africa were reconstructed and act as proxy for continental aridity (Alayne Street and Grove, 1976; Talbot and Delibras, 1980; Shanahan et al., 2006). Dry and wet periods can also be inferred by the occurrence of freshwater algae and diatoms as well as pollen assemblages (Pokras and Mix, 1985; Lèzine, 1991; Lézine et al., 2005). The variation of dry and wet periods reflects generally the variable monsoon intensity (McIntyre et al., 1989).

The last glacial period of NW-Africa is characterised by a significantly higher input of aeolian dust and generally drier climatic conditions (Lèzine, 1991; Matthewson et al., 1995; Moreno et al., 2001). A weakened thermohaline circulation led to a stronger hemispheric temperature gradient coupled with intensified trade winds (Sarnthein et al., 1981; Vidal et al., 1997; Jullien et al., 2007). The resulting southward shift of the ITCZ (Jennerjahn et al., 2004) has reduced the monsoonal precipitation over NW-Africa (deMenocal et al., 2000a) and led to a southward migration of the vegetation zones

(Hooghiemstra et al., 2006). This scenario should be transferred to the much less understood pervious major climatic termination (Termination II).

In contrast, the interglacials like the Holocene, were considered as a relatively stable climatic periods. However, many high resolution marine records in the North Atlantic realm provide evidences for unstable climatic conditions on millennial scale (Bianchi and McCave, 1999; Bond et al., 1999; deMenocal et al., 2000b). The most prominent climatic feature during the Holocene of NW-Africa is the African Humid Period (deMenocal et al., 2000a). This humid period is placed between 14.8 kyr BP until 5.5 kyr BP and is accompanied with rapid hydrological fluctuations and the infill of smaller lakes and a greening of the Sahara (Kocurek et al., 1991; Claussen et al., 1999; Gasse, 2000; Renssen et al., 2006).

In addition, further short-term climatic events like Dansgaard-Oeschger oscillations and Heinrich events are known from the North Atlantic (Heinrich, 1988; Bond et al., 1992; Broecker et al., 1992; Dansgaard et al., 1993; van Kreveld et al., 1996). These rapid events had durations of a few hundred to a thousand years and occurred approximately every 7 - 10 kyr (Bond et al., 1992). Palaeoceanographic studies have revealed that iceberg drifting occurred south of the main ice rafting belt until the Iberian continental margin resulting in sharp drops of the annual sea surface temperatures off Portugal (Abrantes et al., 1998; Abreu et al., 2003). However, the effect of these sub-millennial climatic changes is poorly known in the subtropical North Atlantic (Jullien et al., 2007).

2 Methodological approach

2.1 Sample preparation and proxy approach

The sedimentary record of all cores recovered in the Dakar Canyon and Diola Canyon consists of hemipelagic sediments with intercalated turbidite beds at distinct intervals. The exact differentiation between hemipelagic sediments and turbidites was determined by visual core description and X-ray radiographs, which were performed on 1 cm thick sediment slides. To establish an accurate age model, to analyses the hemipelagic background sediments and to clarify the turbidite emplacement times each turbidite was cut out of the records.

The elemental distribution of the hemipelagic sediments was measured in 1 cm resolution using the X-ray Fluorescence (XRF) Core Scanner. This scanner is a computer-controlled core-scanning tool that analyses the chemical composition on the surface of a split sediment core (Tjallingii, 2006). The high sample resolution and the non-destructive measurement provide continuous information about the elemental distribution in the sediment cores. However, element concentrations are not provided directly by the XRF-measurements but element intensities (in cps) can be converted from these scans (Kuhlmann, 2003).

Based on the core description samples of the hemipelagic sediments were taken between the turbidites in irregular intervals. The sand fraction (>63 μm) was separated from the fine fraction by wet sieving. For grain size analysis of the terrigenous components of the fine fraction, the samples were pre-treated with 10% H_2O_2 and 12.5% HCl in order to remove organic matter and carbonate. In the following, the fine fraction was separated into silt (63 - 2 μm) and clay (< 2 μm) by repeated settling in the Atterberg tubes according to Stokes' law. Each separated fraction were dried and weight percentages (wt%) was determined.

The detailed grain size analysis of the terrigenous components of the silt fraction were performed with the Micromeritics SediGraph 5100 in the range of 63 - 2 μm. The SediGraph measures accurately in the range of 100 - 2 μm and therefore the clay fraction has to be removed due to the cohesive behaviour and aggregate formation (Stein, 1985). The silt size distribution is expressed as equivalent spherical diameter according to settling velocities based on Stokes' law. Two data processing steps have been applied to the

SediGraph cumulative raw data. The data were interpolated at 0.1 φ increments by using a linear interpolation and the interpolated cumulative data has been normalised by subtracting minima and dividing by resulting cumulative maxima. Afterwards the grain size distributions were calculated in the range from 4 - 9 φ (62,5 - 1,95 µm). The biogenic opal content in marine sediments of NW-Africa is negligible (Koopmann, 1981; Holz et al., 2007). Hence we refer to terrigenous silt as carbonate and organic free silt. The composition of aeolian derived terrigenous silt in deep-sea sediments depends on the distance to the source area, the intensity of the transporting winds and climatic variations of the hinterland (Rea, 1994). Therefore, the variation of the terrigenous silt size distribution is used to estimate the paleo-wind intensity whereas coarser silt values reflect stronger wind intensities.

Based on the core description all turbidites in the cores recovered in the axis of the Dakar Canyon were sampled in 1 cm resolution to reconstruct the grain size distribution in the turbidites. All samples were freeze-dried and the sand fraction was separated from the fine fraction (< 63 µm) by wet sieving. The fine fraction was subdivided into silt and clay by repeated settling in Atterberg tubes according to Stokes' law. Each separated fraction was dried and weight percentages were determined. The analysis of the grain size distribution of turbidites allows the reconstruction of the sedimentary architecture of such a deposit. Furthermore, the sediment source can be determined by component analysis of the sand fraction (500 - 250 µm). Unfortunately the results were not very meaningful and a clear identification of the source area was not possible.

The mineral composition of the carbonate and organic matter free clay fraction of core GeoB 9602-3 recovered from the Diola Canyon was analysed on grounded and mounted textually orientated aggregates with a Phillips PW 1830 X-ray diffractometer (CoKα radiation, 40 kV, 40 mA). All samples were measured from 3 - 40° 2Θ. The clay minerals were identified by their basal reflection measuring the individual peak heights using the software package "MacDiff". For semiquantitative evaluations of the content of each clay mineral the empirically estimated weight factors on integrated peak areas were used (Biscaye, 1964; Biscaye, 1965). All concentrations are given in percent of the total clay mineral assemblage. The formation of clay minerals like kaolinite and smectite requires defined source materials and climatic conditions. Intensive chemical weathering under a warm and humid climate are necessary for the formation of both clay minerals. Therefore, the kaolinite/smectite ratio can be used as an indirect indicator of the prevailing climatic conditions in the hinterland.

2.2 Chronographic framework

The planktonic foraminifera *Globigerinoides ruber* (white) was used for all stable isotope measurements. The age model for cores GeoB9612-3 is provided by correlation with the orbitally tuned SPECMAP-record (Martinson et al., 1987) whereas GeoB9602-3 was correlated to the NGRIP ice core record (Svensson et al., 2008). The investigated cores in the Dakar Canyon were correlated to GeoB9612-3 by their typical total reflectance pattern. In addition a few accelerator mass spectrometry (AMS) radiocarbon data samples from different cores support the age model and core correlations. At least 700 individual species of the planktonic foraminifera *G. ruber* (white/pink), *G. sacculifer* and *O. universa* were collected for accelerator mass spectrometry (AMS) radiocarbon dating. Carbonate hydrolysis and CO_2 reduction was carried out at Bremen University and AMS dating was done at the Leibniz Laboratory for Radiocarbon Dating and Isotope Research in Kiel and at the Poznan Radiocarbon Laboratory in Poznan, Poland. A standard reservoir age of 400 yrs is assumed for calibration regarding to the short lasting periods of winter upwelling. The radiocarbon ages younger than 24 ^{14}C kyr BP are corrected and calibrated using CALIB REV5.0.1 (Stuiver et al., 1998). Older radiocarbon ages are subsequently calibrated using he function of Bard et al. (1998). All ages are given in thousands of years before present in the following. Ages of turbidites are considered to be equivalent to the age derived for the onset of hemipelagic sedimentation on the top of the relevant turbidite.

3 Objectives of this study

The present study investigates the timing and composition of turbidity currents in two submarine canyons along the NW-African continental margin based on analysis of gravity cores recovered directly in the canyon axis. In addition, gravity cores from the adjacent levee provide the variations of the terrigenous sediment supply during the late Quaternary. Seismic and Parasound sediment echosounder profiles were used to study the structure and morphology of the investigated canyon systems. The analysis of a core transect in the Dakar Canyon allows to reconstruct the architecture of the turbidite deposits.

The main object of this study, which is imbedded in the interdisciplinary Project C2 of the Research Center Ocean Margin (RCOM/MARUM), was the investigation of sedimentation processes and sediment pathways at the tropical continental margin off Senegal. Therefore the sedimentation processes on the continental slope and the link to the sedimentary history of the associated shelf was investigated. The main goal of this project is the development of a schematic model which describes the transport dynamics of sediment from shallow marine environments into the deep sea. Furthermore, a quantification of sediment budgets in relation to climatically controlled, varying sediment supply should be established.

4 Manuscript #1

Late Quaternary climatic events and sea level changes recorded by turbidite activity, Dakar Canyon, NW-Africa

Roberto Pierau[*], Till J.J. Hanebuth[*], Sebastian Krastel[+], and Rüdiger Henrich[*]

[*] MARUM - Center for Marine Environmental Sciences and Faculty of Geosciences, University of Bremen, Klagenfurter Straße, 28359 Bremen, Germany

[+] IFM-Geomar, Leibinz Institute of Marine Science, Wischhofstr. 1 - 3, 24148 Kiel, Germany

submitted to *Quaternary Research*

Abstract

The mechanisms of gravity-driven sediment transport in submarine canyons during sea level changes have been reported from many regions. However, the relationship of sea level changes and short-term climatic changes with turbidite deposition is poorly documented. This study focuses on the activity of the Dakar Canyon off southern Senegal in response to major glacial/interglacial sea level shifts and variability in the NW-African continental climate. The sedimentary record from the canyon allows us to determine the timing of turbidite events and based on XRF-scanning element data, we have identified the climate signal at a sub-millennial time scale from the surrounding hemipelagic sediments. Over the late Quaternary the highest frequency in turbidite activity in the Dakar Canyon is confined to major climatic terminations when remobilisation of sediments from the shelf was triggered by the eustatic sea level rise. However, episodic turbidite events coincide with the timing of Heinrich events in the North Atlantic. During these times continental climate has changed rapidly, with evidences for higher dust supply over NW-Africa which has fed turbidity currents. Increased aridity and enhanced wind strength in the southern Saharan-Sahelian zone may have provided a considerable source for this dust.

Keywords: turbidite system, sea level change, palaeoclimate, NW-Africa, Heinrich equivalents

1. Introduction

Submarine canyons play a major role as conduits for sediment transport from the continental shelf and upper slope into the deep-sea basins (Weaver et al., 2000). Several canyons that incise the passive NW-African continental margin have been investigated in terms of their general sedimentation processes (Seibold and Fütterer, 1982; Zühlsdorff et al., 2007b). These studies have postulated a major influence of glacial/interglacial sea level changes and climatic variability on the continental sediment supply. The Quaternary and Holocene climate history of NW-Africa is reconstructed from marine and terrestrial archives suggesting significant climate change from arid glacial condition to a more humid climate during the early Holocene (Sarnthein et al., 1982; Rognon and Coudé-Gaussen, 1996; deMenocal et al., 2000a; Kuhlmann et al., 2004). In contrast, the control of sub-millennial climatic changes on sediment dynamics is poorly known in the subtropical North Atlantic realm. In this study we reconstruct the late Quaternary turbidite history of the Dakar Canyon to unravel these sedimentation controlling factors based on a high resolution age model. We discuss the sedimentary imprints of the interplay between sea level and climatic changes, and their potential to trigger turbidity currents.

2. Study area

The cold southward directed Canary Current, as a part of the Eastern Boundary Current System, is the major surface current along the NW-African margin (Mittelstaedt, 1991). The surface water masses in the subtropical North Atlantic south of 20°N are dominate by a wind driven subtropical gyre (Stramma et al., 2005). These surface currents are underlain by the South Atlantic Central Water and the North Atlantic Central Water (Lonsdale, 1982). Deep-water currents are represented by the North Atlantic Deep Water at depths between 1200 - 4000 m (Stramma and Schott, 1999) and the Antarctic Bottom Water (AABW) below a water depth of 4000 m (Wynn et al., 2000).

The seasonal migration of the Intertropical Convergence Zone (ITCZ) is the most important atmospheric feature in NW-Africa (Nicholson, 2000). During boreal summer,

the northward shift of the ITCZ (20°N during August) is accompanied by the humid "SW" monsoon south of the ITCZ. Northeast directed trade winds prevail during winter times when the ITCZ has migrated to the southward position of 5°N. The trade winds and the overlying Sahara Air Layer are the prevailing wind systems over NW-Africa (Fig. 1a) and drive major dust transport from the Sahara-Sahel zone towards the Atlantic Ocean (Koopmann, 1981; Prospero and Lamb, 2003). Fluvial supply in the study area is restricted to the Senegal River north of Dakar but plays only a minor role in sediment supply (Redois and Debenay, 1999). Therefore, the surface sediments on the Senegalese shelf consist of quartz sands and carbonate shell fragments (McMaster and Lachance, 1969; Barusseau et al., 1988; Redois and Debenay, 1999). These sands have originated from palaeo-dunes that, in turn, have formed around the Last Glacial Maximum (LGM) as a result of increased aridity and wind strength (Sarnthein and Diester-Haass, 1977; Lancaster et al., 2002), and low sea level providing widely exposed shelf areas. The Senegalese Shelf varies in width between 50 - 100 km (Hagen, 2001) and the average depth of the shelf break south of 15°N is found in about 100 - 150 m present water depths (McMaster and Lachance, 1969).

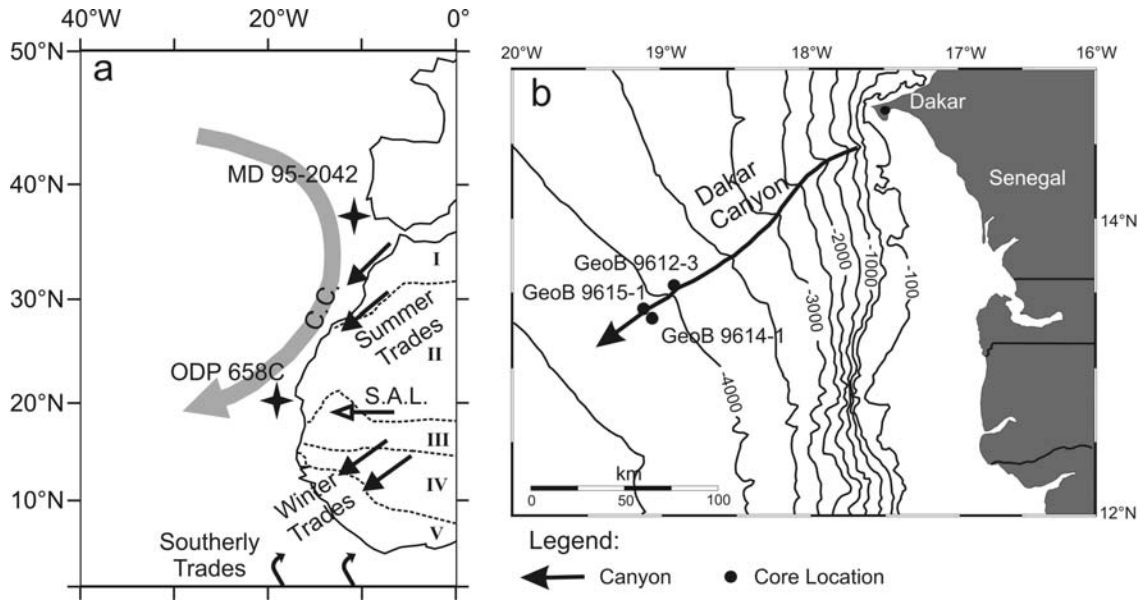

Figure 1: Map of the Dakar Canyon and surrounding area. a) Overview of the study area including the major surface current (C.C. - Canary Current), the prevailing wind systems (S.A.L. - Sahara Air Layer and trade wind system) and the major vegetation zones of NW-Africa (modified after Hooghiemstra et al., 2006, I - Mediterranean vegetation, II - Saharan desert, III - Sahelian vegetation, IV - Sudanian savannah, V - Guinean rain forest). b) Map of the Dakar Canyon including the locations of the presented cores. Bathymetry is taken from GEBCO.

Along the Iberian and NW-African margin the sea surface temperatures (SST) show a range from about 18°C during the Late Glacial to 21,5°C during the early Holocene times, indicating a considerable southward transport of cooler subpolar water masses by the Canary Current (Zhao et al., 1995). Furthermore, cooler SST could also be attributed to enhanced upwelling forced by stronger trade wind intensity (Martinez et al., 1999). Consequently, the inflow of cold surface water masses as far as south into the region off Cape Blanc coincides with low orbital boreal summer insolation and is thought to have additionally influenced the regional atmospheric and climate pattern of NW-Africa (deMenocal et al., 2000b). As a result, due to the arid glacial conditions and intensified trade winds, a period of active dune formation has occurred between 25 - 14.8 ka BP in the western Sahara (Sarnthein, 1978; Lancaster et al., 2002). During the LGM sea level lowstand (ending around 19.0 ka BP) the exposed shelf south of Dakar was also covered by dune fields, whose remnants can still be traced on the shelf today (Barusseau et al., 1988).

3. Material and dating methods

The bathymetry and architecture of the Dakar Canyon (Fig. 2a) were mapped using a bathymetric multibeam system and a sediment echosounder. At the upper slope the canyon incises vertically up to 700 m into the strata and is up to ~10 km wide. The canyon cuts straight downslope and the incision depths of the canyon decrease basinwards down to less than ~20 m at the continental rise in ~4000 m water depth. Irregular high amplitude reflectors indicate a sandy infill of the canyon's thalweg (Fig. 2b, c). At the distal part the canyon splits into a main active channel and a parallel running channel remnant. This study focuses on three gravity cores recovered from the thalweg (GeoB 9614-1, GeoB 9615-1) and its northern levee in the direct vicinity of the canyon (GeoB 9612-3, Fig. 1b, Table 1).

Table 1: Key parameters of cores investigated in this study including core number, geographic position and water depth.

core number	latitude	longitude	water depth (m)
GeoB 9612-3	13° 33.01' N	18° 53.50' W	3893
GeoB 9614-1	13° 20.54' N	19° 03.56' W	4090
GeoB 9615-1	13° 23.68' N	19° 06.27' W	4180

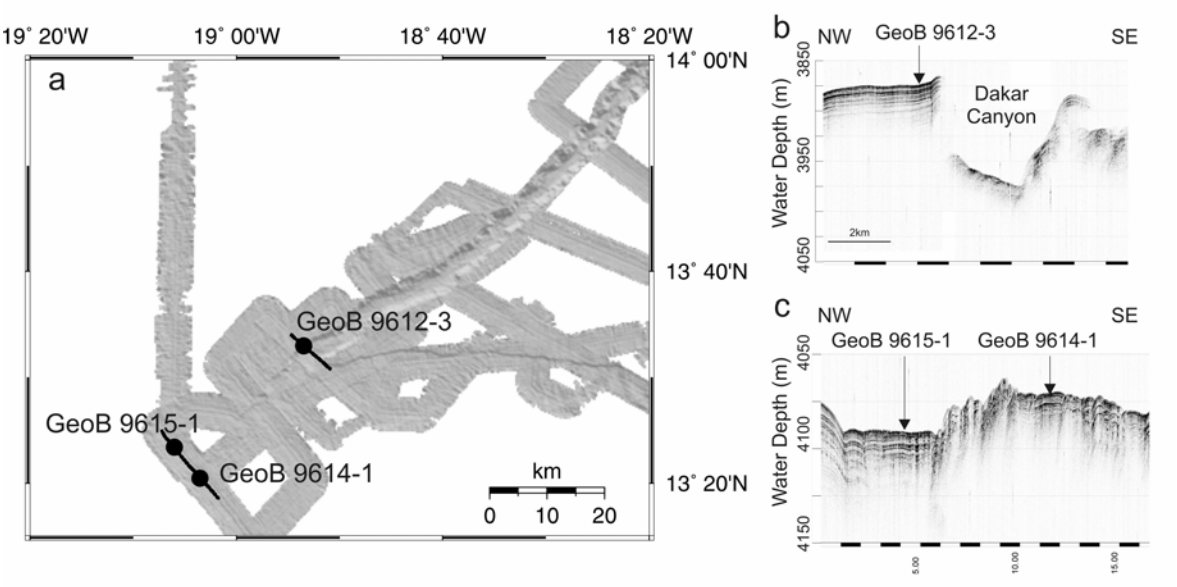

Figure 2: Bathymetric multibeam map of the distal Dakar Canyon (a) including the core locations. The locations of the seismic profiles are shown as black lines. b & c) Narrow beam sediment echo sounder profile crossing the location of Cores 9612-3, 9615-1 and 9614-1. The distance in altitude between the canyon bottom and the top of the levee as depicted in Figure 2b is about 100 m.

The sedimentary records of all these cores consist of hemipelagic sediments composed of silty mud, which are frequently intercalated by fine sandy and silty turbidite beds at distinct intervals. The exact differentiation between hemipelagites and turbidites was determined by visual core description and X-ray radiographies, which were performed on 1cm thick sediment slides. At the northern levee of the canyon the hydroacoustic profile depicts well-stratified deposits (Fig 2b) as identified as hemipelagic sediments in Core 9612-3. The turbidites in this core are of spill-over origin and according to the X-ray radiographies the hemipelagic sediments show no erosional features. Thus this core was selected to provide a suitable startigraphical model which can be transferred as a reference to the other investigated cores.

The planktonic foraminifera *Globigerinoides ruber* (white) was used for $\delta^{18}O$ stable isotope measurements and the planktonic foraminifers *G. ruber* (w/p), *G. sacculifer* and *O. universa* were collected for accelerator mass spectrometry radiocarbon (AMS) dating at the Leibniz Laboratory for Radiocarbon Dating and Isotope Research in Kiel, Germany. The elements Ca and Ti were measured in 1 cm resolution using a non-destructive X-ray Fluorescence (XRF) Core Scanner.

The age model for Core 9612-3 is based on its stable oxygen isotope curve (Fig. 3) which is correlated to the orbitally tuned SPECMAP record (Martinson et al., 1987). Four radiocarbon dates are used to improve the age model for the younger part of the record

(Table 2). A standard reservoir age of 400 yrs is assumed for calibration regarding to short lasting period of winter upwelling. The radiocarbon ages younger than 24 ^{14}C ka BP are corrected and calibrated using CALIB REV5.0.1 (Stuiver et al., 1998). Older radiocarbon ages are subsequently calibrated using the function of Bard et al. (1998). All ages are given in calibrated thousands of years before present in the following (ka BP).

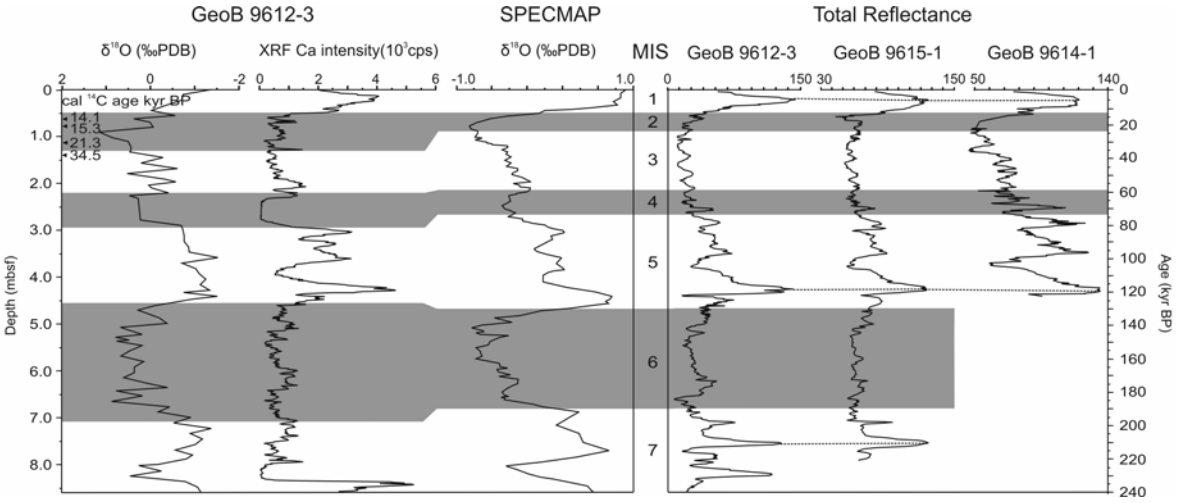

Figure 3: Oxygen isotope record and XRF Ca intensity of Core 9612-3 against core depth (mbsf - meters below seafloor) compared to the SPECMAP record. The shaded areas indicate glacial isotope stages. Cores 9614-1 and 9615-1 were correlated with 9612-3 by their characteristic total reflectance pattern of the hemipelagites (dotted lines). Turbidites were cut out of these records.

4. Results

In this paper we focus on the occurrence of turbidites in the Dakar Canyon during the late Quaternary. Thickness of the turbidites varies from a few centimetres (minimum 1 cm) to a comparably thick turbidite of 135 cm in Core 9615-1 (Fig. 4, Tab. 3). According to the analysis of the X-ray radiographies all turbidites shows a clear fining-upward sequence and consists mostly of cross-laminated fine sands overlain by laminated silts and homogenous mud.

Table 2: AMS radiocarbon dating and calibrated ages of Core 9612-3.

core depth (cm)	Lab ID	conventional age (yrs)	calibration two sigma range (cal yr BP)	calib. age (kyr BP)
55	KIA30490	12650	13860 - 14610	14.1
68	KIA30506	13380	15030 - 15690	15.3
111	KIA30488	18400	20810 - 21910	21.3
133	KIA30487	29530		34.5

The cores recovered in the canyon axis consist of relatively thick turbidites (Tab. 3) with coarse sandy material at their base. The T_A and T_B units as parts of the lower Bouma-Sequence (Bouma, 1962) are only partly preserved. The fine-grained deposits, reflected in the T_C to T_D units, occur in most of the turbidites. This fine material was deposited a) as spill-over turbidites in the levee Core 9612-3 and b) as fine sediment suspension in the canyon axis. The top sections of the turbidites are often destroyed by intensive bioturbation. Therefore, it is partly problematic to distinguish a turbidite top from the overlying hemipelagic sediments. In such a case the beginning of the hemipelagic sedimentation was defined by increased numbers of foraminifers (Zühlsdorff et al., 2007b). To determine the age of the cores we subtracted the turbidite sections out of all records, receiving a continuous hemipelagic sedimentation succession, and correlated the two other investigated cores (9615-1, 9614-1) by their characteristic total reflectance pattern (Fig. 3). Ages of turbidites are considered to be equivalent to the age derived for the onset of hemipelagic sedimentation on the top of the relevant turbidite. Based on core correlation and age determination of the turbidites, we combined the turbidite records of all three cores to provide a stacked turbidite sequence for the Dakar Canyon. This stacked record consists in total of 40 individual turbidite beds (Tab. 3).

The highest turbidite frequency is recorded during the two past glacial/interglacial transitions, and thus coincides with the respective rise in the eustatic sea level (Fig. 5a). For Termination I (T1, 15.7 - 13.9 ka BP) five events/ka have occurred whereas a lower frequency of 1.2 events/ka is recorded for Termination II (T2, 137.2 - 126.6 ka BP). Furthermore, turbidites that are concentrated around these terminations show the highest thickness (Fig. 4). In addition, some thin turbidites occur around 60, 49, 28 and 23 ka BP as well as prior to T2 (at 220, 170 and 164 ka BP, Fig. 5a), which could not have been triggered by major rises in sea level. These events coincide, however, with lower SST (Fig. 5b, c) along the Iberian and NW-African continental margin (Zhao et al., 1995; Pailler and Bard, 2002) and coeval with the timing of Heinrich events in the North Atlantic (Thouveney et al., 2000; Moreno et al., 2002). Furthermore, higher Ti/Ca ratios (Fig. 5d) are recorded in the hemipelagites in Core 9612-3 during these Heinrich equivalent time intervals (HE). The marine carbonate content is reflected by the XRF Ca intensity, whereas Ti is related to siliciclastic components of terrigenous origin. The Ti/Ca ratio is, therefore, commonly used as a proxy for the influx of terrigenous material in marine sediments (Arz et al., 1998). Due to the absence of riverine input in the study area, this ratio reflects here the variability of dust input from the continent.

Table 3: Age, thickness and Bouma Units of the turbidites in Cores 9612-3, 9614-1, 9615-1 and the stacked turbidite record of the Dakar Canyon. Columns marked by xx consist of turbidites without age determination due to the direct covering of two individual turbidites. Bouma Units which are marked with (?) were not clearly identified.

GeoB 9612-3			**GeoB 9615-1**			**GeoB 9614-1**			**Stacked turbidite record**	
age (ka BP)	thickness (cm)	Bouma Unit	age (ka BP)	thickness (cm)	Bouma Unit	age (ka BP)	thickness (cm)	Bouma Unit	Turbidite No.	age (ka BP)
12.3	1	?	14.3	6	T_B - T_C	14.7	8	T_C - T_E	1	12.3
13.9	4	T_C	**xx**	1	T_B	18.2	17	T_A - T_B	2	13.9
14.6	2	?	15.1	14	T_B - T_E	22.4	15	T_B - T_E	3	14.3
14.8	2	T_C	15.3	6	T_B - T_E	23.2	13	T_C	4	14.6 / 14.7
14.9	11	T_B - T_C	**xx**	8	T_C - T_E	48.8	5	T_C	5	14.8
22.1	3	?	15.4	5	T_C - T_E	122.4	8	T_C	6	14.9 / 15.1
29.3	10	T_A - T_D	**xx**	2	T_C	123.8	20	T_B - T_E	7	15.3
57.2	4	?	15.5	5	T_C				8	15.4
123.5	3	?	15.7	4	?				9	15.5
126.6	3	T_C	**xx**	3	T_C				10	15.7
xx	5	T_C	24.2	135	T_A - T_C				11	18.2
128.2	2	?	28.5	38	T_B - T_C				12	22.1 / 22.4
128.3	4	?	57.2	6	T_C - T_E				13	23.2
128.7	3	?	60.2	5	?				14	24.2
129.3	5	T_C	82.9	4	?				15	28.5 / 29.3
129.6	3	T_C	131.6	4	T_D				16	48.8
132.9	9	T_B - T_C	132.3	4	T_D				17	57.2
xx	3	?	136.5	5	T_C - T_D				18	60.2
133.6	3	?	137.2	10	T_C - T_D				19	82.9
134.0	4	T_C - T_D	**xx**	16	?				20	122.4
135.0	5	?	141.3	21	T_A - T_C				21	123.5 / 123.8
136.3	2	?	**xx**	7	T_C - T_E				22	126.6
xx	3	?	**xx**	3	T_C				23	128.2
170.3	2	?	163.8	3	?				24	128.3
173.7	4	?	171.7	21	T_B - T_E				25	128.7
216.7	3	?	173.3	15	T_B- T_E				26	129.3
219.7	8	T_C							27	129.6
									28	131.6
									29	132.3 / 132.9
									30	133.6
									31	134.0
									32	135.0
									33	136.3 / 136.5
									34	137.2
									35	141.3
									36	163.8
									37	170.3 / 171.7
									38	173.3 / 173.7
									39	216.7
									40	219.7

Two episodes of very high Ti/Ca ratios (Fig. 5d) and extremely low XRF Ca intensities (Fig. 3) are observed around 220 and 70 ka BP in Core 9612-3. This core was recovered in a water depth of 3900 m and could be influenced by depth changes of the carbonate unsaturated AABW (Sarnthein et al., 1982) which, in turn, would led to carbonate solution in the sediment. According to this effect, low Ca values led to irregularly high values of the Ti/Ca ratio.

5. Discussion

Both continental climatic changes and sea level oscillations controlled the turbidite activity in the Dakar Canyon. During T1 the steadily rising sea level (Peltier and Fairbanks, 2006), due to the melting of the Northern Hemisphere ice sheets, was interrupted by one or more short time intervals of very rapid rises known as meltwater pulses (Fairbanks, 1989).

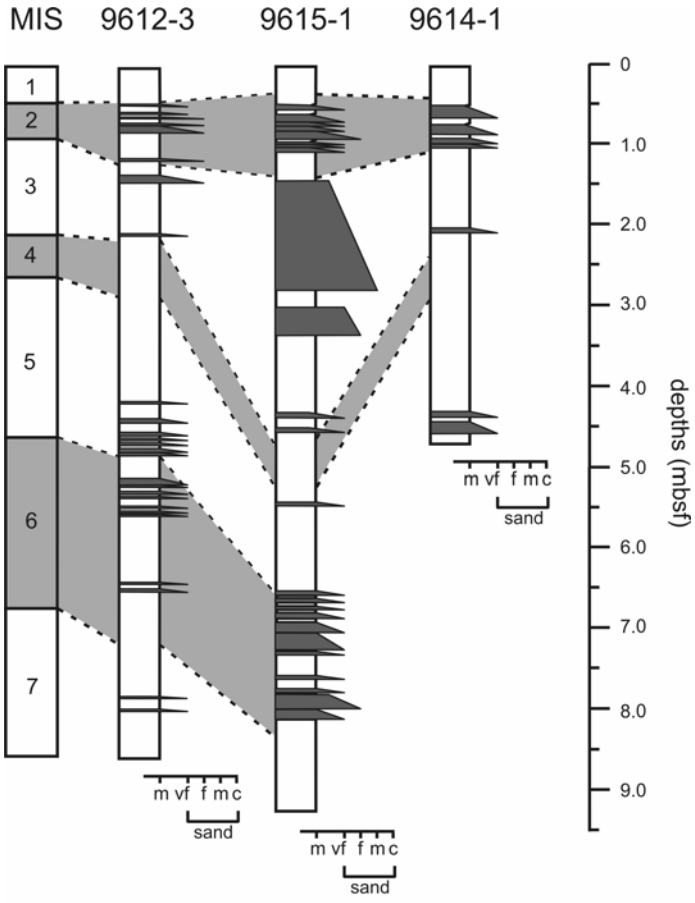

Figure 4: Schematic sedimentary columns of Cores 9612-3, 9615-1 and 9614-1 against age and depths (mbsf). The grain size distributions of the turbidites are expressed in mud (m) and sand content (vf - very fine, f - fine, m - medium, c - coarse).

The interval of very high turbidite activity during T1 partly coincides with MWP1A (14.6 - 14.3 ka BP, Fig. 6) when the sea level rose as much as 15 m within a few centuries (Hanebuth et al., 2000). Furthermore, a high Ti/Ca ratio is recorded at 15 ka BP that fits with the timing of Heinrich event 1 in the North Atlantic (Fig. 6). This period coevals with generally dry conditions over the NW-African continent (Lèzine, 1991). Contemporaneously, a weakened thermohaline circulation led to a stronger hemispheric temperature gradient coupled with intensified trade winds (Vidal et al., 1997; Jullien et al., 2007). The resulting southward shift of the ITCZ (Jennerjahn et al., 2004) has reduced the monsoonal precipitation over NW-Africa (deMenocal et al., 2000a) and led to a southward

migration of the vegetation zones (Hooghiemstra et al., 2006). In general, the aeolian dust input off NW-Africa was significantly higher during glacial periods (Matthewson et al., 1995; Moreno et al., 2001). The Ti/Ca ratio of Core 9612-3 supports this observation, reflected by higher Ti/Ca ratios during periods of enhanced dust supply (Fig. 6). Furthermore, along NW-Africa, the river discharge during the LGM was nearly not existent due to the arid climate conditions (Barusseau et al., 1988).

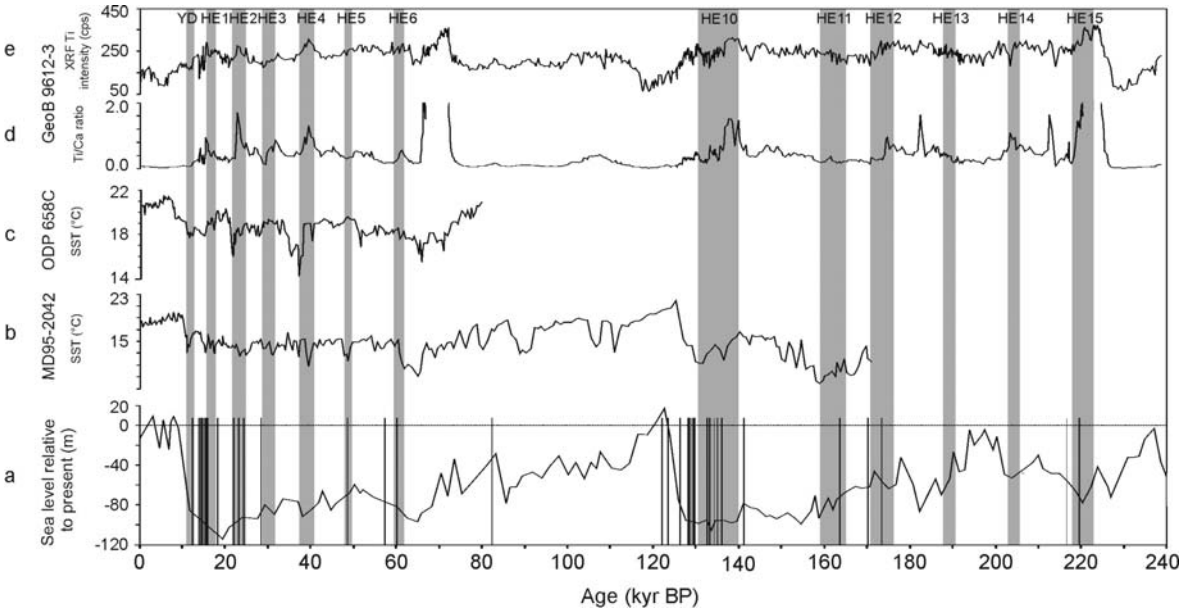

Figure 5: Comparison of the 9612-3 sediment record with regional and global climate proxy data. Fig. 5a illustrates the stacked turbidite record (each black bar indicates a single turbidite event) of the Dakar Canyon in relation to the global sea level curve (Siddall et al., 2003). Abrupt drops in SST (Fig. 5b, 5c) of MD95-2042 (Pailler and Bard, 2002) and ODP 658C (Zhao et al., 1995) demonstrate the influence of cold surface water along the Portuguese and NW-African continental margin during HE (marked in grey). The changes of Ti/Ca ratio of Core 9612-3 and XRF Ti intensity (Fig. 5d, 5e) coeval with HE and shows synchronous millennial-scale oscillations with shifts in SST of Cores MD95-2042 and ODP 658C.

Enhanced climate-induced dust supply towards the exposed shelf and active dune formation between 16 and 14 ka BP (Sarnthein, 1978; Lancaster et al., 2002) has provided a considerable sediment source for gravity-driven mass flows off the shelf break. The dune fields have formed at the lee side of the tectonic high of Ndiass horst, east of Dakar, and extended parallel to the former coastline (Barusseau et al., 1988). These dune remnants are obviously found on the entire modern shelf up to a water depth of 20 m and have even been discovered close to the shelf break in 120 m modern water depth (Barusseau et al., 1988). The loose sands of these dunes were probably very efficiently remobilised during the subsequent rapid transgression and their material was collected by and transported downslope through the canyon. The large volume of reworked sediments is expressed in

massive thickness and high frequency of turbidite deposition during T1 (Fig. 4). The interaction of these climatically controlled sediment supply onto to the exposed shelf and the following rapid transgression were responsible for the high turbidite occurrence during the T1.

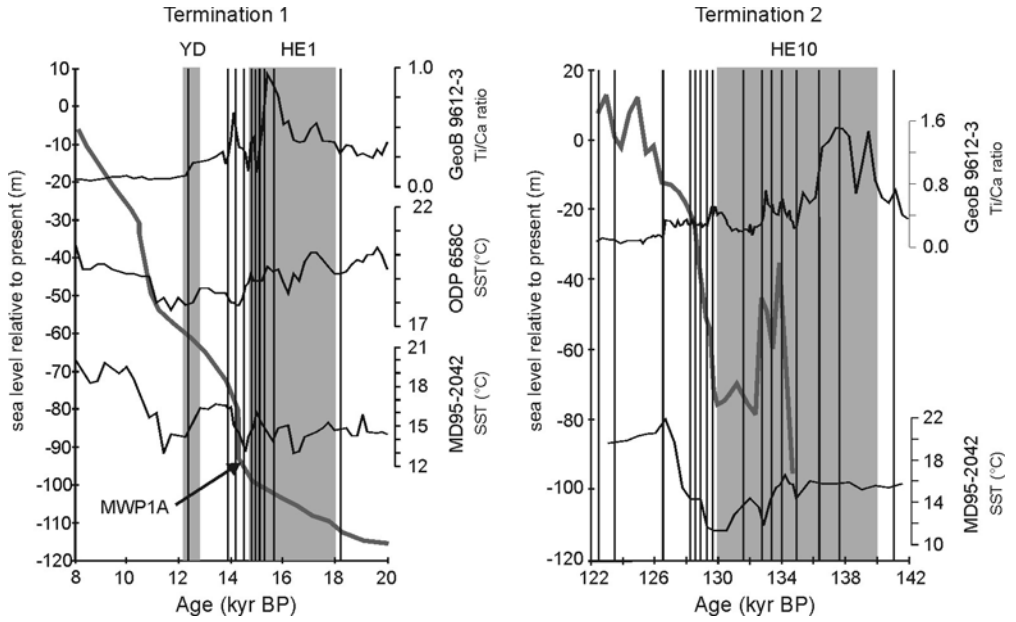

Figure 6: Turbidite activity during T1 and T2 in the Dakar Canyon in comparison with sea level change, SST and Ti/Ca ratio of Core 9612-3. The thick grey line indicates the sea level and the grey marked areas illustrate periods of short-term climatic changes. Each black bar represents a single turbidite. The highest activity of turbidite deposition during both terminations correlates well with episodes of rapid sea level rise.

A low Ti/Ca ratio after 14 ka BP displays the onset of the African Humid Period (14.8 ka BP) when the climate has changed rapidly towards humid conditions (deMenocal et al., 2000a). The latest turbidite bed coincides remarkably with a short interruption of this wet period by the arid Younger Dryas (Gasse et al., 1989) which was centred around 12.6 ka BP (Fig. 6, deMenocal et al., 2000a). Comparably, humid conditions and the general sea level stability have prevented further turbidity activity during the Holocene (Fig. 5a).

The results can be transferred to the much less understood Termination II. During this climatic transition two phases of increased turbidite activity are recorded at 136 - 132 ka BP and at 130 - 128 ka BP (Fig. 6). Moreover, some single turbidite events have occurred in the time interval from 126 - 122 ka BP. High Ti/Ca ratios occur around 138 ka BP in Core 9612-3. Elevated Ti/Ca ratios are also detected during these two phases of high turbidite activity and coincide with decreases in SST recorded in Core MD95-2042 (Fig. 6, Pailler and Bard, 2002). In general, we assume a comparable situation for the turbidite depositional history during T2 as described for T1. The sea level history during T2 was

possibly characterized by an early, temporary highstand (ca. 134 ka BP) at intermediate levels, followed by a fall in sea level with a subsequently stable period at 133 - 130 ka BP and finally by the ultimate sea level rise into the marine isotope stage (MIS) 5e (Siddall et al., 2006).

The turbidite activity, that has started around 136 ka BP, coincides with the initiation of the early sea level rise (Fig. 6). No activity is recorded during the succeeding phase of sea level stagnation whereas a second period of high turbidite deposition occurred contemporaneous with the second interval of sea level rise. A relatively high Ti/Ca ratio is registered prior to the early sea level rise (Fig. 6), which indicate an episode of enhanced dust supply. Dune fields have probably formed on the exposed shelf prior to T2 as well. Subsequently, during rapid sea level rise, the dunes may have been eroded and the material was transported trough the canyon by turbidity currents as observed as efficient mechanism during T1. The low Ti/Ca ratio through MIS 5 (Fig. 5d) probably indicates more humid conditions and less dust supply. This reduced dust input and a high sea level might have impeded further turbidite activity.

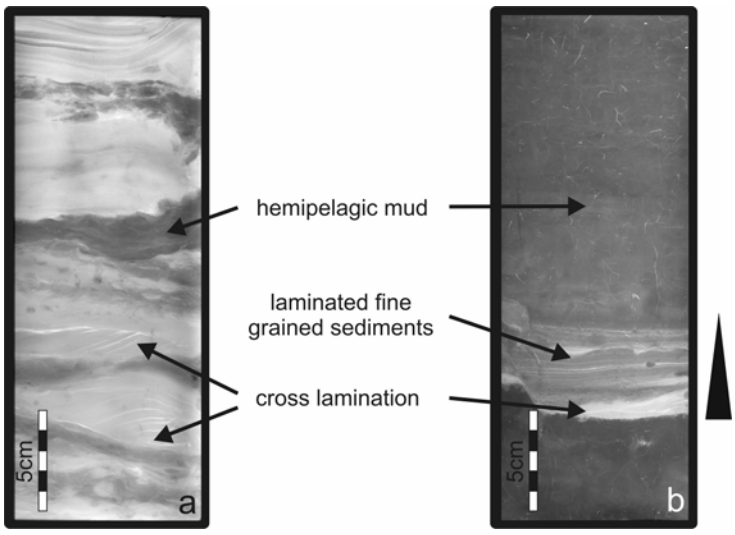

Figure 7: X-ray radiographs of Core 9615-1 showing different sedimentary structures of turbidites. Fig. 7a of 75 - 100cm core depths display a sector of frequent turbidite deposition during Termination 1. The turbidites consists of relative thick and coarse sediments. Fig. 7b (425 - 450cm core depths) shows a thin fining upward turbidite sequence deposited during a Heinrich time equivalent.

Sporadically appearing turbidites are recorded during MIS 6 and MIS 3 (Fig. 5a). These turbidites consist of laminated fine-grained sediments. They are, in general, thinner and finer than those turbidites that have deposited during the two major climate transitions (Fig. 7). The ages of these turbidites coincide with HE (Fig. 5a). The occurrence of HE is

associated with significant peaks in the Ti/Ca ratio of Core 9612-3 (Fig. 5d) and is accompanied by intervals of low SST as recorded in the Cores MD95-2042 and ODP 658C (Zhao et al., 1995; Pailler and Bard, 2002). These observations seem to indicate episodes of short-term climatic changes in the hinterland influencing the seaward flux of dust. Jullien et al. (2007) argue that a southward shift of the ITCZ reorganises the atmospheric pattern of NW-Africa which results in arid conditions in the hinterland with enhanced trade wind intensity. During HE sea level oscillations have also occurred but surely at significantly lower amplitudes then during major climate terminations (Lambeck et al., 2002). During these times, sea level was 60 - 90 m lower than present (Yokoyama et al., 2001). The shelf was partly exposed and these arid episodes were probably responsible for the deposition of dust and the enhanced sediment accumulation on the shelf. Slightly rising sea level during these HE could have remobilised dust from the shelf. According to the detailed sea level reconstruction of coral terraces from the Huon Peninsula during these HE, sea level rose rapidly towards the end of a HE (Yokoyama et al., 2001). We conclude that during HEs dust was deposit on the shelf which were subsequently remobilised at the termination of a HE recorded in the turbidite activity.

6. Conclusions

Two main phases of turbidite activity coinciding with the past two glacial terminations are identified in the Dakar Canyon. They are linked to major climatic transitions in association with rapidly rising eustatic sea level. The turbidite activity during these terminations was triggered by the remobilisation of sediments which had previously been deposited on the exposed shelf in form of aeolian dunes under arid glacial climate conditions and an intensified trade wind regime. The significant influence of MWP1A is detectable by an exceptional high turbidite activity. The dynamic of turbidite activity during Termination 2 seems to reinforce the recent progress in sea level reconstructions. The onset of humid conditions after major climate terminations has coincided with a die-off of turbidite activity probably due to reduced dust supply. High and relatively stable sea levels during MIS 5 and the Holocene have additionally impeded further turbidite activity.

The short-lasting climatic changes during HE are characterized by reduced monsoon intensity and southward migration of the vegetation zones resulting in enhanced dust flux. Increases in the Ti/Ca ratios indicate a higher aeolian input and coeval with the deposition of turbidites. This observation probably shows that the influence of HE extended as far

south as into the study area resulting in a large-scale reorganisation of the atmospheric and climatic pattern.

This study points out the potential of sedimentary canyon records as archives to reconstruct the interplay of even short-lasting climatic episodes and global sea level oscillations considering the turbidite history.

Acknowledgements

The captain, crew, and shipboard participants of cruise M65/2 are thanked for their assistance. Swantje Boeschen, Brit Kockisch and Helga Heilmann are acknowledged for laboratory assistance. We also thank Christine Zühlsdorff, Dave Heslop, Ulrike Proske and Helge Meggers for useful comments on an early version of the manuscript. This work was funded funded through DFG-Research Center / Excellence Cluster „The Ocean in the Earth System“. This is MARUM publication no. ####.

5 Manuscript #2

Sediment transport and turbidite architecture in the submarine Dakar Canyon off NW-Africa

Roberto Pierau[*], Rüdiger Henrich[*], Inga Preiß-Daimler[*], Sebastian Krastel[+], and Jacob Geersen[*]

[*] MARUM - Center for Marine Environmental Sciences and Faculty of Geosciences, University of Bremen, Klagenfurter Straße, 28359 Bremen, Germany

[+] IFM-Geomar, Leibinz Institute of Marine Science, Wischhofstr. 1 - 3, 24148 Kiel, Germany

submitted to *Marine and Petroleum Geology*

Abstract

The submarine Dakar Canyon is located at the passive continental margin off NW-Africa and act as an effective pathway for gravity-driven sediment transport. Four gravity cores directly recovered from the canyon axis were investigated in order to reconstruct the sedimentation processes in the Dakar Canyon during the Late Quaternary. In addition, the hemipelagic sediments of a gravity core from the northern levee of the Dakar Canyon provide the variations of dust input. Coarse terrigenous silt size data and high Ti/Ca ratios reflect overall increased higher dust supply during the last two peak glacials resulting in the formation of extensive sand sea covering the exposed shelf. The interglacials were characterised by less intensive wind stress. Two major periods of turbidite deposition are recorded between 141 to 131 kyr BP and from 23.2 to 14.2 kyr BP due to the remobilisation of dune material by eustatic sea level rise. These turbidite deposits consist of sandy to silty sediments. Detailed grain size analyses were used to reconstruct the sedimentary characteristics and flow processes of these turbidity currents. With increasing distance to the source area a downslope sorting trend in the grain size distribution towards finer grain sizes were observed. A much higher frequency in turbidite activity occurred around 135 kyr BP in contrast to the second interval around 18 kyr BP, suggested a higher

sediment budget in the source area. The correlation of turbidites is based on their stratigraphic position. However, a single turbidite can exactly be dated at all core location in the thalweg. Hence, this turbidite was used to estimate its volume of 9.9 x 10^6 m^3 in the investigated area of the canyon. Based on the sedimentological investigation of the turbidites we provide a schematic model for the sedimentation processes in the Dakar Canyon.

Keywords: submarine Dakar Canyon, sedimentation processes, turbidity currents, NW-Africa

1. Introduction

1.1 General aspects of mass wasting systems along the NW-African margin

The passive Northwest African continental margin is strongly influenced by large-scale mass wasting processes (Jacobi, 1976; Weaver et al., 2000; Wynn et al., 2000; Antobreh and Krastel, 2006; Krastel et al., 2006; Talling et al., 2007). Numerous submarine canyons incise the continental margin of Northwest and West Africa (Dietz et al., 1968; Dietz and Knebel, 1971; Jacobi and Hayes, 1982; Wissmann, 1982; Weaver et al., 2000; Krastel et al., 2004). These canyons are major pathways for significant volumes of gravity-driven sediment transport from shallow-marine environments into the deep sea (Dietz et al., 1968; Wynn et al., 2000; Babonneau et al., 2002; Antobreh and Krastel, 2006; Zühlsdorff et al., 2007b). The shelf act thereby as temporary sediment storage and bypass area. Several processes, such as earthquakes, sea level changes, and rapid sediment loading might cause sediment instabilities and are necessary to trigger turbidity currents. Submarine canyons are important repositories and conduits for terrestrial derived clastic sediments in deep marine environments and play a major role as hydrocarbon reservoirs (Emery and Myers, 1996; Weimer and Slatt, 1999; Stow and Mayall, 2000). Therefore, outcrops of fossil submarine canyon systems were studied to reconstruct reservoirs and provide essential inputs for 3D geological models that were used for further predictions of the reservoir behaviour (Eschard et al., 2003; Satur et al., 2005). Modern canyon systems can be used as analogues for ancient deep-water clastic systems, and therefore detailed investigations of modern systems provide valuable information about structure, architecture and

evolutionary trends in sedimentary regimes in canyon systems. The aim of this study is to reconstruct the sedimentological characteristics of turbidite deposits in the submarine Dakar Canyon off Senegal. We present a detailed reconstruction of the sedimentation processes in the Dakar Canyon based on sediment echosounder data and gravity cores, directly recovered from the canyon thalweg. In addition, the climatic conditions were investigated on a sediment sequence recovered at the northern levee using chronological, sedimentological, geochemical and mineralogical methods.

1.2 Oceanographic and sedimentary regimes of NW-Africa

The south-westward flowing Canary Current is the major surface current along NW-Africa (Mittelstaedt, 1991) and the surface currents south of 20°N are dominate by the Guinea Dome (Stramma et al., 2005). During boreal winter a southward directed surface current (African Coastal Current, Fig. 1) flows along the coast of Mauritania and Senegal (Stramma and Schott, 1999). Instead, during summer the study area is influenced by the northward flowing Mauritania Current (Fig. 1). The migration of the Intertropical Convergence Zone (ITCZ) is the most important atmospheric feature over Northwest Africa (Nicholson, 2000). During boreal summer the ITCZ shifts northward and NW-Africa is influenced by the humid SW monsoon flow south of the ITCZ. During winter when the ITCZ migrates southward, the NE trade winds dominate the study area.

The trade winds and the overlying Saharan Air Layer (SAL) are the prevailing wind systems of NW Africa and are responsible for transport of dust across the Northwest African continent to the Atlantic Ocean (Sarnthein et al., 1982; Swap et al., 1996). Large dust plumes play a major role in terrigenous sediment supply along the Northwest African continental margin (Koopmann, 1981; Holz et al., 2004; Stuut et al., 2005). Fluvial supply in the study area is restricted to a few small rivers draining onto the shelf. Therefore, surface sediments of the Senegalese Shelf are dominated by aeolian derived quartz sands (Debenay and Redois, 1997). These sands were generally wind-derived and originated from paleo-dunes ("Ogolian erg") whose remnants are still preserved on the shelf south of Cape Verde (Barusseau et al., 1988). These paleo-dunes formed during the last glacial maximum (LGM), when active desert dunes migrated seaward over the exposed shelves in response to overall increased wind strengths (Matthewson et al., 1995; Rognon and Coudé-Gaussen, 1996; Martinez et al., 1999). The Senegalese shelf varies in width between 20 - 100 km in order with the geographical position (Debenay and Redois, 1997; Hagen, 2001).

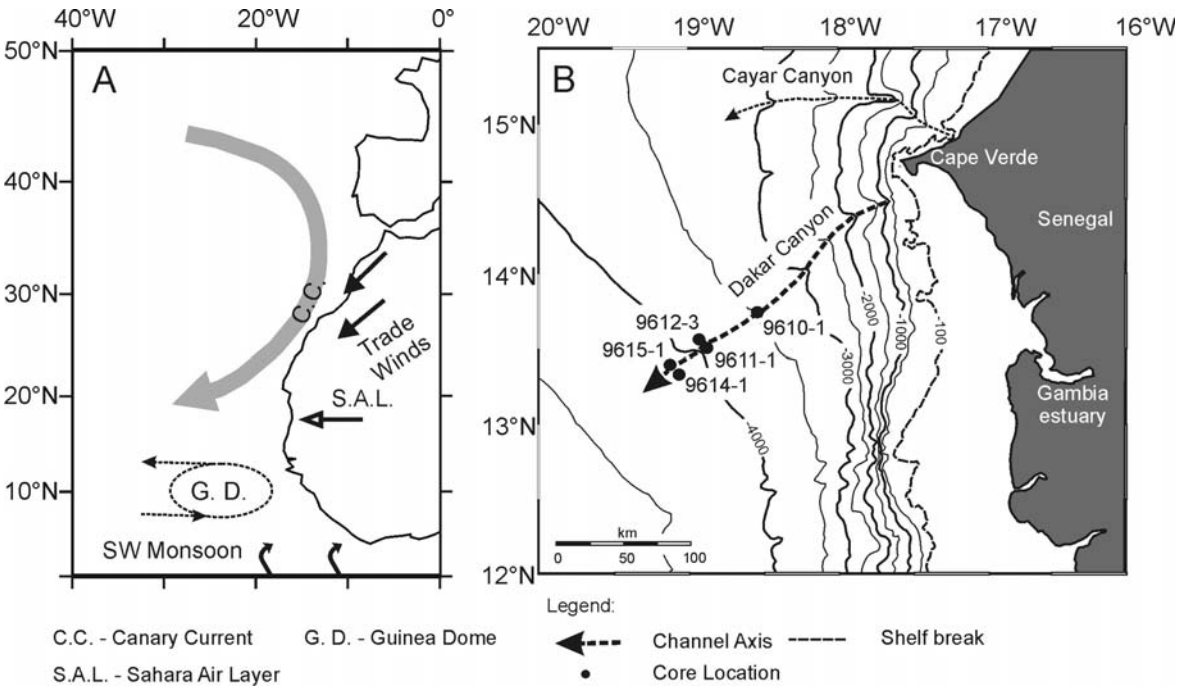

Figure 1: A) Overview map of NW-Africa with the most important oceanographic and climatic features. B) Detailed map of the study area showing the Dakar Canyon, the core locations and prominent geographic features.

The mean depth of the shelf break south of 15°N is located in water depths of 100 - 150 m associated with a continental slope with typical slope angles from 1° - 6° (McMaster and Lachance, 1969; Wynn et al., 2000).

The Northwest African continental margin is strongly affected by gravity-driven sedimentation processes (Weaver et al., 2000). Well known large debris flows and slide complexes are the Saharan Debris Flow, the Mauritania Slide Complex and the recently discovered Dakar Slide in the study area (Masson et al., 1996; Krastel and cruise participants, 2006; Antobreh and Krastel, 2007; Henrich et al., 2008). Theses mass wasting features transport significant volumes of sediment over long distances from the shelf into deep sea basins (Talling et al., 2007). In addition, numerous canyons along the passive northeast Atlantic continental margin are associated with turbidite activity like the Agadir Canyon, Cape Timiris Canyon, Cayar Canyon as well as some canyon systems south of the study area (Dietz et al., 1968; Dietz and Knebel, 1971; Babonneau et al., 2002; Wynn et al., 2002; Antobreh and Krastel, 2006; Zühlsdorff et al., 2007b). The principal controlling factors of the sedimentation processes of NW-Africa are the relief and climate of the hinterland, the width of the shelf, the inclination of continental slope, upwelling and sea level changes (Seibold and Fütterer, 1982).

1.3 The Dakar Canyon

The Dakar Canyon incises the continental slope of Senegal slightly south of Cap Verde, near the city off Dakar (Fig. 1). During the RV "Meteor" cruise M65/2 in 2005 the canyon was investigated by a combination of seismic and hydroacoustic as well as sedimentological and geochemical approaches (Krastel and cruise participants, 2006). The canyon was mapped for a length of about 200 km along the canyons thalweg from the upper slope at a water depth of 1300 m to water depths of 4100 m where the canyon runs out into the deep-sea basin (Fig. 2a).

The most proximal part of the canyon could not be mapped, due to the proximity of the harbour of Dakar. A tributary system of smaller gullies is depicted in the hydroacoustic profile at the most proximal profile to the coast (Fig. 2b). At this position the canyon is incised into the sediments up to 700 m and the width of the main canyon is ca. 10 km. The canyon is almost straight and runs in a NW-SE direction. The Dakar Canyon is typically V-shaped it the proximal sector and changed into a more U-shape pattern at the distal part (Fig 2b). Typical canyon structures such as steep sidewalls and terraces are imaged in the hydroacoustic profiles crossing the canyon (Fig. 2c). The incision depths decrease basinwards to less than 20 m at the continental rise at 4100 m water depth. The canyon bottom is filled with coarse material, illustrated by irregular high amplitude reflectors on the hydroacoustic profiles (Fig. 2c). At the most distal part, the canyon splits into a main channel and a southern, parallel running channel remnant.

2. Material and methods

The bathymetry and architecture of the Dakar Canyon were mapped using a Hydrosweep bathymetric multibeam system and a narrow beam PARASOUND sediment echosounder providing morphological and seismic facies information (Krastel and cruise participants, 2006). This study focuses on gravity cores recovered from the canyon thalweg (GeoB 9610-1, GeoB 9611-1, GeoB 9614-1 and GeoB 9615-1) and the associated northern levee (GeoB 9612-3, Tab. 1). Cores 9610-1 and 9611-1 yields information on the sedimentation processes at the "middle" part of the canyon thalweg in water depths between 3270 m and 3980 m, while cores GeoB 9614-1 and GeoB 9615-1, display the discharge towards the deep-sea basin (Fig. 2a).

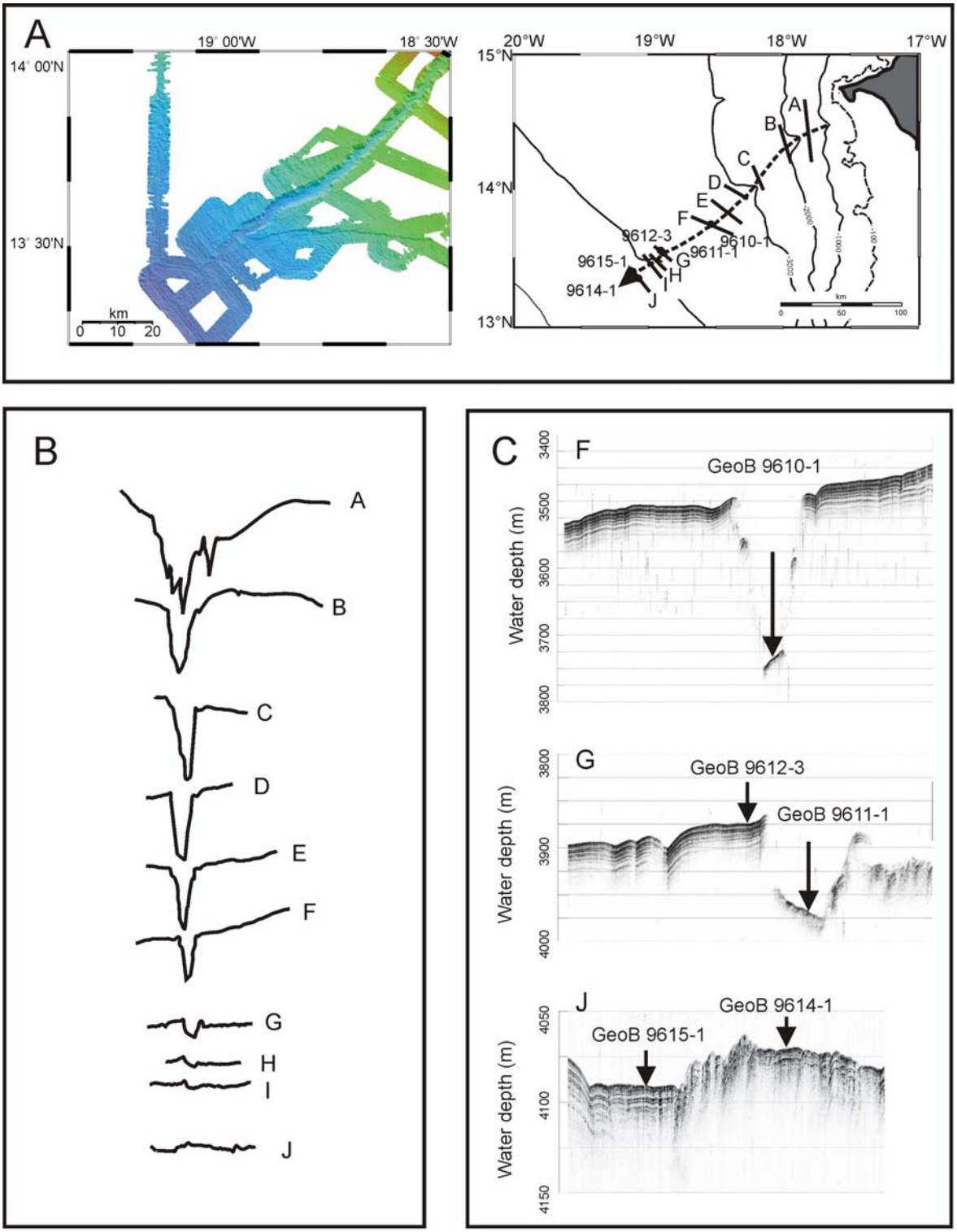

Figure 2: A) Bathymetric multibeam map of the investigated area of the Dakar Canyon plotted from Hydrosweep data. The positions of the Parasound profiles and the core locations are shown in the overview map. B) Cross-sectional bathymetric profiles perpendicular to the canyon axis, generated from bathymetric data. C) Parasound profiles including core locations. Typical morphologic elements like steep sidewalls and terraces can be observed in the cross profiles.

Table 1: Latitude, longitude, water depths and position of the analysed cores.

core number	latitude	longitude	water depth (m)	Area	core length (m)
GeoB 9610-1	13°45.27'N	18°32.75'W	3268	canyon axis	2.54
GeoB 9611-1	13°32.30'N	18°52.60'W	3983	canyon axis	1.47
GeoB 9612-3	13°33.01'N	18°53.50'W	3893	levee	8.78
GeoB 9614-1	13°20.54'N	19°03.56'W	4090	canyon axis	4.78
GeoB 9615-1	13°23.68'N	19°06.27'W	4180	canyon axis	9.30

Additionally, core GeoB 9612-3 was taken from the northern levee and provides the age model (Pierau et al., in review-a) . The joint sedimentary record of all cores allows us to reconstruct the sedimentation processes throughout the canyon. Detailed analyses of the turbidite sequences were determined using X-ray radiographies. Therefore, 1cm thick sediments slide were made to improve the visual core description.

Based on the core description all turbidites in Cores 9610-1, 9611-1, 9614-1 and 9615-1 were sampled in 1 cm resolution to reconstruct the grain size distribution (GSD) in the turbidites. All samples were freeze-dried and the sand fraction (> 63 μm) was separated from the fine fraction by wet sieving. The fine fraction (<63 μm) was subdivided into silt (63 - 2 μm) and clay (<2 μm) by repeated settling in Atterberg tubes according to settling velocities based on Stokes' law. Each separated fraction was dried and weight percentages (wt%) was determined.

Core GeoB 9612-3 was select for detailed grain size analyses of the terrigenous silt fraction of the hemipelagic background sediments using the Micromeritics SediGraph 5100. The Sedigraph 5100 measures accurately in the range of 100 - 2 μm and therefore the clay fraction has to be removed due to the cohesive behaviour and aggregate formation (Stein, 1985). Silt size distributions are expressed as equivalent spherical diameter according to settling velocities based on Stokes' law. The hemipelagic sediments were sampled in a 10 cm resolution. After freeze-drying and wet sieving, the organic matter and carbonate content were removed from the fine fraction (>63 μm) using 10% H_2O_2 respective 10% HCl to extract the terrigenous content of the hemipelagic sediments. Subsequently the silt fraction was separated from the clay fraction using the Atterberg settling method. Two data processing steps have been applied to the SediGraph cumulative raw data. The data were interpolated at 0.1 φ increments by using a linear interpolation and the interpolated cumulative data has been normalised by subtracting minima and dividing by resulting cumulative maxima. Afterwards the grain size distributions were calculated in

the range from 4 - 9 φ (62,5 - 1,95 µm). The opal content in marine sediments of NW-Africa is negligible (Koopmann, 1981; Holz et al., 2007; Zühlsdorff et al., 2007b). Hence we refer to terrigenous silt as carbonate and organic matter free silt.

2.1 Age model and core correlation

The age model of Core GeoB 9612-3 and the correlation of GeoB 9614-1 and GeoB 9615-1 are presented in Pierau et al.(in review-a) . The turbidite sections were subtracted from the cores to receive a continuous hemipelagic sediment record (Fig. 3). Ages of turbidites are considered to be equivalent to the age derived for the onset of hemipelagic sedimentation on the top of the relevant turbidite. The age model of GeoB 9610-1 and GeoB 9611-1 is based on 7 accelerator mass spectrometry (AMS) radiocarbon dates (Tab. 2).

Carbonate hydrolysis and CO_2 reduction was carried out at Bremen University and all AMS dating was done at the Leibniz Laboratory for Radiocarbon Dating and Isotope Research in Kiel. A conservative reservoir age of 400 yrs is assumed for radiocarbon age calibration due to seasonal upwelling. The radiocarbon ages up to 24 kyr BP were corrected and calibrated into calendar years using CALIB REV5.0.1 (Stuiver et al., 1998). Older radiocarbon ages were subsequently converted into calendar years using the calibration function of Bard et al. (1998). All calibrated ages are given in calibrated thousands of years before present (kyr BP).

Table 2: AMS radiocarbon dates of the investigated cores including sampled horizon, Laboratory ID, analysed material and age calibration. Data marked with (*) are presented in Pierau et al. (in review-a).

Core number	Core depth (m)	Lab ID	Analyses material	Conventional age (yrs)	Calibration two sigma range (cal yr BP)	Calib. age (kyr BP)
GeoB 9610-1	0.82	KIA30501	G. sacculifer, G. ruber	12770	14050 - 14820	14.4
GeoB 9610-1	2.44	KIA30499	bulk carbonate	14060	15830 - 16720	16.3
GeoB 9611-1	0.30	KIA30513	G. ruber, G. sacculifer	10080	10870 - 11210	11.0
GeoB 9611-1	0.56	KIA30502	G. ruber, G. sacculifer	12640	13850 - 14580	14.2
GeoB 9611-1	0.70	KIA30512	bulk carbonate	13600	15250 - 16030	15.6
GeoB 9611-1	0.83	KIA30511	bulk carbonate	13870	15590 - 16460	16.0
GeoB 9611-1	1.27	KIA30508	bulk carbonate	15210	17560 - 18540	18.0
GeoB 9612-3*	0.55	KIA30490	G. sacculifer, G. ruber, G. bulloides	12650	13860 - 14610	14.1
GeoB 9612-3*	0.68	KIA30506	G. sacculifer, G. ruber, G. bulloides	13380	15030 - 15690	15.3
GeoB 9612-3*	1.11	KIA30488	G. sacculifer, G. ruber, G. bulloides	18400	20810 - 21910	21.3
GeoB 9612-3*	1.33	KIA30487	G. sacculifer, G. ruber, G. bulloides	29530		34.5
GeoB 9614-1	0.48	KIA30507	G. ruber	12930	14240 - 15010	14.6
GeoB 9614-1	0.67	KIA30505	G. ruber	18780	21320 - 22260	21.8
GeoB 9614-1	1.34	KIA30504	G. ruber	30390		35.4
GeoB 9615-1	0.30	KIA30492	G. ruber	10630	11830 - 12080	11.9
GeoB 9615-1	0.59	KIA30491	G. sacculifer, G. ruber, G. bulloides	13230	14890 - 15480	15.2
GeoB 9615-1	1.05	KIA30509	bulk carbonate	13730	15410 - 16240	15.8

3. Results

3.1 Age determination

The determination of the basal ages of Cores 9612-3, 9614-1 and 9615-1 is based on the correlation by their characteristic total reflectance pattern (Pierau et al., in review-a). The sedimentary records of Core 9612-3 has a basal age of 240 kyr BP, Core 9615-1 of 222 kyr BP and Core 9614-1 spans an interval of 120 kyr BP (Fig. 3). The calibrated AMS radiocarbon dates provide the ages of Core 9610-1 and 9611-1. Both cores cover the Marine Isotope Stages (MIS) 1 and 2. Concerning to the age determination, we are able to reconstruct the sediment dynamics in Dakar Canyon in detail for MIS 1 and 2 and in less detail up to MIS 7 due to the lack of data for this period (Fig. 3).

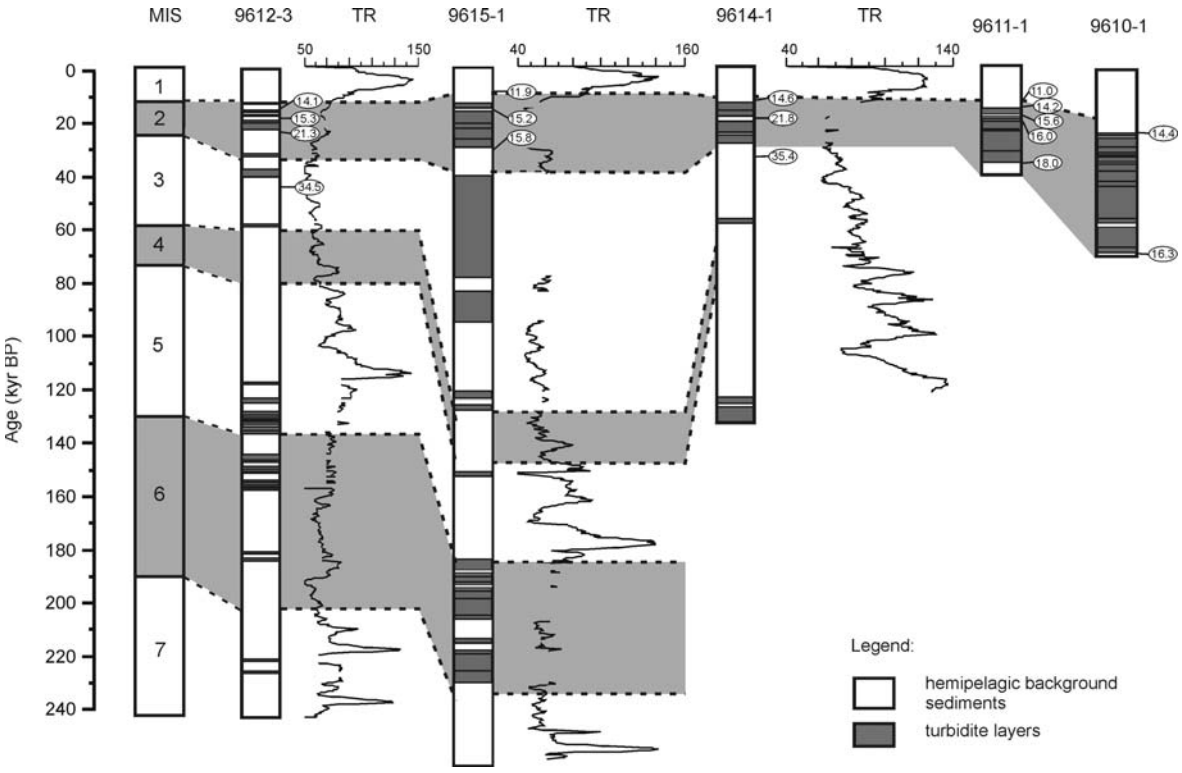

Figure 3: Correlation of the analysed cores by the total reflectance (TR) pattern. The encircled numbers are calibrated radiocarbon ages. The turbidites are highlighted by dark grey boxes.

The youngest turbidite in Cores 9610-1, 9611-1 and 9615-1 can be correlated from core-to-core by the AMS radiocarbon data of 14.2/14.3 kyr BP (Tab 3). The age of this turbidite marks the end of the turbidite activity in the canyons thalweg, whereas a younger turbidite is recorded in Core 9612-3 on the northern levee. Further correlation of other turbidites in

the canyon axis by the radiocarbon ages was not possible. It is important to recognize, that a correlation based on the age determination is just an approximation.

Table 3: Key characteristics of the analysed turbidites including depth of the turbidite bottom, thickness and relevant BOUMA units. All turbidites are numbered from top to base of the core.

	GeoB 9610-1		**GeoB 9611-1**		**GeoB 9612-3**		**GeoB 9614-1**		**GeoB 9615-1**	
Turbidite Nr.	Core depth (m)	age (kyr BP)	Core depth (m)	age (kyr BP)	Core depth (m)	age (kyr BP)	Core depth (m)	age (kyr BP)	Core depth (m)	age (kyr BP)
1	0.84	14.2	0.56	14.2	0.46	12.3	0.49	14.7	0.47	14.3
2	0.91	?	0.65	15.6	0.54	13.9	0.57	18.2	0.59	15.2
3	1.03	?	0.73	16.0	0.64	14.6	0.71	22.4	0.73	?
4	1.13	?	0.76	?	0.68	14.8	0.89	23.2	0.79	?
5	1.15	?	0.83	?	0.71	14.9	2.03	48.8	0.87	?
6	1.23	?	1.10	?	1.14	22.1	4.33	122.4	0.93	15.5
7	1.33	?			1.34	29.3	4.43	123.8	0.96	15.8
8	1.49	?			2.07	57.2			1.43	24.2
9	1.54	?			4.19	123.5			2.99	28.5
10	2.00	?			4.38	126.6			4.33	57.2
11	2.07	?			4.41	?			4.50	60.2
12	2.38	?			4.58	128.2			5.39	82.9
13					4.61	128.3			6.58	131.6
14					4.68	128.7			6.63	132.3
15					4.76	129.3			6.73	136.5
16					4.82	129.6			6.79	137.2
17					5.10	132.9			6.93	141.3
18					5.19	?			7.09	?
19					5.27	133.6			7.30	?
20					5.33	134.0			7.63	163.8
21					5.45	135.0			7.77	171.7
22					5.53	136.3			7.81	173.3
23					5.57	?			8.02	?
24					6.42	170.3				
25					6.52	173.7				
26					7.68	216.7				
27					8.02	219.7				

3.2 Grain size distribution and Ti/Ca ratio of the hemipelagic sediments

Core GeoB 9612-3 recovered at the northern levee (Fig. 2c) consists of olive-grey silty-muddy hemipelagic sediments with intercalated turbidite beds at distinct intervals (Krastel and cruise participants, 2006). This core provides the longest sedimentary record and was chosen to analyse the variations of the GSD in the hemipelagic background sediments. Within these hemipelagic sediments thin (cm-thick) turbidites are recorded at two distinct intervals around the major climate terminations (Fig. 3). According to the analyses of the X-ray radiographs, these turbidites shows no erosional features and are interpreted as spill-over turbidites (Pierau et al., in review-a).

The GSD of the bulk hemipelagic sediment of core GeoB 9612-3 is dominated by the silt and clay fraction (Fig. 4). The content of the sand fraction is generally low (maximum

30 wt%) and reflects the proportion of foraminifers. The bulk silt fraction varies from 26 to 90 wt% and shows the highest contents in two periods between 180 to 120 kyr BP and 40 to 15 kyr BP. Maxima in the clay content (up to 67 wt%) are recorded around 185, 150 kyr BP and between 100 to 70 kyr BP.

The downcore record of the terrigenous silt (wt%) and the detailed analyses of the terrigenous silt fraction of GeoB 9612-3 displays significant variations in grain size diameter throughout the record. The variations of grain size data of aeolian derived sediments allows estimations of the continental aridity and wind strength (Matthewson et al., 1995; Stuut et al., 2002).

In general, the terrigenous silt size distributions is dominated by a spectrum of coarse silt between 15 - 50 µm and minor amounts of the fine silt fraction (< 6 µm) are recorded (Fig. 4). The terrestrial silt size also shows strong variation between glacial and interglacial periods. A first prominent shift from finer to coarser silt sizes occurred from 230 to 220 kyr BP, when modal sizes increased from 20 to 40 µm and peak heights increased from 3 to 5 % (Fig. 4). Sporadic events of coarser silt sizes (40 - 20 µm) are recorded until 150 kyr BP interrupted by short periods of finer silt sizes. Between 150 to 120 kyr BP, a transition to overall coarser silt sizes of up to 50 µm occurs, which displays the coarsest terrigenous silt size distribution in the record.

Distinct finer silt sizes of 4 to 10 µm characterise the following MIS 5. During the MIS 4 and 3 also relative fine terrigenous silt sizes between 8 to 20 µm were deposited, which again were interrupted by short periods of coarser grain sizes (at around 70 and 40 kyr BP). A transition to a trend of increasing silt sizes is recorded at 28 kyr BP until 15 kyr BP, whereas finer grain sizes occurred during the MIS 1. Generally, a positive correlation between the terrigenous silt size and the Ti/Ca ratio of the hemipelagic background sediments can be registered (Fig. 4).

The XRF Ti intensity represents the input of dust, whereas the marine carbonate content is reflected by the XRF Ca intensity, therefore the Ti/Ca ratio is used as a proxy for the variability of the dust influx. The Ti/Ca ratio is characterised by abrupt changes during MIS 7 - 6 as well as during MIS 3 - 2. Lower values are recorded during the interglacial MIS 5 and 1 (Fig. 4). Significant and long range peak values are recorded between 150 - 125 kyr BP and 28 - 15 kyr BP.

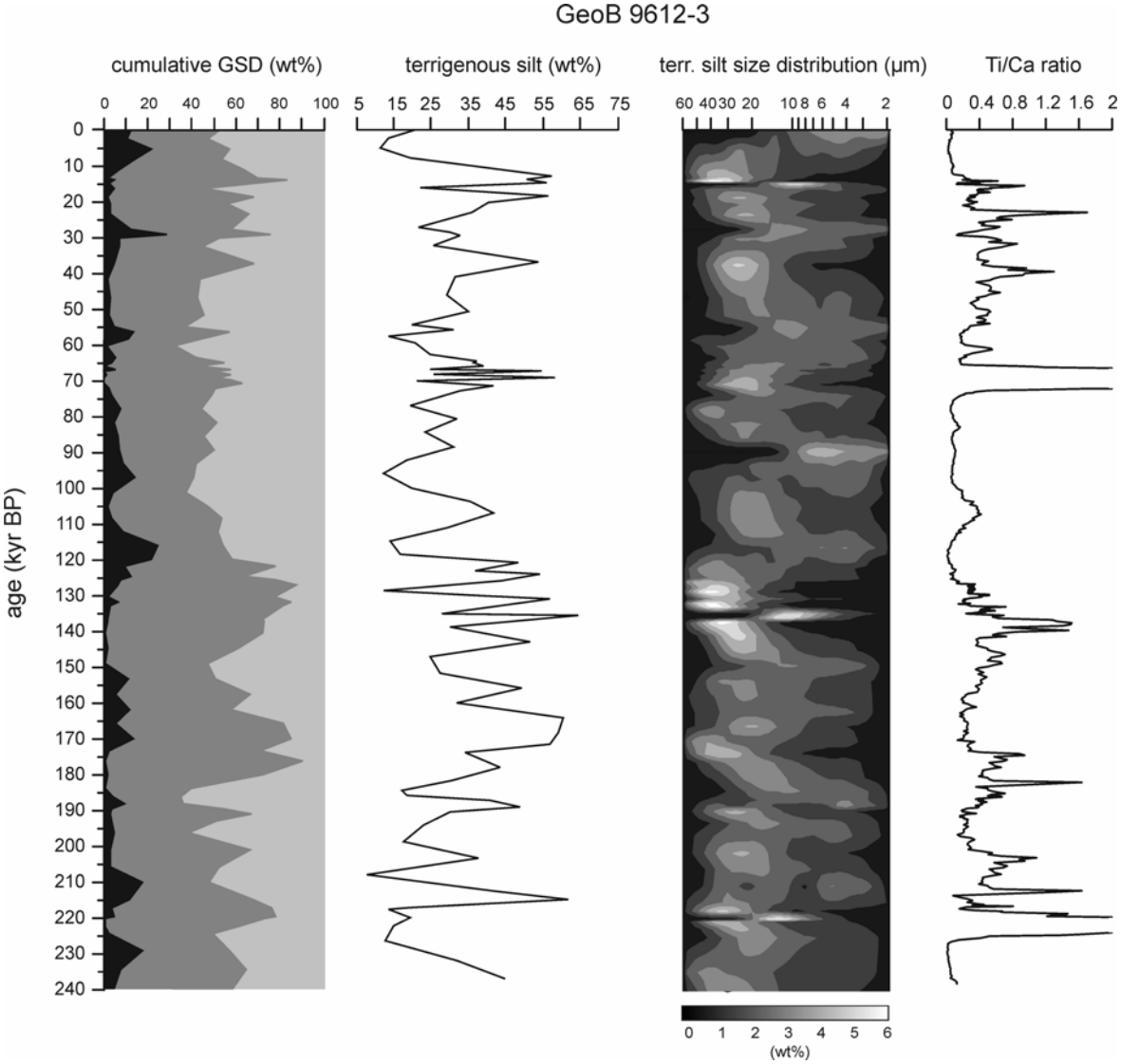

Figure 4: Cumulative grain size distribution (GSD) with sand, silt and clay from left to right, terrigenous silt (wt%) and detailed analysis of the terrigenous silt size distribution (wt%) and Ti/Ca ratio of the hemipelagic background sediments of Core 9612-3 recovered at the northern levee of the Dakar Canyon. Please note, that the turbidites are cut out of the record.

3.3 Turbidite sequences in the Dakar Canyon

Based on the analyses of the X-ray radiographs, turbidite depositions can be clearly distinguished from the hemipelagic background sediments and the internal structure are visible. The coarse grained units T_A - T_B of the BOUMA - sequence (Bouma, 1962) are often lacking and only the finer uppermost intervals (T_C - T_D) are developed (Tab. 4). All analysed turbidites are characterised by greyish brown to light olive brown material and shows typical finning-upward units. Most of the turbidites are several cm thick sandy to silty turbidites (Tab. 4).

Table 4: Turbidite numbers and age determination of investigated cores. Columns marked by (?) consist of turbidites without age determination due to the direct covering of individual turbidites.

GeoB 9610-1			GeoB 9611-1			GeoB 9614-1			GeoB 9615-1		
core depth (m)	thickness (cm)	Bouma Unit	core depth (m)	thickness (cm)	Bouma Unit	Core depth (m)	thickness (cm)	Bouma Unit	Core depth (m)	thickness (cm)	Bouma Unit
0.84	3	T_D	0.56	8	T_C - T_E	0.49	7	T_C - T_E	0.47	6	T_B - T_C
0.91	12	T_C - T_D	0.65	4	T_C - T_D	0.57	9	T_C	0.59	14	T_B - T_E
1.03	9	T_C - T_E	0.73	3	TC	0.71	15	T_A - T_B	0.73	6	T_B - T_C
1.13	2	T_D	0.76	6	T_C - T_D	0.89	13	T_B - T_E	0.79	8	T_C - T_D
1.15	6	T_D - T_E	0.83	27	T_C - T_E	2.03	3	T_C	0.87	5	T_C - T_E
1.23	10	T_C - T_E	1.10	14	T_B - T_E	4.33	8	T_C	0.93	2	T_C
1.33	16	T_C - T_E				4.43	20	T_B - T_E	0.96	9	T_C
1.49	5	T_D - T_E							1.43	135	T_A - T_C
1.54	45	T_A - T_E							2.99	38	T_B - T_C
2.00	4	T_D							4.33	6	T_C - T_E
2.07	30	T_A - T_E							4.50	5	?
2.38	4	T_C - T_D							5.39	4	?
									6.58	4	T_D
									6.63	4	T_D
									6.73	5	T_C - T_D
									6.79	8	T_C - T_D
									6.93	16	T_A - T_C
									7.09	21	T_C - T_E
									7.30	5	?
									7.63	3	?
									7.77	3	?
									7.81	21	T_B - T_C
									8.02	16	T_B - T_E

The turbidite displays significant differences in the investigated cores. Cores 9610-1 and 9611-1, recovered in the canyon axis, show stacked and frequent turbidite emplacements. Core 9610-1 contains 12 turbidites (Tab. 4) with relative thick turbidite beds of 30 cm and 40 cm at the base (Fig. 5). The turbidite sequences of this core were deposited between 16.3 and 14.3 kyr BP. The GSD of the turbidites in core GeoB 9610-1 can be divided into two groups. The basal turbidites are dominated by a high contents of coarse to medium sand (1 mm - 250 µm) up to 80 wt%, resulting in a high sand/mud ratio (Fig. 5). The GSD of the upper 8 turbidites are characterised by silty material and higher clay contents. The dominance of fine material in these turbidites is also reflected in a very low sand/mud ratio. A very high sand/mud ratio is found at the base of core GeoB 9611-1 (Fig. 5), reflecting a high amount of coarse sand. This core includes 6 turbidites with a sequence of relative thick turbidites (14 cm, 27 cm) at the base of the core. The time of deposition correspond to core 9610-1 from 18 to 14.2 kyr BP. The sand fraction dominates the turbidites beds at the bottom of Core 9611-1 (up to 80 wt%). Increasing contents of fine material is recorded in the uppermost 5 turbidites. T4 and the upper interval of T1 were not analysed due to missing samples.

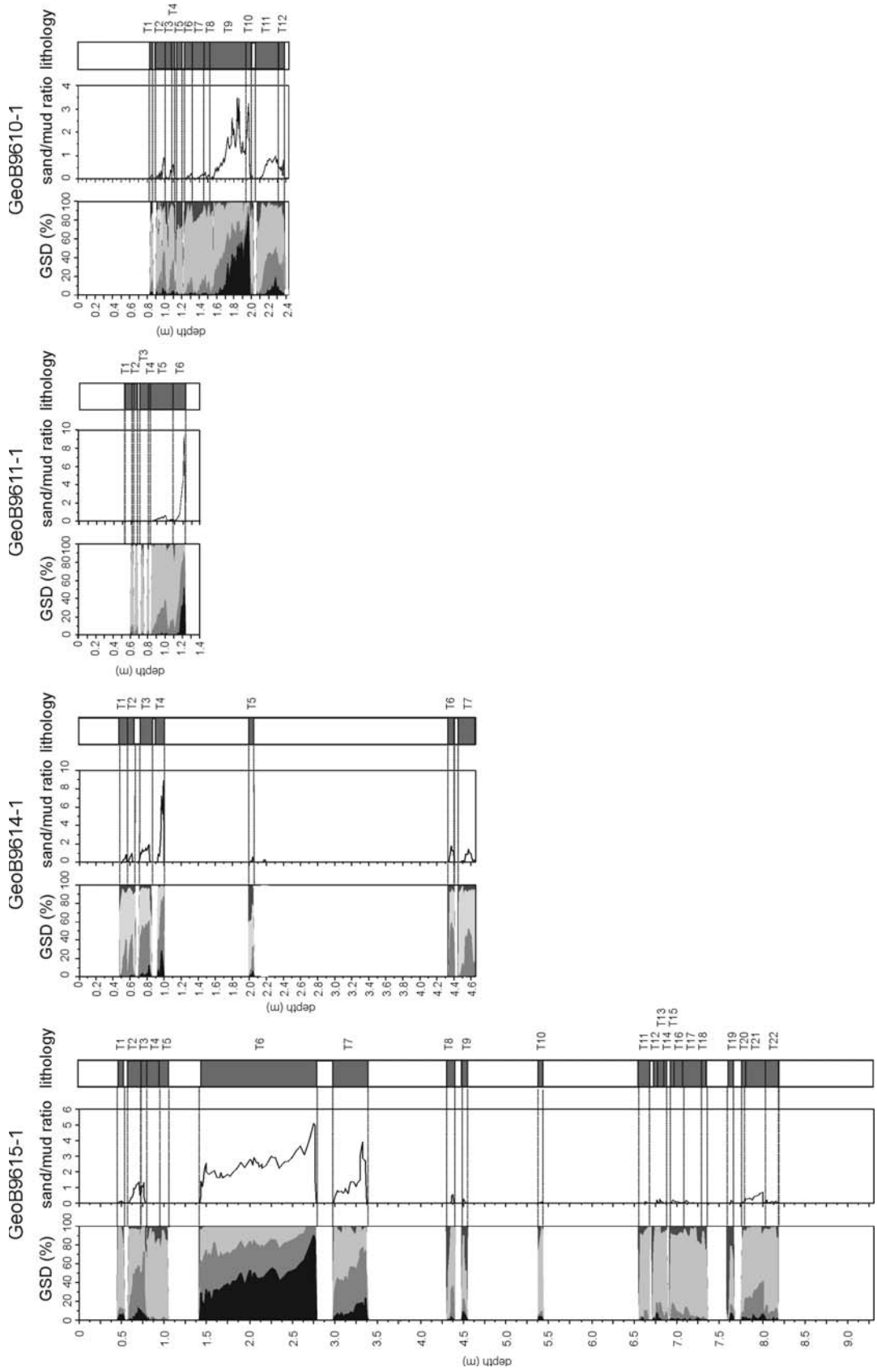

Figure 5: Cumulative grain size distribution (GSD) with coarse to medium sand (1mm - 250 µm), fine sand (250 - 63 µm), silt and clay from left to right, sand/mud ratio and numbered turbidites of the cores in the Dakar Canyon.

In contrast core GeoB 9614-1, retrieved in the southern channel remnant at the distal part of the Dakar Canyon, consists mainly of hemipelagic sediments with intercalated turbidites at two main intervals (Fig. 5). Two turbidites were recorded at the base of the core with ages around 122 kyr BP. Furthermore, a turbidite was deposited at 48 kyr BP. The interval with the highest activity in this core is recorded between 23 - 14 kyr BP. The two turbidites (T7 & T6) at the base of the core are characterised by relative high fine sand contents (50 - 60 wt%). The thin T5 (3 cm) consists mainly of silty material. The highest sand/mud ration in Core 9614-1 is recorded in T4. The overlying turbidites again consist of fine sandy, silty material (Fig. 5).

A high turbidite occurrence with 22 individual events is found in core GeoB 9615-1 located in the distal part of the main canyon axis (Fig. 5). Most turbidites occurred in two main episodes of turbidite deposition between 142 and 131 kyr BP and from 15.8 to 14.3 kyr BP and coincide with the major climate terminations. Some events occurred during MIS 6 and 3. The turbidites deposited during Termination II mainly consists of silty material and minor fine sand contents. The GSD of the thin turbidites deposited during MIS 6 and 3 are also dominated by the silt fraction. Instead, T7 is dominated by high coarse to medium sand contents. Turbidite T6 in Core 9615-1 is the thickest event (135 cm) identified in the Dakar Canyon and consists of high amounts of sand. Furthermore, this turbidite shows a clear fining-upward trend, but a fine grained top section is not found. The second episode of frequent turbidite activity is recorded between 16 and 14 kyr BP. Turbidites T5 and T4 are deposited at the beginning of this time interval and were characterised by high amounts of silt and the absence of the sand fraction. The uppermost 3 turbidites again consists of higher sand contents (Fig. 5).

4. Discussion

4.1 Dust input and sediment flux

The combination of terrigenous silt size data and XRF core scanning data of Core 9612-3 is used to reconstruct the variability of dust input from the continent and the resulting effects on the sediment supply. Wind intensities and climate conditions off the NW-African continent, which are responsible for dust supply to the ocean, changed significantly during these time span (deMenocal et al., 1993; Matthewson et al., 1995).

The composition of aeolian derived terrigenous silt in deep-sea sediments depends on the distance to the source area, the intensity of the transporting winds and climatic variations in the hinterland (Rea, 1994). Various studies of deep-sea cores and seabed sediments along the NW-African continental margin demonstrate that terrigenous sediments with modal grain sizes > 6 µm are attributed to aeolian dust plumes, whereas finer particles were transported by fluvial input (Koopmann, 1981; Holz et al., 2004; Stuut et al., 2005). Generally, the Ti/Ca ratio reflects the input of siliciclastic components (Arz et al., 1998). Fluvial discharge is of subordinate importance along the NW-African continental margin up to the mouth of the Senegal river (Holz et al., 2004). South of Cape Verde some smaller rivers drain onto the shelf and riverine input becomes more important south of the Gambia estuary. Resuspension of fluvial material from the broad shelf south of Cape Verde and offshore transport can not be excluded and probably explain the relative high clay contents around 185, 150 kyr BP and between 100 - 70 kyr BP (Fig. 4). Detailed information about the circulations patterns of surface currents at the shelf south of Cape Verde are unknown. Therefore, we use the Ti/Ca ratio of Core 9612-3 as a proxy for dust input (Pierau et al., in review-a). Prominent peaks of the Ti/Ca ratio often correspond with coarser terrigenous silt sizes (Fig. 6). However, the low sample resolution of the silt size record does not allow a suitable correlation to the high resolution of the Ti/Ca ratio. Nevertheless, both proxies display comparable trends.

An increasing trend in the terrigenous silt size distribution as well as higher Ti/Ca ratios are recorded around the major climate terminations (Fig. 6). These significant shifts are attributed to a stronger wind regime (Matthewson et al., 1995). In general, the input of aeolian dust increases during arid glacials (Sarnthein et al., 1981; Moreno et al., 2001; Stuut et al., 2002). This is also recorded in maxima of the terrigenous silt sizes and high Ti/Ca ratios in Core 9612-3 around 140 kyr BP and 18 kyr BP, reflecting the last two peak glacials (Fig. 6). During these peak glacials, climate-induced dust supply was responsible for the formation of large dune fields at the exposed shelf along NW-Africa (Sarnthein and Diester-Haass, 1977; Sarnthein, 1978; Lancaster et al., 2002). These dune fields migrated onto the exposed Senegalese shelf towards the coastline and were subsequently remobilised during the eustatic sea level rise and deposited in the Dakar Canyon (Barusseau et al., 1988).

The interglacials (MIS 5 and 1) are characterised by finer terrigenous silt sizes and low Ti/Ca ratios (Fig. 6). This indicates the onset of humid climate conditions in the hinterland and a less intensive wind regime both resulting in a reduced dust influx (Sarnthein et al.,

1981; deMenocal et al., 2000a). The strengthening of the monsoon resulting in a greater moisture flux from the ocean to the African continent (Sarnthein et al., 1981; Gasse and Van Campo, 1994).

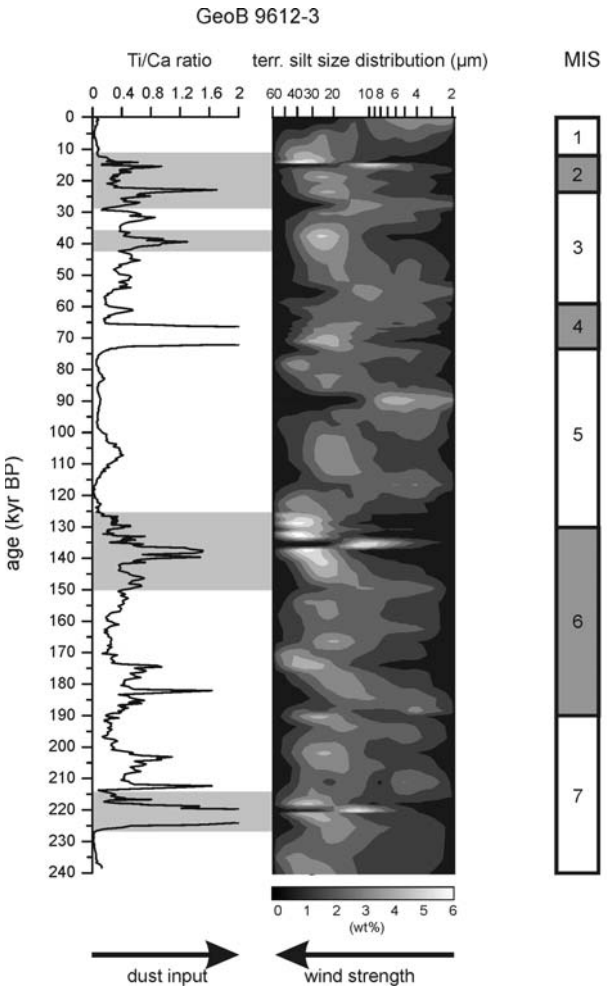

Figure 6: Reconstruction of the Late Quaternary climatic and environmental conditions of NW-Africa. Ti/Ca ratio is used as a proxy for general dust input and terrigenous silt size data represent variations of the wind strengths. The shaded area indicates prominent peaks of the Ti/Ca ratio which corresponds with coarser terrigenous silt sizes.

The humid climate conditions between 11 - 5 kyr BP were responsible for dune stabilisation throughout the Sahara (Kocurek et al., 1991; Swezey, 2001). A reduced climate induced sediment supply and a relative high sea level prevents the deposition of turbidites in the Dakar Canyon during the interglacials (Pierau et al., in review-a). According to the Ti/Ca ratio short episodes of enhanced dust input probably forced by increasing wind stress occurred during MIS 7, 6 and 3 (Fig 6.). These short periods coincide with Heinrich time equivalents (Pierau et al., in review-a), but they do not coeval with significant higher mean silt sizes probably owed to the low sample resolution (Fig. 6). This wind driven sediment input and the slightly rising sea level triggered the deposition of turbidites during these periods. Hence we postulate that the sediment influx during MIS 7, 6 and 3 did not have a considerable influence on the turbidite deposition.

4.2 Turbidite sequences in the Dakar Canyon: sedimentological characteristics and source area

Two main intervals of turbidite deposition occur between 141 to 131 kyr BP and from 23.2 to 14.2 kyr BP which coeval with the last two major climate terminations. The turbidite activity in the canyon axis during Termination II around 135 kyr BP is recorded in Core 9615-1 and in Core 9614-1 (Fig. 3). The turbidite activity as recorded in Core 9615-1 started at 142 kyr BP and finished at 131.6 kyr BP. Time equivalent turbidites are also recorded during this period in Core 9612-3 recovered at the northern levee. In contrast, only two turbidites are identified in Core 9614-1 located at the southern channel remnant at 123.8 and 122.4 kyr BP. The sedimentary section of Core 9614-1 probably does not contain the entire interval of turbidite activity. Both events are distinct younger than the turbidites occurrence in Core 9615-1. Furthermore, the 123.8 kyr BP event can be correlated with a turbidite recorded during the same time at the northern levee in Core 9612-3. This observation can reflect a minor period of turbidite activity during that time span. The simultaneous occurrences of turbidites at the northern levee and in the southern channel remnant can suggest a deposition of turbidites in a secondary pathway at the distal part of the canyon.

A less frequent number of turbidites are recorded in Core 9615-1 during the second interval of turbidite activity between 15.7 to 14.3 kyr BP. Turbidite deposition in the southern canyon remnant (Core 9614-1) occurred from 23.2 to 14.7 kyr BP. Cores 9610-1 and 9611-1, recovered in the upper part of the canyon axis, were characterised by high frequent and stacked turbidite deposition between 16.3 to 14.1 kyr BP. During the peak glacial sea level lowstands around 140 and 18 kyr BP (Fairbanks, 1989; Siddall et al., 2003) the exposed shelf was covered by dune fields (Barusseau et al., 1988; Lancaster et al., 2002), which provides a considerable sediment source. These so called “aeolian-sand turbidites” (Sarnthein and Diester-Haass, 1977) might be generated by voluminous slides of sand wedges which were located at the coastline during this time.

The turbidites in the Dakar Canyon consists mainly of silty material with minor amounts of sand (Fig. 5). The source area of the turbidites is most likely located at the upper slope or outer shelf. In general, the coarsest grain size distribution in turbidites is recorded in the most proximal canyon core 9610-1, except for T8 & T7 in Core 9615-1. This observation implies a downslope sorting of grain sizes, whereas the coarsest material was deposited at the most proximal part of the investigated canyon area. We can not exclude that erosion by

turbidity currents in the thalweg reworked former deposited material. However, this erosion could only include minor sediment volumes, because there are no startigraphic gaps in the cores. All MIS are always represented in the sections (Fig. 3). With increasing distance to the sediment source area, a downstream sorting trend towards finer grain sizes can be observed. So we postulated that coarse material (e.g. coarse sand) is deposited in the thalweg and finer material like medium to fine sand is transported into the deep sea basin and probably build up typically sandy lobes. The occurrence of sand lobes was not observed and mapped during the cruise. These downslope evolution of the sedimentary characteristics of turbidite beds in the Dakar Canyon is consistent with physical and numerical models for transport and sorting of fine grained turbidity currents (Stow and Bowen, 1980; Salaheldin et al., 2000).

A general trend to finer grain sizes in the upper section in the progressively younger turbidite beds occurs during the interval of turbidite activity around the Termination I (Fig 5.). The turbidites deposited during the initial phase of the sea level rise are characterised by relative coarse beds, followed by a vertical pattern with decreasing GSD and bed thickness. Similar climate and environmental condition occurred during this period as proposed for the previous glacial maximum. The influx of climate induced dust and sand supply onto the exposed shelf during the glacial sea level lowstand, provides again the sediments in the source area. Dust can be uplifted by the prevailing wind system over the African continent and is transported as aerosol over large distances (Prospero, 1996), whereas sand is mostly been transported by sliding, rolling and saltating of grains at the bedrock (Kleinhans, 2004). The GSD indicates that the coarsest material was transported downslope during the initiation of the sea level rise. The sediment source of this coarse material should be located in front of the dune fields in the direct vicinity of the former coast line, which would indicate a second but minor sediment source. The sedimentary facies distribution of the present outer shelf is characterised by coarse grained sands with median particle size > 300 μm (Redois and Debenay, 1999). These sands are found to in water depths between 100 - 200 m at the present shelf break. This facies type may be regarded as potential sediment reservoir for the relative coarse grained turbidites. The feeder system at the canyon head may have therefore mobilised shelf sediments with different sedimentary compositions.

The following turbidites consists of finer material which would suggest finer sediments in the source area. These sediments should be originated from the dune fields. The surface layer of modern aeolian sand ergs around Cape Timiris, Mauritania, consists of moderately

well sorted medium sand (Kocurek et al., 1991). This grain size spectrum is significant finer than the coarse grain facies type found at the present outer shelf and it is reflected in the GSD of the upper turbidites (Fig. 5). The thickness of turbidites is effected by the GSD and the sediment source (Stow and Bowen, 1980; Satur et al., 2000). Therefore less voluminous turbidity currents might reflect a finer GSD as well as a lower sediment reservoir in the source area.

Two thick (dm-m scale) turbidites are recorded in Core 9615-1 (Fig. 5). Both events are characterised by a coarse bed and a fining-upward sequence with a missing very fine grained top. The thickness and the sedimentary composition is similar to aeolian sand turbidites, described by Sarnthein and Diester-Haass (1977). These deposits require high-energy and high-concentration flows and might be generated by voluminous slides of sand wedges. These turbidites were deposited at 28.5 and 24.2 kyr BP. The relative low sea level during MIS 3 and enhanced influx of aeolian sediments probably formed first dune fields on the exposed parts of the shelf. Sediment instabilities and the resulting aeolian sand turbidites might be initiated by further sea level lowering.

4.3 Variations of the sediment budgets in the source area

A significantly higher number of turbidites are recorded in Cores 9612-3 and 9615-1 during the previous peak glacial centred at 135 kyr BP in contrast to the second interval of main activity around 15 kyr BP (Fig. 3). If we assume, that all turbidity currents were originated at the exposed shelf and transported through the canyon, this observation would suggest varying sediment budgets in the source area during both intervals of turbidite activity. The remarkable frequent turbidite occurrences during the Termination II could indicate an enlarge sediment reservoir in the source area in contrast to Termination I. This assumption is underlined by the terrigenous silt size data of Core 9612-3. These data displays a significant increase and a long-term input of coarse silt between 150 - 125 kyr BP. Enhanced wind stress over this relative long period should result in the development of extensive sand seas at the exposed shelf. The relative short interval of enhanced wind stress during the LGM was probably not sufficient enough to transport comparable amounts of sediment onto the exposed shelf. These potential contrasts in the volume of sand seas during the last two glacial periods of NW-Africa probably corresponds to comparative contrasts in the overall size and expansion of the Northern Hemisphere Ice Sheets, which could be resulting in a much more efficient overall compression of global

atmospheric pattern and increase of wind speed during the previous glacial maximum compared to the LGM (Sarnthein et al., 1981; Clark et al., 1999). Turbidite beds of similar thickness were deposited in Core 9615-1 during both intervals of turbidite activity. A less frequent number of turbidites, however, is recorded in this core around 15 kyr BP. An equal sediment budget should result in similar frequencies and volumes of turbidite deposits during both intervals of main turbidite activity. The thickness of turbidites is effected by the grain size distribution and the sediment source (Stow and Bowen, 1980; Satur et al., 2000). Therefore less voluminous turbidity currents could reflect finer grain size composition as well as a lower sediment volume in the source area. Dietz et al (1968) descript the Cayar Canyon, originated north of Cape Verde (Fig. 1b), as effective sediment trap and pathway for gravity driven sediment transport. Any sediment transport from the north should be captured by the Cayar Canyon. Hence, the source area of the turbidites in the Dakar canyon is rather limited to the north and only small volumes of sediment can be reworked, resulting of the generally small scale turbidite deposits.

4.4 Turbidite correlation and estimations of turbidite volume

Generally turbidity currents should flow through the canyon and their deposits should be found in all investigated cores. A correlation of single turbidite beds in cores of the Dakar Canyon has been attempted by their relative stratigraphic position. Other suitable correlation tools like turbidite colour, component analyses of the sand fraction and magnetic susceptibility were ineffective. A different mineralogy would essentially have simplified the correlation of turbidites. Therefore, the remaining correlation tool was the relative stratigraphic position of the turbidites.

Two intervals of turbidite activity in the Dakar Canyon can be observed around 135 kyr and 15 kyr BP. The stacked turbidite sequences in Cores 9610-1 and 9611-1 prevent a detailed age determination and stratigraphic correlation and hence only the time interval can be detected. However, some depositional ages can be clearly distinguished. Turbidite T1 in Cores 9610-1, 9611-1 and 9615-1 can exactly be correlated by radiocarbon dating (14.3 kyr BP event) on top of this turbidite (Tab. 4). This event is used as an example for turbidite correlation along the thalweg. Further correlations of single turbidite beds by their depositional age are possible between Cores 9612-3, 9614-1 and 9615-1. The sedimentary composition of the relative thick turbidites at the bottom of Cores 9610-1 (T9, T11) and 9611-1 (T5, T6) allow only a tentative correlation. Furthermore, the correlation of T1 in

the three cores allows an estimation of the sediment volume deposited by this turbidite along the investigated sector. The calculation is based on the turbidite thickness and the spatial distribution in Dakar Canyon as identified in the echosounder profiles (Fig. 7).
We want to point out that the calculated values are only estimates because control by cores is sparse and the interpretation of the sediment structures on the echosounder profiles only allows a rough estimation of the spatial distribution of turbidite beds at the canyon bottom. The turbidite thickness and the spatial distribution at the core location as well as the distance between the core locations are the factors which were incorporated in the volume estimation. The thin turbidite (3 to 8 cm thick, Tab. 3) covers an area between the core location 9610-1 and 9615-1 of approximately 165 km^2 and the resulting volume is 9.9 x 10^6 m^3 (~0.01 km^3). This is a minimum estimate because it does not consider the turbidite deposits upslope of Core 9610-1 and downslope of Core 9615-1. Comparable turbidite volumes in submarine canyons at the NW-African continental margin are unknown. Large volume turbidites were deposited in the deep water basin of the Moroccan Turbidite System which reaches total volumes between 1 - 300 km^3 (Wynn et al., 2002).

4.5 Flow processes of turbidity current

The age determination reveals that a number of turbidites can be correlated between Core 9612-3 from the northern levee and Cores 9614-1 and 9615-1 at the distal part of the canyon (Tab. 4). A correlation by depositional ages of the turbidite sequences in Cores 9610-1 and 9611-1 to these cores, however, is not possible except for the 14.3 kyr BP event. A high frequency stacked turbidite sequence is recorded in Core 9610-1 and 9611-1 in the time between 16.3 - 14.3 kyr BP which is not found in Cores 9614-1 and 9615-1 during the same interval. This observation implies a more frequent turbidite deposition in the upper part of the investigated canyon area and demonstrates that not all turbidity current reached the lower part of the canyon.
Additionally, numerous small scale turbidite deposits (cm - scale) are recorded in the turbidite sequence in Core 9612-3, recovered at the northern levee. The ages of these turbidites partly coincide with the ages of turbidites in Cores 9614-1 and 9615-1 (Tab. 4). This observation contrasts the assumption that all turbidity currents were transported through the canyon. A core transect across the canyon comprises of Core 9612-3 from the northern levee, Core 9611-1 at the canyon floor and a gravity core at the southern flank outside the canyon (Fig. 2c).

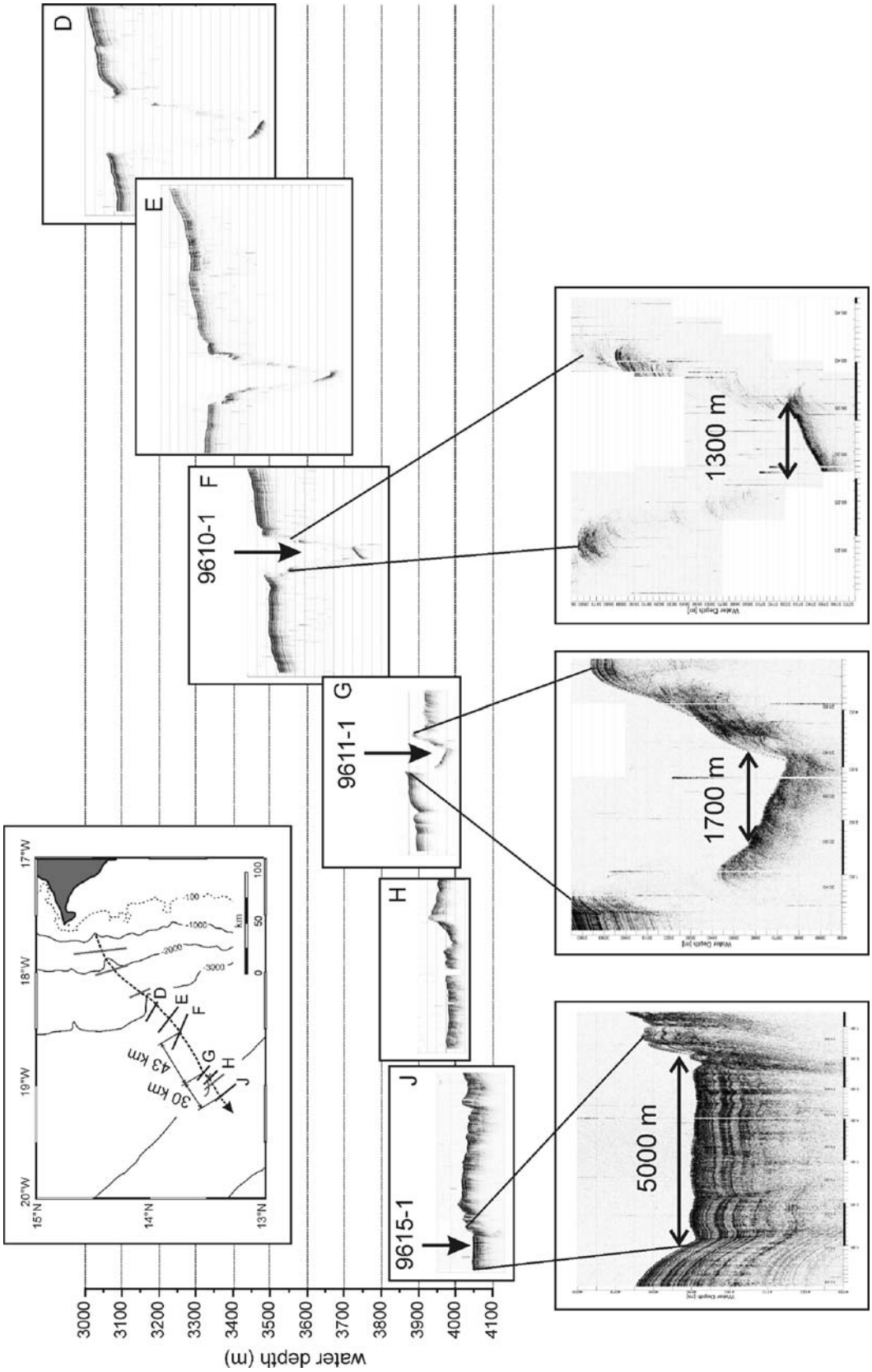

Figure 7: Cross sections including core locations of the Dakar Canyon. The locations of the profiles are shown in the map above. Note that a northern levee is not developed at profiles H and J. The close-ups display the widths of the canyon at the core locations. The calculation of the volume of T1 I based on these canyon widths, the distance between the core locations (shown in the map) and the thickness of T1.

The core south of the canyon consists of hemipelagic sediments with only two small scale turbidites (Krastel and cruise participants, 2006) and was therefore not investigated in detail due to the low content of turbidites. If the suspension cloud fills the entire canyon, so called spill-over turbidites can be generated and deposited at the surrounding levees. The less frequent turbidite deposition at the southern levee indicates that the suspension cloud was deflected to a northern direction by the Coriolis forces, which is expected as general feature in many turbidite systems (Nakajima et al., 1998).

4.6 Schematic model of the sedimentation processes in the Dakar Canyon

Based on the results we present a schematic conceptual model of the sedimentation processes in the Dakar Canyon during the most important time slices. During the peak glacials (Fig. 8a) a large sediment reservoir was build up at the exposed shelf. The low sea level and the enhanced wind stress were responsible for the formation of dune fields. During this time the canyon was inactive. The dune fields were remobilised by the rising sea level and were transport downslope by turbidity currents (Fig. 8b). The highest turbidite activity occurred during the sea level rise. Typical clastic deep sea systems are associated with a fan system, but due to the lack of seismic data we only assume such a feature (dotted line). The interglacials are characterised by sea level highstands (Fig. 8c). The dune fields were widely reworked and only remnants are visible on the shelf. The exploit sediment source and the high sea level prevent further turbidite depositions.

5. Conclusion

The intervals of main turbidite activity in the Dakar Canyon between 141 - 131 kyr BP and from 23.2 to 14.2 kyr BP coincide with the last two peak glacials. The frequent turbidite depositions during these intervals indicates that the Dakar Canyon act as an effective pathway for gravity-driven sediment transport at the continental margin off NW-Africa.
The variations of the environmental and climate condition throughout the last 240 kyr BP are the most important factor of the sedimentation processes in the Dakar Canyon. The peak glacials were characterised by high aeolian sediment input and the formation of large dune at the exposed shelf. These sand bodies provide a considerable sediment source for gravity-driven turbidity currents in the Dakar Canyon.

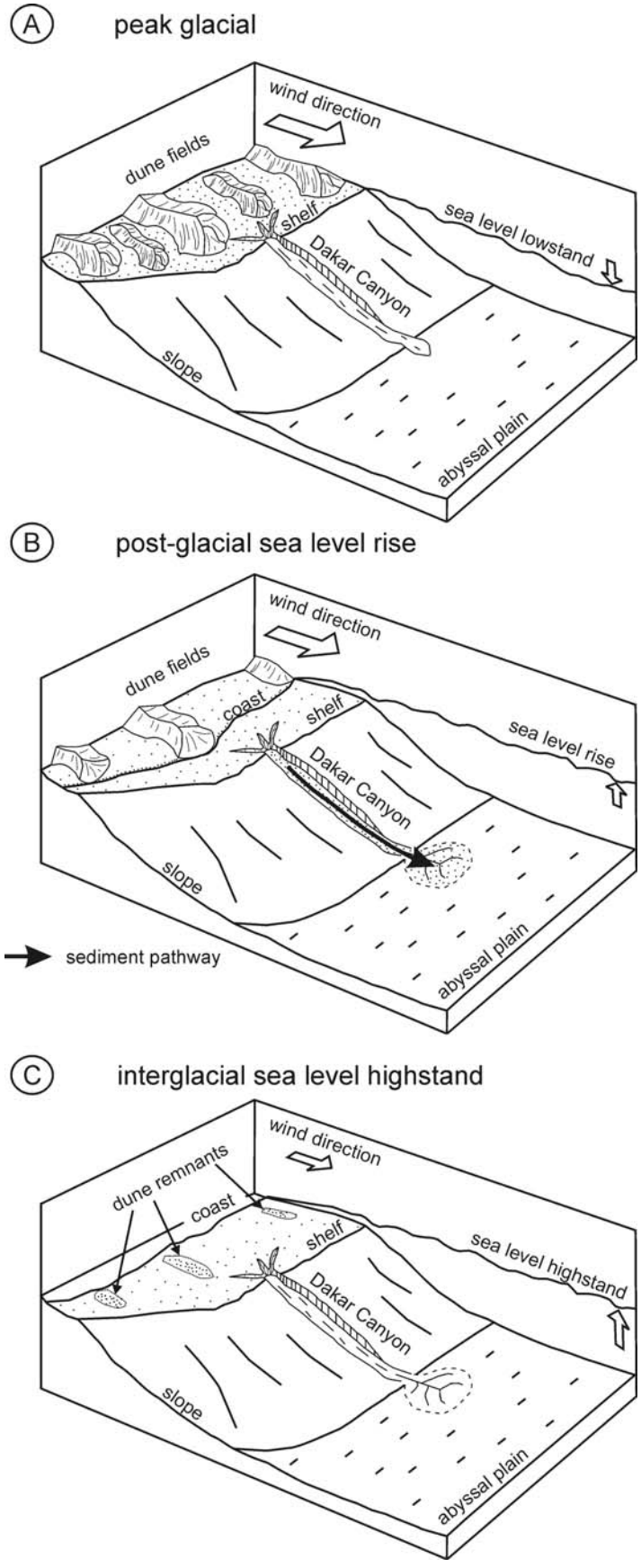

Figure 8: Schematic conceptual model of the sedimentation processes in the Dakar Canyon during the most important time slices.

A relative long-term period of arid climate conditions and enhanced wind stress occurred during the previous glacial maximum from 150 to 120 kyr BP. In contrast, a comparable but much shorter arid period occurred during the last glacial between 28 and 15 kyr BP. A significant higher number of turbidites were deposited in the distal part of the canyon during the Termination II in contrast to Termination I, indicating an enlarged sediment reservoir at the exposed shelf during the Termination II. Finer terrigenous silt sizes and low Ti/Ca ratios are recorded during interglacial periods. The reduced sediment influx prevents further turbidite depositions.

A downslope sorting in the grain size distribution of the turbidites can be observed The coarsest material was deposited in relative thick turbidite beds at the most proximal part of the investigated area of the canyon, whereas only small scale and fine grained turbidity currents reach the lower part of the canyon. A much higher frequency in turbidite deposition is recorded in the proximal Dakar Canyon around 18 kyr BP in comparison to the distal part which implies that not all turbidity currents reached the lower part of the canyon. The correlation of single turbidite beds through the canyon is based on their relative stratigraphic position. Turbidite T1 in Cores 9610-1, 9611-1 and 9615-1 can exactly be correlated by its radiocarbon age. The estimated volume of this turbidite in the investigated areas is ca. 9.9 x 10^6 m^3. Based on these results we present a schematic conceptual model for the sedimentation processes in the Dakar Canon.

Acknowledgments

We would like to thank the crew and scientific party of cruise M65/2 for their assistance. We are grateful to thank Swantje Böschen for preparing the grain size analyses. Brit Kockisch and Helga Heilmann are acknowledged for laboratory assistance. This work was funded by DFG-Research Center/Excellence Cluster „The Ocean in the Earth System“. This is MARUM publication no. ####.

6 Manuscript #3

Trigger mechanism of turbidity currents in two neighbouring submarine canyons at the Senegalese continental margin: a comparison of the Diola and Dakar Canyon

Roberto Pierau[*], Sebastian Krastel[+], Jacob Geersen[*], Till J.J. Hanebuth[*], and Rüdiger Henrich[*],

[*] MARUM - Center for Marine Environmental Sciences and Faculty of Geosciences, University of Bremen, Klagenfurter Straße, 28359 Bremen, Germany

[+] IFM-Geomar, Leibinz Institute of Marine Science, Wischhofstr. 1 - 3, 24148 Kiel, Germany

submitted to *Marine Geology*

Abstract

Submarine canyons systems are major pathways for gravity-driven sediment transport at continental margins. In this study we focus on the mechanisms of gravity-driven sediment transport in two canyons located at the passive continental margin off NW-Africa. The sedimentary history was reconstructed on sediment cores recovered directly from the canyons thalweg and the adjacent levees. The turbidite emplacement times were reconstructed using high resolution age models. Furthermore, detailed silt analysis; XRF-core scanning data and the clay mineral analysis of the hemipelagic background sediments allowed the identification of different sediment transport pathways. The investigated canyon systems are affected by the seasonal shifts of the Intertropical Convergence Zone and the discharge of the West African rivers.

The Dakar Canyon is located directly in front of Cape Verde. The highest frequency of turbidite deposition is found at the major climatic terminations when huge amounts of sediment were remobilised from the shelves in the course of the eustatic sea level rise. In addition, the occurrence of episodic turbidites coincides with the timing of Heinrich events. During these events the continental climate changed rapidly towards drier conditions in the study area, being displayed by increased dust supply in the sediments. In contrast,

sedimentation in the Diola Canyon is strongly influenced by the West African rivers. During the late Quaternary a mixture of fluvial derived material and aeolian dust was deposited at the exposed shelf. Frequent turbidite deposition in the Diola Canyon is recorded between 52 kyr BP and 34 kyr BP when minor sea level rise forced the remobilisation of this sediment mixture. Furthermore, the post-glacial sea level rise removed the remaining sediment deposits from the now flooded shelf region. This study highlights the influence of sea level rise and the subsequent remobilisation of shelf sediments as well as short-lasting climatic changes which act as main factors controlling the sediment flux in the investigated canyon systems.

Keywords: Diola Canyon, Dakar Canyon, NW-Africa, submarine canyons, sedimentation processes, turbidity currents

1. Introduction

The sedimentation processes along the passive continental margin of NW-Africa are affected by different climatic zones and are influenced by hemipelagic sedimentation, seasonal upwelling, as well as aeolian and fluvial input (McMaster and Lachance, 1969; Seibold and Fütterer, 1982; Weaver et al., 2000; Wynn et al., 2000; Zühlsdorff et al., 2007b). Variations of the climatic conditions during the Quaternary and especially the Holocene control the flux of terrigenous sediments into the Atlantic Ocean. The Quaternary and Holocene climate history of NW-Africa is reconstructed from marine and terrestrial archives suggesting significant climate change from arid glacial condition to a more humid climate during the early Holocene (Sarnthein et al., 1982; Rognon and Coudé-Gaussen, 1996; deMenocal et al., 2000a; Moreno et al., 2001; Kuhlmann et al., 2004). Most of these archives are located in front of Mauritania or round the Canary Islands. Up to now only a few studies are available for the marine sector of south Senegal and Guinea-Bissau. Thus the understanding of the climatic history remains vague.

Several canyon systems incise the NW-African continental margin and act as major pathways of gravity-driven sediment transport (Wynn et al., 2000; Antobreh and Krastel, 2006; Krastel et al., 2006; Talling et al., 2007; Zühlsdorff et al., 2007a). These canyon systems transport significant amounts of sediment from shallow-marine environments into the deep sea basins. Mechanisms that are generally considered to trigger gravity-driven

sediment transport are seismic activity, sea level changes, gas charging as well as rapid sediment loading and oversteepening. Many studies on large deep-sea fans point out that sea level fall and lowstand enhance turbidite activity, whereas these systems were inactive during sea level rise (Prins et al., 2000). In this study we reconstruct the sedimentation dynamics of the newly investigated Diola Canyon. In the following, these dynamics are compared with the Dakar Canyon, located north of the Diola Canyon. Both canyons were subjected to different climatic settings throughout the Quaternary although they are situated close to each other. The transition zone from arid climatic conditions in the north to humid conditions in the south conditions is located between both canyons. Thus, dust outbreaks should dominate the Dakar Canyon, whereas the influence of fluvial runoff is increased in the southern part of the study area. These different climatic settings should have been affected the trigger mechanisms of gravity-driven sediment transport within these canyons. The aim of the paper is to unravel these mechanisms to understand the sedimentation patterns in these two canyons throughout the late Quaternary.

2. Study area

2.1 Oceanic and climatic stetting

The surface currents off NW-Africa are dominated by the cold southward directed Canary Current (Fig. 1), whereas south of 20°N the surface water masses are mainly influenced by the wind driven Guinea Dome (Mittelstaedt, 1991; Stramma et al., 2005). The present-day climatic conditions at the NW-African continent is controlled by the seasonal migration of the Intertropical Convergence Zone (ITCZ), separating northern dry conditions from equatorial wet monsoonal conditions (Nicholson, 2000). During boreal summer, the SW monsoon shifts northward together with the ITCZ at which the later one reaches latitudes of ~ 20°N. North of the ITCZ the NE directed trade winds prevail, influencing the study area during the winter times when the ITCZ has migrated to its southward position (5°N). The trade winds and the overlying Sahara Air Layer (S.A.L.) are the most relevant wind systems off NW-Africa (Fig. 1a), forcing the westward transport of dust from the continent to the ocean as well as coastal upwelling (Koopmann, 1981; Sarnthein et al., 1982; Mittelstaedt, 1991; Prospero and Lamb, 2003). These dust plumes dominate the terrigenous sediment supply along the NW-African continental margin (Koopmann, 1981; Holz et al., 2004; Stuut et al., 2005). Fluvial supply is restricted to some smaller rivers, whereas in the

southern part of the study area river discharge becomes more important (Fig. 1b). Therefore, the surface sediments on the NW-African shelves are dominated by aeolian derived quartz sands and silts whereas higher amounts of fluvial derived silt and clay can be found at the shelf between The Gambia and Geba River (McMaster and Lachance, 1969; Debenay and Redois, 1997).

The NW-African margin is bordered by a generally flat, 40 - 100 km wide shelf (Wynn et al., 2000). The shelf width increases south of the Gambia River reaching a maximum expansion of ca. 150 km in the investigated area (Fig. 1b). Many active rivers reach the coast south of the Cape Verde peninsula whose main sediment load is trapped in estuaries along the inner shelf (McMaster and Lachance, 1969).

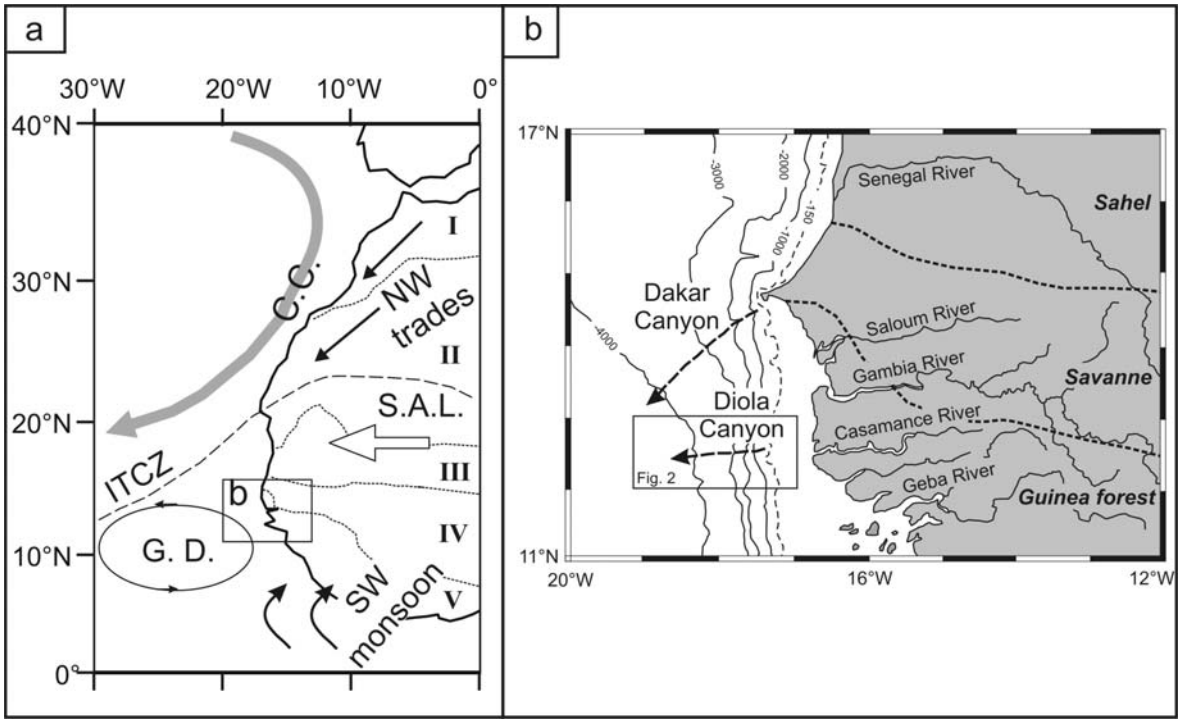

Figure 1: A) Overview map of NW-Africa with the most important oceanographic and atmospheric features as expected during the boreal summer (C.C. - Canary Current, G.D. - Guinea Dome, ITCZ - Intertropical Convergence Zone, S.A.L. - Sahara Air Layer). The major vegetation zones are redrawn after Hooghiemstra et al. (2006). (I - Mediterranean vegetation, II - Saharan desert, III - Sahelian vegetation, IV - Sudanian savannah, V - Guinean rain forest). B) Detailed map of the study area including the Dakar Canyon and the Diola Canyon, the major vegetation zones and the rivers draining the hinterland.

2.2 Morphology of the Diola and Dakar Canyon

The Diola Canyon is located at the continental slope of southern Senegal and The Gambia, in the vicinity of the Casamance and Gambia River (Fig. 1b). The morphology of the

canyon was mapped by one proximal seismic profile at water depths of ca. 2100 m (Fig 2) and two distal profiles at ~4000 m (Fig. 3).

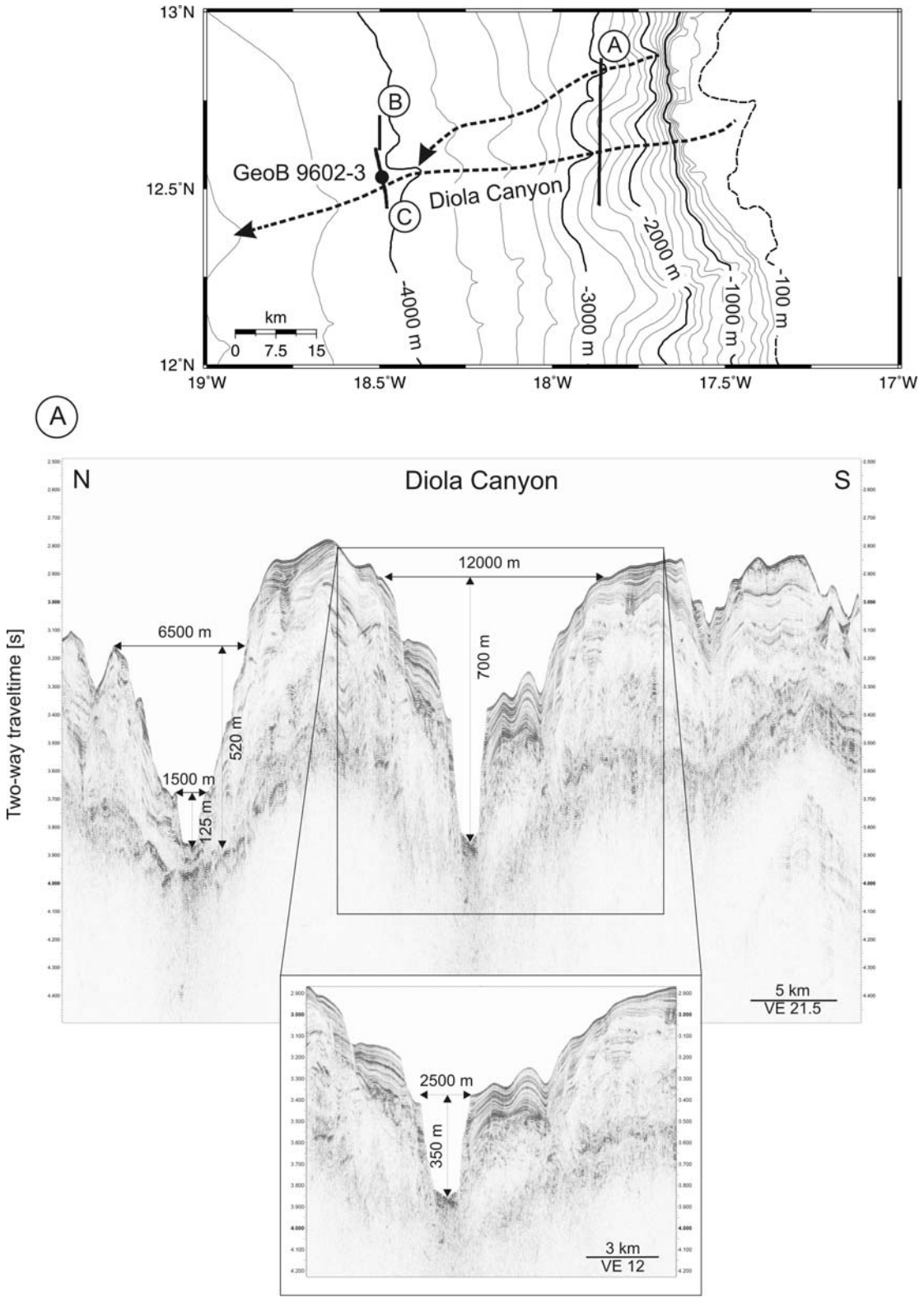

Figure 2: Proximal seismic profile of the Diola Canyon. The dotted lines in the map mark the course of the Diola Canyon and the unnamed tributary canyon. The seismic profiles are marked with encircled capitals and the location of core GeoB 9602-3 with a black dot.

Two deep incisions of ca. 500 m and 700 m are shown at the proximal profile and can be interpreted as two independent canyons (Fig. 2). The southern canyon corresponds to the Diola Canyon while the northern canyon is unnamed.

The Diola Canyon runs almost straight in an E - W direction (Fig. 2). A typically V-shaped pattern and canyon structures like steep sidewalls as well as terraces are imaged at the proximal part of the Diola Canyon (Fig. 3). A ~2500 m wide inner canyon incises the surrounding sediments to a depth of about 350 m marking the main canyon axis. In addition, the inner canyon is imbedded in a 12 km wide and ca. 700 m deep outer canyon. Here, characteristic levee structures are not developed due to the deep incision. However, well stratified sediments are visible at the top of both canyon flanks. Irregular high amplitude reflectors at the canyon bottom indicate the infill of coarse material. Similar morphological features as shown in the Diola Canyon can be observed in the northern unnamed canyon. High amplitude reflectors, however, are not observed at the base of this canyon. This unnamed canyon is also imbedded in a deeply incising V-shaped structure (650 m deep, 6.5 km wide). The unnamed canyon cannot be detected in the distal profiles (Fig. 3). Hence, both canyon axis probably join somewhere between the profiles and form a combined thalweg running further downslope.

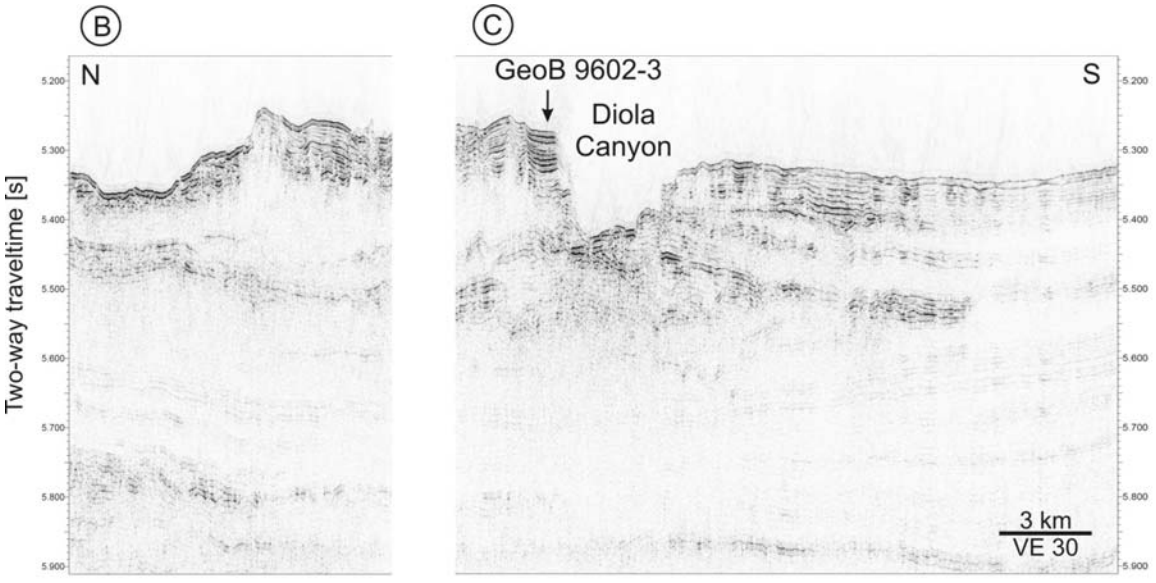

Figure 3: Distal seismic profiles of the Diola Canyon. Profile C shows the proximal Diola Canyon including the core location of GeoB 9602-3 recovered at the northern levee. The unnamed tributary canyon is not visible in profile B.

The incision depth of the Diola Canyon decreases quickly basinwards. The distal profile of the Diola Canyon (Fig. 3) about 90 km off the coast is characterized by an asymmetrical profile with a gentle dipping ca. 70 m high southern flank and a steeper >100 m high northern flank. At this position the width of the canyon is ~ 4 km. The southern flank shows some small terraces. The sediments south of the canyon are characterised by a wavy, subparallel pattern. The northern flank shows well stratified sediments. Core GeoB 9602-3 was recovered at this flank and consists of hemipelagic sediments with intercalated turbidite beds. The attempt to recover a core from the canyons thalweg was not successful.
The Dakar Canyon incises into the continental slope of Senegal slightly south of the Cap Verde peninsula (Fig. 1b, 4). The canyon was mapped for a length of ~200 km from the upper slope starting at the upper slope at a water depth of 1300 m down to water depths of 4100 m where the canyon runs out into the deep-sea basin (Pierau et al., in review-b).

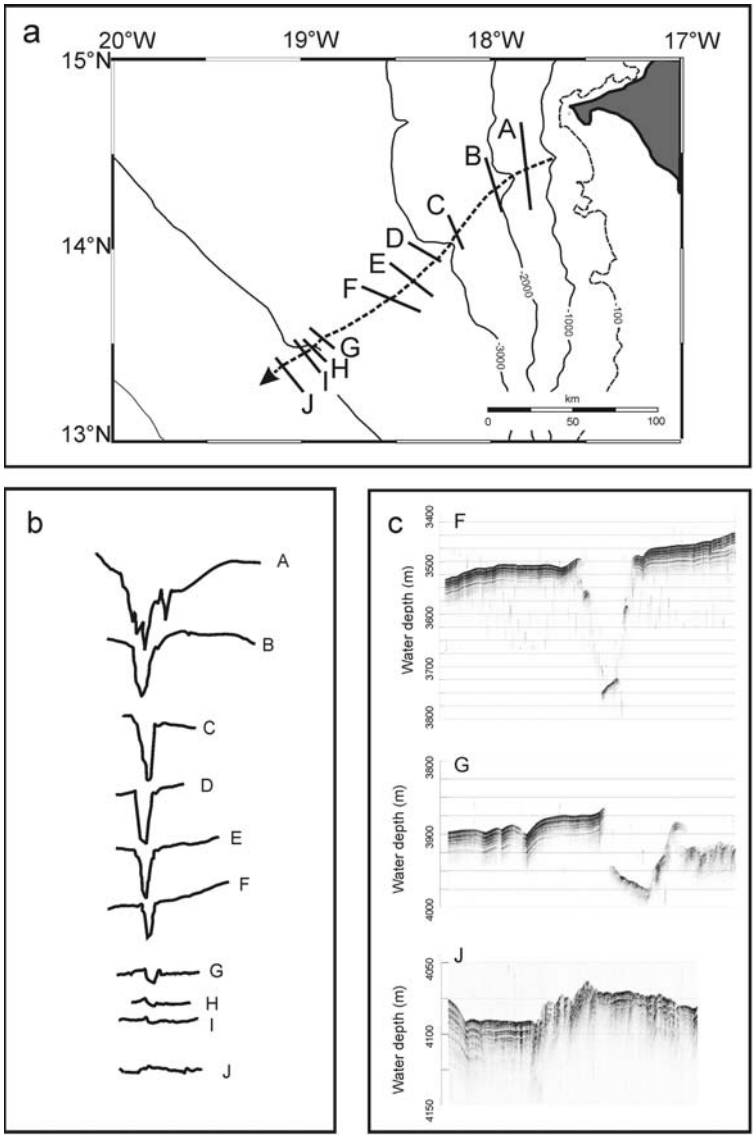

Figure 4: Overview map of the Dakar Canyon. A) Positions of the Parasound profiles. B) Cross-sectional profiles perpendicular to the canyon. C) Selected Parasound profiles showing morphologic features like steep side walls and terraces of the Dakar Canyon.

A tributary system of smaller gullies is depicted at the most proximal profile. At this position the canyon is incised into the sediments up to 700 m and the width of the main canyon is ca. 10 km. The almost straight Dakar Canyon is V-shaped in the proximal sector and typical canyon structures such as steep sidewalls and terraces are imaged in hydroacoustic profiles (Pierau et al., in review-b). At the distal part the canyon changes into a more U-shape pattern. A nearly identical morphology can be observed in the Diola Canyon. Therefore we assume that the sediment dynamics in both canyon systems can be compared due to the similar morphology.

3. Material and methods

In this study we present sedimentological and geochemical data of the 4.83 m long gravity core GeoB 9602-3 (12°35.25'N; 18°30.4'W) recovered at 3981 m water depth in the Diola Canyon. The coring location was chosen in order to retrieve a high resolution sedimentary record of the turbidite activity in the Diola Canyon. X-ray radiographs were made on thin sediment slices to improve the visual core description. This technique helps to determine the exact position of turbidites in the core. To provide a qualified age model and to clarify the turbidite emplacement times each turbidite was cut out of the record.

The elemental distribution was measured in 1 cm resolution using the X-ray Fluorescence (XRF) Core Scanner. Based on the core description the samples of the hemipelagic background sediments were taken between the turbidites in irregular intervals. The sand fraction (> 63 μm) was separated from the fine fraction by wet sieving. For grain size analysis of the terrigenous components of the fine fraction, the samples were pre-treated with 10% H_2O_2 and 12.5% HCl in order to remove organic matter and carbonate. In the following, the fine fraction was separated into silt (63 - 2 μm) and clay (<2 μm) by repeated settling in Atterberg tubes according to Stokes' law. The detailed grain size analyses of the terrigenous components of silt fraction were performed with the Micromeritics SediGraph 5100 in the range of 63 - 2 μm. The biogenic opal content in marine sediments of NW-Africa is negligible (Koopmann, 1981; Holz et al., 2007). The mineral composition of the carbonate and organic matter free clay fraction was analysed on grinded and mounted texturally oriented aggregates with a Philiphs PW 1830 X-ray diffractometer (CoKα radiation, 40 kV, 40 mA). All samples were measured from 3 - 40° 2Θ. The clay minerals were identified by their basal reflections. For semiquantitative evaluations of the content of each clay mineral the empirically estimated weight factors on

integrated peak areas were used (Biscaye, 1964; 1965). All concentrations are given in percent of the total clay mineral assemblage.

The planktonic foraminifera *Globigerinoides ruber* (white) was used for stable isotope measurements and at least 700 individual species of the planktonic foraminifera *G. ruber* (w/p), *G. sacculifer* and *O. universa* were collected for accelerator mass spectrometry (AMS) radiocarbon dating at the Poznan Radiocarbon Laboratory in Poznan, Poland.

High-resolution multi-channel seismic reflection profiles were collected with the Bremen high resolution seismic system. A 1.7l GI-Gun was used as source. The energy was recorded with a 600 m long 96 channel streamer. The processing procedure included trace editing, setting up geometry, static corrections, velocity analysis, normal moveout corrections, bandpass frequency filtering (frequency content: 55/110 - 600/800 Hz), stack, and time migration. A common midpoint spacing of 10 m was applied throughout.

4. Results

4.1 Stratigraphy

The age model for Core 9602-3 is based on its stable oxygen isotope curve (Fig. 5a) correlated to the NGRIP record (Svensson et al., 2008). The turbidite sections were cut out of the core to provide an almost continuous hemipelagic sediment record. Five radiocarbon dates are used to improve the age model for the younger part of the record (Table 1). A standard reservoir age of 400 yrs is assumed for calibration which takes the short lasting period of winter upwelling into account. The radiocarbon ages younger than 24 ^{14}C ka BP are corrected and calibrated using CALIB REV5.0.1 (Stuiver et al., 1998). Older radiocarbon ages are subsequently calibrated using the function of Bard et al. (1998). In the following all ages are given in calibrated thousands of years before present (kyr BP). Ages of turbidites are considered to be equivalent to the age derived for the onset of hemipelagic sedimentation on the top of the relevant turbidite.

Table 1: Radiocarbon dates and age calibration of GeoB 9602-3

Core depth (m)	Lab ID	Analyses material	Conventional age (yrs)	Calibration two sigma range (cal yr BP)	Calib. age (kyr BP)
0.05	Poz-22953	G. sacculifer, G. ruber, G. bulloides	4475	4604 - 4730	4.7
0.99	Poz-22954	G. sacculifer, G. ruber, G. bulloides	13140	14913 - 15167	15.0
1.25	Poz-20280	G. sacculifer, G. ruber, G. bulloides	14030	16013 - 16406	16.2
1.70	Poz-20281	G. sacculifer, G. ruber, G. bulloides	18650	21544 - 21965	21.7
2.78	Poz-22955	G. sacculifer, G. ruber, G. bulloides	27670		32.4

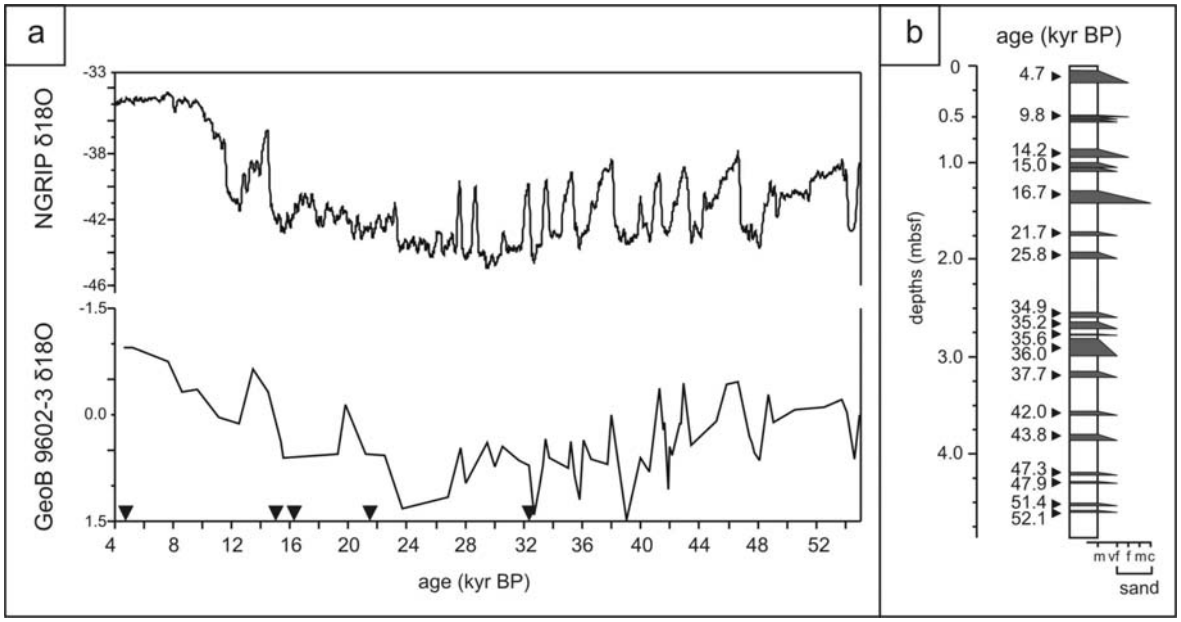

Figure 5: Oxygen isotope record of GeoB 9602-3 compared to the NGRIP record. The triangles mark AMS dating points. Turbidites were cut out of these records. On the left, the core log of GeoB 9602-3 illustrates the timing, thickness and simplified sedimentary composition of the turbidites.

4.2 Turbidite activity and sedimentary properties in the Diola Canyon

Core GeoB 9602-3 mainly consists of olive-grey silty-muddy hemipelagic sediments with intercalated turbidite beds. The turbidite beds are thinly bedded varying from 1 cm to 18 cm in thickness. The cm-scale turbidites consist of very fine grained material. In addition, coarse grained turbidites are also preserved showing typical finning-upward trends. The turbidite activity in the Diola Canyon during the last 55 kyr BP is characterised by a sporadic and irregular turbidite occurrence (Fig. 5b). A relative regular turbidite deposition of 6 events is recorded between 52.1 and 42.0 kyr BP. A high turbidite activity occurred between 37.7 and 34.9 kyr BP. During this time span the thickest turbidite (19 cm) in the whole record was deposited at 36.0 kyr BP. In the following, two single events are recorded at 25.8 and 21.7 kyr BP. A higher activity was recorded again between 16.7 to 14.2 kyr BP. Three small scale and stacked turbidites were deposited around 9.8 kyr. The most recently event is recorded at 4.7 kyr BP.

Based on the age model of Core GeoB 9602-3 we reconstructed the variations of the hemipelagic background sedimentation of the last 55 kyr BP in the Diola Canyon (Fig. 6). It should be noted that all turbidites were cut out of the record to provide a continuous record of the hemipelagic background sedimentation. The downcore record of the carbonate and organic matter free fine fraction (terrigenous silt and clay) can be used to

reconstruct the input of aeolian dust (terr. silt) versus fluvial input (terr. clay). The terrigenous silt is characterised by relative constant amounts of ca. 20 wt%. However, peak values ranging from 45 to 30 wt% occur at 41 kyr BP, 30 - 28 kyr BP and 17 - 15 kyr BP (Fig. 6). In contrast the terrigenous clay shows pronounced variations throughout the record. Relative high values of ca. 30 wt% occur between 53 kyr to 30kyr BP, often interrupted by lower values (ca. 20 wt%). A slight increase of the terrigenous clay content from 10 to 35 wt% is recorded from 26 to 18 kyr BP, followed by a sharp decrease to lower values of 10 wt% from 18 - 15 kyr BP (Fig. 6). Again, a shift to higher values occurs between 14 - 10 kyr BP. The mean of the terrigenous silt size distribution displays the variability of aeolian dust input (Matthewson et al., 1995; Stuut et al., 2002). The mean of the terrigenous silt size distribution shows variations between 9 to 21 µm throughout the record (Fig. 6). Maxima are recorded between 53 - 51 kyr BP, 47 - 46 kyr BP, 41 - 39 kyr BP, 37 - 35 kyr BP, 30 - 28 kyr BP, 16 - 13 kyr BP and at 10 kyr BP. The clay mineral assemblage is dominated by kaolinite, reaching values up to 85 wt% (Fig. 6). Relative low values are recorded between 20 - 18 kyr BP (72 - 75%). Smectite and illite show strong fluctuations between 55 - 26 kyr BP. Pronounced maxima are recorded in the illite composition at 52, 48, 43, 39, 18 and 16 kyr BP. Chlorite occurs sporadically with values <4 wt%. The XRF dataset of core GeoB9602-3 is also characterised by strong variations of the elemental composition between 55 and 16 kyr BP and a shift to relative stable values in the younger part of the record (Fig. 6). Al, K, and Fe show parallel variations with high values recorded around 50, 41 and 31 kyr BP. These elements show a negative correlation to the Ca values. The resulting K/Al and Fe/Ca ratios show also higher values around 50, 41, 31 and 18 kyr BP.

5. Discussion

5.1 Sedimentary properties

Terrigenous material can reach the shelf in the study area as a) river suspended matter transported by the West African rivers or b) as aeolian dust mainly controlled by the NW-Trade winds. A direct quantification between aeolian and fluvial derived material is not possible on the data base represented in this study. High amounts of silt and clay can be found on the shelf between the Gambia and Geba river, whereas medium sand is found at the outer shelf (McMaster and Lachance, 1969).

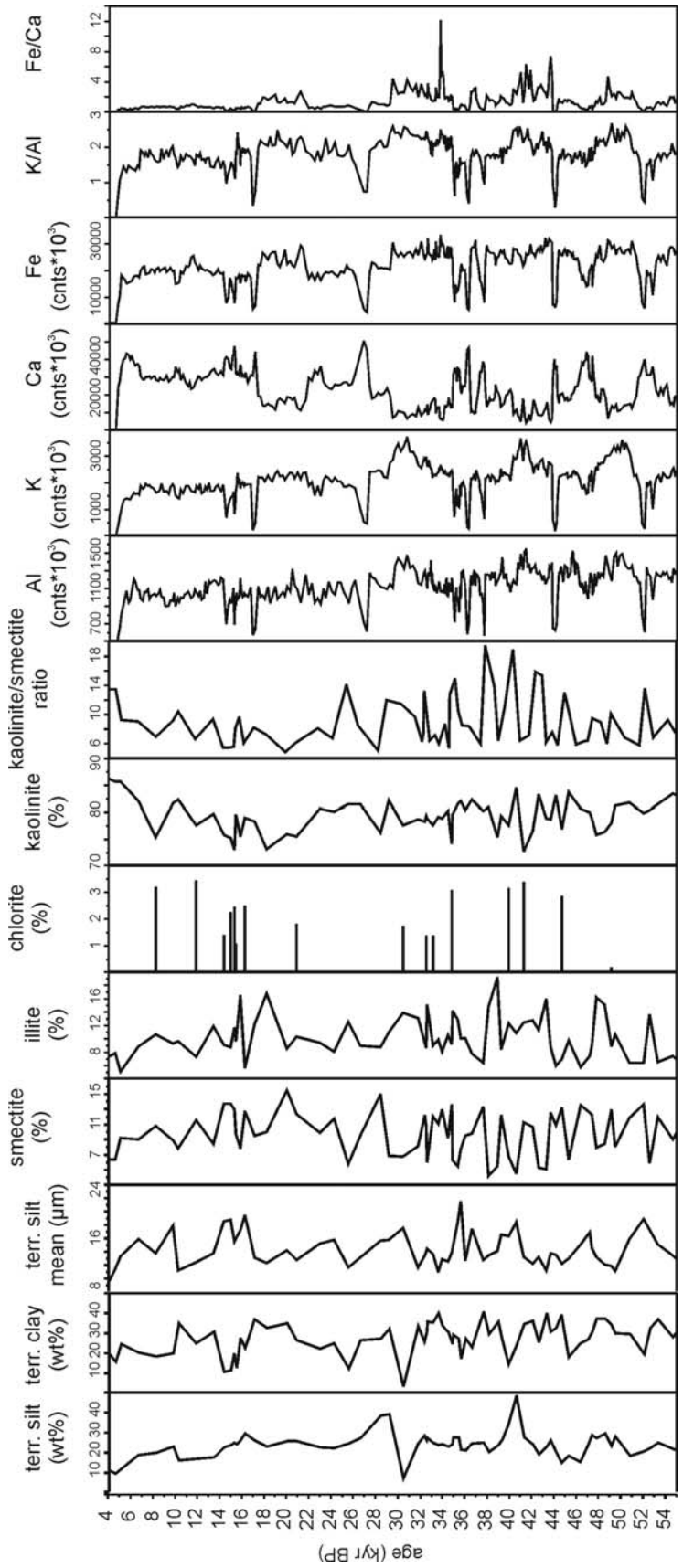

Figure 6: Sedimentary properties of GeoB 9602-3 including the terrigenous grain size distribution, clay mineral assemblage, XRF measurements and the resulting ratios.

Therefore we propose that the southern Senegalisian shelf is dominated by fluvial material derived from different rivers draining the hinterland.

The composition of aeolian derived material in deep-sea sediments depends on the distance to the source area, the intensity of the transporting wind system and the climatic variations in the hinterland (Rea, 1994). Studies of sediment cores and surface samples along the NW-African continental margin demonstrate that terrigenous sediment with mean grain sizes > 6μm are attributed to aeolian dust (Koopmann, 1981; Holz et al., 2004). The mean of the terrigenous silt size distribution of GeoB9602-3 shows pronounced variations and is characterised by values >10μm. These variations can be used to the reconstruction of the general dust input from the continent to the ocean. GeoB9602-2 is located in the transition zone between semiarid and arid open vegetation (Lèzine, 1991) and should be influenced by the NE trade winds and permanent fluvial input originated from the Guinea-South-Senegal region. Therefore this area is very sensitive to climatic changes which should be recorded in variations of sedimentological properties and XRF intensities.

Pronounced maxima in the terrigenous silt size distribution are recorded at 53 - 51, 47 - 46, 41 - 39, 35, 30 - 28, 16 - 13 and around 10 kyr BP (Fig. 7) suggesting episodes of enhanced wind stress. Partly these episodes are coeval with Heinrich events in the North Atlantic (Abreu et al., 2003). These short-term climatic changes are characterised by intensified trade winds over NW-Africa resulting in a higher dust flux (Jullien et al., 2007). The highest input of aeolian dust is being recorded in marine sediment cores in front of NW-Africa during glacial periods (Matthewson et al., 1995; Moreno et al., 2001; Pierau et al., in review-a). The peak glacial are characterised by a weakened thermohaline circulation which led to a stronger hemispheric temperature gradient coupled with intensified trade winds (Sarnthein et al., 1981; Vidal et al., 1997; Jullien et al., 2007). The resulting southward shift of the ITCZ (Jennerjahn et al., 2004) has reduced the monsoonal precipitation over NW-Africa (deMenocal et al., 2000a) and led to a southward migration of the vegetation zones (Hooghiemstra et al., 2006).

Coarser terrigenous silt sizes in GeoB9602-3 are recorded between 16 - 13 kyr BP (Fig. 7) reflecting a relative short period of enhanced wind stress. Generally, the NW-African continent and also the study area should be affected by the enhanced wind stress during the peak glacial. Probably the hinterland of south Senegal and Guinea was covered by a patchy vegetation cover which impeded the transport of dust. Therefore, the dust particles in the hemipelagic sediments in this part originate from more proximal parts on the continent causing the coarsening of the sediment.

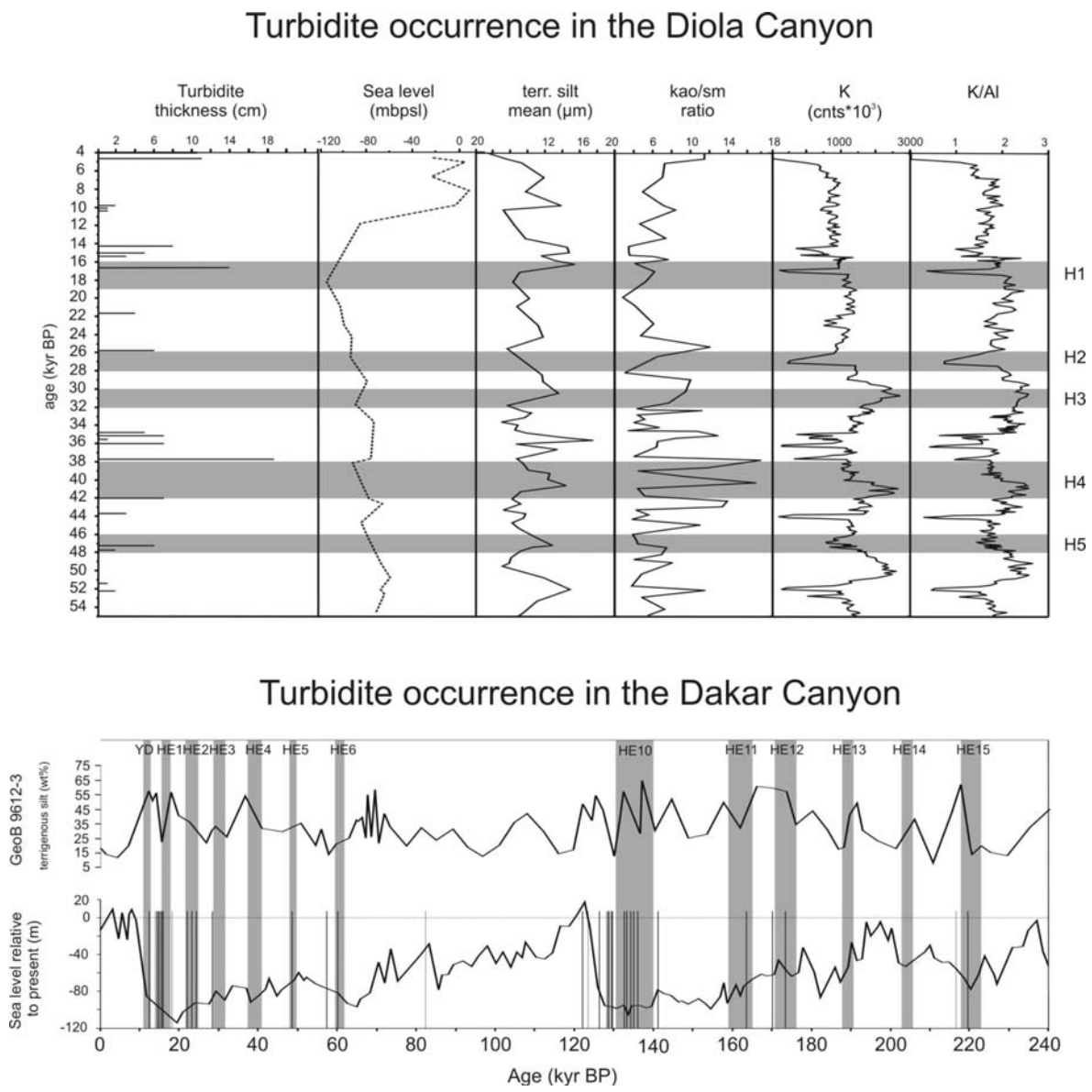

Figure 7: Comparison of the turbidite emplacement times in the Diola Canyon with the global sea level history (Siddall et al., 2003), terrigenous silt size distribution, kaolinite/smectite ratio, XRF K counts and K/Al ratio. The grey shaded areas indicate Heinrich time equivalents.

Additionally, the mean of the terrigenous silt size reaches comparable values as recorded during the Heinrich equivalent time intervals which would suggest similar wind intensities. The distribution of clay minerals on the North African continent is controlled by the geographical position and the prevailing climate conditions (Lange, 1982). High concentration of kaolinite is restricted to regions with intensive chemical weathering under warm and humid conditions. Therefore, major sources for kaolinite are found in the southern Sahara-Sahel zone (Schütz and Sebert, 1987). The formation of smectite also requires chemical weathering whereas the source rock of smectite are volcanic outcrops

(Petschick et al., 1996) which are sporadically found in the Senegal Basin (Brownfield and Charpentier, 2003).

In general, the clay minerals are mainly transported from the source areas to the ocean by wind or rivers (Foucault and Mèliéres, 2000). Concerning the study area, the S.A.L. gathers dust from the exposed kaolinite rich lateritc soils in the southern Sahara (Lange, 1982). When these deposits are covered by vegetation as for instance in the areas south of the Saharan margin, kaolinite is mainly eroded during heavy rainfalls and transported by rivers. Hence, high concentrations of kaolinite are found in seabed samples in front of river mouths (Petschick et al., 1996; Gingele et al., 1998). Gingele et al. (1998) used the kaolinite/smectite ratio to estimate the intensity of freshwater discharge from the Zaire River. Increased freshwater output and thus higher kaolinite/smectite ratios are forced by an intensified monsoon. Humid periods correspond to maximum summer insolation in the Northern Hemisphere resulting in enhanced rainfall on land (Rossignol-Strick, 1985; deMenocal et al., 1993; Kutzbach and Liu, 1997). According to the North African Monsoon Index a relative strong monsoon occurred around 40 kyr BP and less intense monsoon conditions prevailed between 30 - 20 kyr BP (McIntyre et al., 1989). Furthermore, strong monsoon intensity over Central Africa with increased freshwater discharge of the Zaire River was suggested at 28 and 18 kyr BP (Pokras, 1987). Based on pollen reconstruction of a marine sediment core close to the investigated core location, wet periods have been registered around 44 kyr BP and 12 kyr BP (Lèzine, 1991). These observations are reflected in the course of the kaolinite/smectite ratio of GeoB 9602-3 (Fig. 7). Higher and strongly fluctuating kaolinite/smectite ratios were recorded between 44 and 30 kyr BP which would suggest pronounced humid conditions during this time span in the hinterland of South Senegal and Guinea. It should be noted, that probably only the strongest freshwater pulses are recognised in the record. Drier climate conditions reflected in low kaolinite/smectite ratios could have existed prior 44 kyr BP and from 22 to 11 kyr BP.

The elements Al and K can also be used for the reconstruction of the variations in fluvial discharge (Zabel et al., 2001; Kuhlmann et al., 2004). Generally, the flux rate of these elements from the continent to the ocean depends on physical erosion which is mainly controlled by the monsoon intensity and the resulting vegetation coverage. K is associated with potassium feldspar and illite (Martinez et al., 1999), whereas Al can be assigned to fine grained detritus of aluminosilicate origin (Calvert, 1976; Karageorgis et al., 2005). A precise affiliation of both elements to specific minerals does not exist. Nevertheless, the

K/Al ratio can be used as proxy for chemical weathering (Zabel et al., 2001) which is controlled by variations of the moisture supply. Variations in the K intensity and the K/Al ratio show higher values between 51 - 49, 44 - 37 and 33 - 27 kyr BP (Fig. 7), suggesting humid periods coinciding with increased riverine runoff. This observation supports the results of the clay mineralogy.

5.2 Turbidite deposition

The first period of turbidite deposition between 53 - 35 kyr BP is characterised by thinly bedded turbidites consisting mainly of fine to very fine grained sediments (Fig. 5). Comparable deposits can be found in the Dakar Canyon, north of the Diola Canyon. These turbidites consists also of fine sand to silt material and are coeval with the wind intensive Heinrich equivalent time intervals (Pierau et al., in review-a). The sedimentary properties of GeoB9602-3 indicate periods with increased fluvial input (51 - 49, 44 - 37, 33 - 27 kyr BP). Relative high fluvial input is recorded between periods of turbidite activity in the Diola Canyon (Fig. 7). The global sea level was more than 70 m below the present level (Siddall et al., 2003) and the rivers should drain directly onto the exposed shelf. Probably a "Paleo-Casamance River" was directly connected to the head area of the Diola Canyon (Fig. 2). We would expect that strong freshwater pulses should trigger turbidity currents in the Diola Canyon, but the turbidite emplacement times contradict this assumption. The turbidite activity cannot be explained by an intensification of the fluvial input or by enhanced dust input. On the other hand the interplay of both processes is responsible for the build up of a sediment reservoir at the canyon head area providing the sediment source for turbidites in the Diola Canyon. These turbidites were triggered by minor sea level changes (Fig. 7) which in turn probably correspond to Heinrich equivalent time intervals, during which the sea level can rise up to 15 m in a few hundred years (Chappell, 2002). The composition of the small scale turbidites shows no clear evidences for solely dust derived material emphasising the inhomogeneity of the sediment. The high amounts of fine material in the thinly bedded turbidites thus can also reflect the influence of fluvial input which would be underlined by the high kaolinite/smectite and K/Al ratios between 50 - 28 kyr BP.

The second period of turbidite activity between 17 - 10 kyr BP are characterised by a less frequent turbidite deposition (Fig. 7). Three turbidites were deposited between 17 - 14 kyr BP being coeval with the early postglacial sea level rise (Fairbanks, 1989; Hanebuth et al.,

2000). The climatic conditions at the NW-African continent were generally dry during that time (Lèzine, 1991). Reduced monsoonal precipitation led to a southward shift of the vegetation zones (deMenocal et al., 2000a; Hooghiemstra et al., 2006), resulting in a higher dust flux and enhanced wind stress (Sarnthein et al., 1981; Matthewson et al., 1995; Moreno et al., 2001). Evidences for dry climate conditions and reduced fluvial input are recorded in GeoB9602-3 by low kaolinite/smectite ratios and a clear decrease in the K/Al ratio after 24 kyr BP. Furthermore, abrupt increases of the terrigenous silt sizes at 16 and 10 kyr BP indicate several periods of stronger wind stress and drier climatic conditions. These dry episodes are also known from deep-sea cores in front of Mauritania (Matthewson et al., 1995; Holz et al., 2007). Around 18 kyr BP the sea level reaches the glacial lowstand (Fairbanks, 1989; Bard et al., 1990) and large areas of the shelf in the study area were exposed. The enhanced wind stress leads to the accumulation of aeolian derived material at the shelf. This material was subsequently reworked by the postglacial sea level rise (Pierau et al., in review-a). A relatively thick turbidite (14 cm) was deposited at 16.7 kyr BP. This turbidite shows a well developed BOUMA - sequence (Bouma, 1962) and contains a mixture of medium sand and material originating from the shelf (Fig. 8). The thick and relatively coarse turbidite indicates the remobilisation of a relatively huge and coarse sediment reservoir located at the outer shelf or shelf break. South of Cape Verde dune remnants can be observed on the shelf (Barusseau et al., 1988). These “paleodunes” are limited to an area south of Cape Verde until 14°N. Therefore we can exclude that dune fields are the sediment source for this turbidite. The following turbidites are distinctly thinner and consist of fine material. The major portion of the sediment reservoir on the shelf was reworked and deposited by the 16.7 kyr BP turbidite. Thus only small amounts of sediment were available for the downslope transport. A series of three turbidites is recorded around 10 kyr BP corresponding to the final phase of the postglacial sea level rise and being coeval with the deposition of coarser terrigenous silt sizes in the hemipelagic background sediments (Fig. 7).

The input of fluvial material at the core location clearly decreased after 24 kyr BP. The overall dry climatic conditions during the LGM resulted in a reduced freshwater discharge and a limited sediment delivery. The climate of NW-Africa changed into more humid conditions with the onset of the African Humid Period (AHP) at 14.8 kyr BP (deMenocal et al., 2000a). This shift is also reflected in the sedimentary properties of the hemipelagic background sediments of GeoB9602-3. However, due to the high sea level during the Holocene the accumulation of fluvially derived material is predominately stored in the

estuaries and on the shelf (McMaster and Lachance, 1969; Ausseil-Badie et al., 1991) causing sediment starvation in the Diola Canyon.

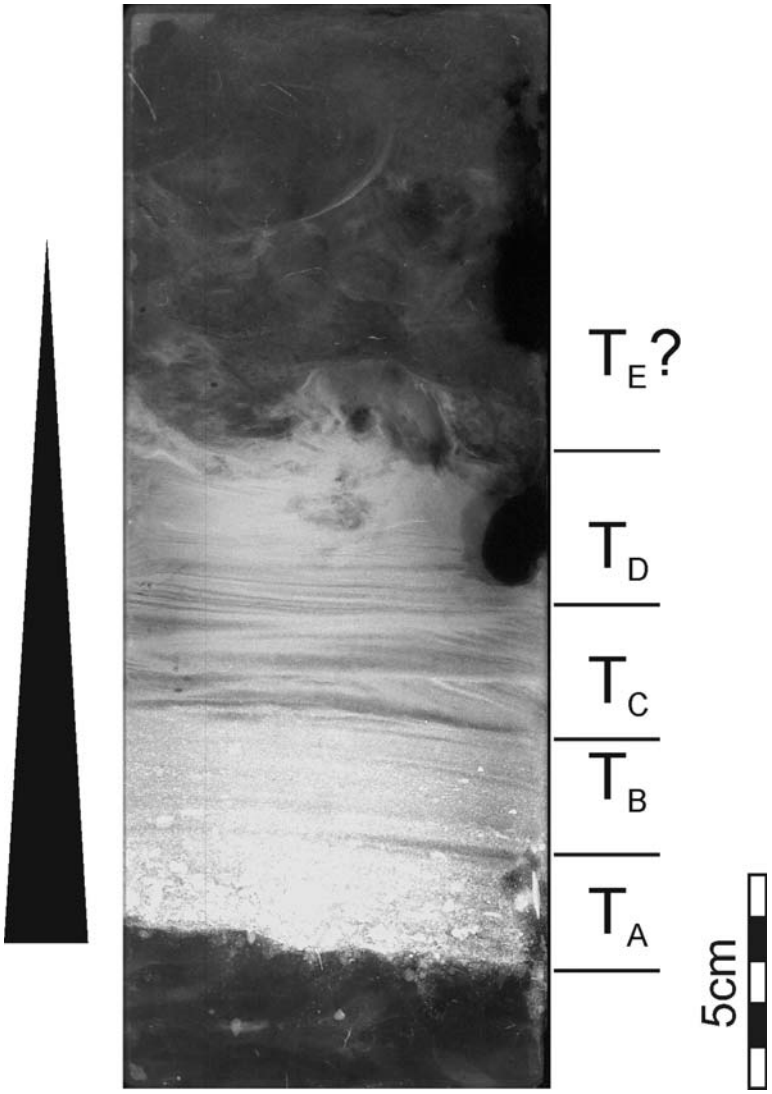

Figure 8: Well developed turbidite with complete BOUMA-sequence. The base of this turbidite consists of a mixture of medium sand and fragments of shelf material. The muddy top is destroyed by intensive bioturbation.

6. Comparison of the Dakar and Diola Canyon

Several submarine canyon systems along the NW-African continental margin were studied in detail in order to reconstruct the turbidite emplacement times and the sedimentation processes (Dietz et al., 1968; Zühlsdorff et al., 2007a; Pierau et al., in review-a). This chapter focuses on two submarine canyon systems, the Dakar Canyon and the Diola Canyon, located close to each other. We compare the variability of the hemipelagic

background sedimentation and the processes triggering the turbidite deposition in these canyons.

Although both canyons are located close to each other, the hemipelagic background sedimentation shows distinct differences. The amount of terrigenous silt in the background sediments around the Dakar Canyon shows strong variations throughout the record and pronounced maxima occurs during the glacials and Heinrich equivalent time intervals (Pierau et al., in review-b). Generally, higher amounts of terrigenous silt are recorded in the hemipelagic sediments around the Dakar Canyon compared to the Diola Canyon. The variations in the terrigenous silt allows estimations about the wind stress (Matthewson et al., 1995; Stuut et al., 2002). Therefore, we assume that the background sedimentation of the Dakar Canyon is strongly controlled by aeolian dust. Instead, the background sediments around the Diola Canyon are predominantly influenced by terrigenous clay supplied by the West African rivers.

The sedimentation processes in the Dakar Canyon were reconstructed at four gravity cores directly recovered from the canyon axis (Pierau et al., in review-b). Two main phases of turbidite activity coinciding with the last two major climatic terminations can be identified in the Dakar Canyon (Pierau et al., in review-a). The turbidite activity was triggered by the remobilisation of aeolian derived sediments during the rapidly rising sea level. These sediments were deposited in paleo-dunes at the exposed shelf under arid glacial conditions and intensified trade winds. The onset of humid conditions during the postglacial to early interglacial times reduced the dust supply from the continent to the ocean. In the last interglacial the high and relative stable sea level has additionally impeded further turbidite activity (Pierau et al., in review-a). In addition, the emplacement of some turbidite deposits is coeval with Heinrich equivalent time intervals. These short lasting climatic changes are characterised by enhanced dust flux due to intensified wind stress (Jullien et al., 2007; Pierau et al., in review-a).

The sediment dynamics in the Diola Canyon is characterised by a frequent deposition of turbidites from 53 - 35 kyr BP. The sedimentary properties of GeoB 9602-3 suggest periods of enhanced fluvial runoff during that time span. Probably a river may have been directly connected to the head area of the canyon. We exclude that only strong freshwater pulses were responsible for triggering turbidity currents in the Diola Canyon. The deposition of fluvial and aeolian derived material on the exposed shelf caused the build-up of the sediment reservoir at the canyon head area. Minor sea level changes, probably during Heinrich time equivalents, may have triggered these turbidity currents.

The intervals of main turbidite activity in the Dakar Canyon coincide with the last two postglacial sea level rises. The peak glacials were characterised by high aeolian sediment input and the formation of large dune at the exposed shelf. These dunes were subsequently remobilised by the rapid rising eustatic sea level. Enhanced but less frequent turbidite deposition is also recorded in the Diola Canyon during the period of the post-glacial sea level rise. A few number of turbidites are recorded which would suggest a smaller sediment budget in the head area compared to the Dakar Canyon.

7. Conclusions

The turbidite activity in the Dakar and Diola Canyon shows some similarities but also differences. A sporadic turbidite activity is recorded during Heinrich equivalent time interval in the Dakar Canyon. These periods of enhanced dust supply due to short-term climatic changes and subsequent turbidite events are not recorded in the Diola Canyon. A mixture of fluvial and aeolian derived material episodically filled up the sediment reservoir at the canyon head which was remobilised during minor sea level changes. The main turbidite activity in the Dakar Canyon occurred during the major climatic terminations. The deposition of siliciclastic turbidites around the major climatic terminations results from the remobilisation of aeolian derived material from the shelf during the rising eustatic sea level. The Dakar Canyon is strongly influenced by dust fluxes from the Sahara, whereas the Diola Canyon is predominately influenced by fluvial discharge. Only three single turbidites are recorded in the time between 17 to 14 kyr BP during the initiation of the eustatic sea level rise. These results suggest that dust outbreaks play a subordinated role in the sediment dynamics of the Diola Canyon. The transition zone of arid/semiarid to more humid climatic conditions during the LGM in NW-Africa could be located south of the Dakar Canyon around 13°N. No turbidite activity is recorded during the interglacials in the Dakar Canyon. A reduced dust supply due to more humid climatic conditions and the high sea level prevent further turbidite activity. Three turbidites were deposited during the early Holocene (9.8 kyr BP) in the Diola Canyon and a single event is recorded at 4.7 kyr BP. The turbidite deposition during the early Holocene most probably was triggered by the final sea level rise.

Acknowledgements

The authors would like to thank the crew and scientific party of cruise M65/2 for their assistance. We are grateful to thank Gitte Graubner, Brit Kockisch and Helga Heilmann for laboratory assistance. We would like to thank Susanne Wiebe from AWI-Bremerhaven for technical support during clay mineral preparation. Vera Lukies is thanked for her help with the XRF core scanner measurements. Ulrike Proske is thanked for her helpful comments. This work was funded by DFG-Research Center/Excellence Cluster „The Ocean in the Earth System“. This is MARUM publication no. ####.

7 Outlook and future perspectives

The primary objectives and aims of this study were nearly achieved. The trigger mechanisms and timing of turbidity currents in the Dakar Canyon and Diola Canyon were clarified. Furthermore, a schematic model of the sedimentation dynamics in the Dakar Canyon was developed. This information enlarges the knowledge of sedimentation processes in submarine canyons. However, a transition of the results to other submarine canyons should be well considered due to the prevailing environmental conditions in the study area.

Based on the turbidite emplacement times in the Dakar Canyon, turbidites can be used as an indirect indicator for global sea level oscillations. This study provides further information about the climatic history of NW-Africa during the late Quaternary with special reference to the major climatic termination and short lasting climatic events. This aspect points out that the sedimentary record of the Dakar Canyon can be used as archive to reconstruct the interplay of global sea level variations and short-lasting climatic episodes.

However, some open questions are still remaining. The source area of the turbidites is located on the shelf. Therefore, it is important to investigate and characterise the spatial sediment distribution on the shelf. The sedimentary composition of the shelf south of the Cape Verde peninsula is not known in detail. The head area of the submarine canyon is often characterised by a feeder system of tributary gullies, which is also assumed for the Dakar Canyon. These gullies incise the outer shelf and conduct the available sediments. Furthermore detailed information about the sediment dynamics at the upper slope are required to understand the sorting and deposition of gravity-driven sediment transport processes. Finally, the submarine fan system should be cored to understand how much sediment reaches the deep-sea basin. A detailed knowledge of the sedimentary composition of the shelf and the submarine fan is essential for the calculation of sediment budgets. If possible, alternative coring techniques should be used to recover longer and probably older sediment sequences in all investigated areas. This information could enlarge our knowledge of sedimentation processes of the past.

8 References

Abrantes, F., Baas, J., Haflidason, H., Rasmussen, T., Klitgaard, D., Loncaric, N. and **Gaspar, L.,** 1998. Sediment flux along the northeast European Margin: inferring hydrological changes between 20 and 8 kyr. Marine Geology, 152, 7-23.

Abreu, L. d., Shackelton, N. J., Schönfeld, J., Hall, M. and **Chapman, M.,** 2003. Millennial-scale oceanic climate variability off the Western Iberian margin during the last two glacial periods. Marine Geology, 196, 1-20.

Adkins, J., de Menocal, P. and **Eshel, G.,** 2006. The "African humid period" and the record of marine upwelling from excess ^{230}Th in Ocean Drilling Program Hole 658C, Paleoceanography, 21

Alayne Street, F. and **Grove, A. T.,** 1976. Environmental and climatic implications of late Quaternary lake-level fluctuations in Africa. Nature, 261, 385-390.

Antobreh, A. A. and **Krastel, S.,** 2006. Morphology, seismic characteristics and development of Cap Timiris Canyon, offshore Mauritania: A newly dicovered canyon preserved-off a major arid climatic region. Marine and Petroleum Geology, 23, 37-59.

Antobreh, A. A. and **Krastel, S.,** 2007. Mauritania Slide Complex: morphology, seismic characterisation and processes of formation. International Journal of Earth Sciences, 96, 451-472.

Arz, H. W., Pätzold, J. and **Wefer, G.,** 1998. Correlated millennial-scale changes in surface hydrography and terrigenous sediment yield inferred from last-glacial marine deposits off Northeastern Brazil. Quaternary Research, 50, 157-166.

Ausseil-Badie, J., Barusseau, J. P., Descamps, C., Salif Diop, E. H., Giresse, P. and **Pazdur, M.,** 1991. Holocene deltaic sequence in the Saloum Estuary, Senegal. Quaternary Research, 36, 178-194.

Babonneau, N., Savoye, B., Cremer, M. and **Klein, B.,** 2002. Morphology and architecture of the present canyon and channel system of the Zaire deep-sea fan. Marine and Petroleum Geology, 19, 445-467.

Bard, E., Arnold, M., Hamelin, B., Tisnerat-Laborde, N. and **Cabioch, G.,** 1998. Radiocarbon calibration by means of mass spectrometric 230Th/234U and 14C ages of corals. An updated data base including samples from Barbados, Mururoa and Tahiti. Radiocarbon, 40, 1041-1085.

Bard, E., Hamelin, B. and **Fairbanks, R. G.,** 1990. U-Th ages obtained by mass spectrometry in corals from Barbados: sea level during the past 130,000 years. Nature, 346, 456-458.

Barusseau, J. P., Giresse, P., Faure, H., Lezinet, A. M. and **Masse, J. P.,** 1988. Marine sedimentary environments on some parts of the tropical and equatorial Atlantic margins of Africa during the Late Quaternary. Continental Shelf Research, 8, 1-21.

Bianchi, G. G. and **McCave, I. N.,** 1999. Holocene periodicity in North Atlantic climate and deep-ocean flow south of Iceland. Nature, 397, 515-517.

Biscaye, P. E., 1964. Distinction between kaolinite and chlorite in recent sediments by X-ray diffraction. American Mineralogist, 49, 1281-1289.

Biscaye, P. E., 1965. Mineralogy and sedimentation of recent deep sea clay in the Atlantic Ocean and adjacent seas and oceans. GSA Bulletin, 76, 803-832.

Blumberg, S., Lamy, F., Arz, H. W., Echtler, H. P., Wiedicke, M., Haug, G. H. and **Oncken, O.,** 2008. Turbiditic trench deposits at the South-Chilean active margin: A Pleistocene-Holocene record of climate and tectonics. Earth and Planetary Science Letters, 208, 526-539.

Bond, G. C., Heinrich, H., Broecker, W., Labeyrie, L., McManus, J., Andrews, J., Huon, S., Jantschick, R., Clasen, S., Simet, C., Tedesco, K., Klas, M., Bonani, G. and **Ivy, S.**, 1992. Evidences for massive discharge of icebergs into the North Atlantic ocean during the last glacial period. Nature, 360, 245-249.

Bond, G. C., Showers, W., Elliot, M., Evans, M., Lotti, R., Hajdas, I., Bonani, G. and **Johnson, S.** 1999. The North Atlantic's 1-2kyr Climate Rhythm: Relation to Heinrich Events, Dansgaard/Oeschger Cycles and the Little Ice Age. Mechanisms of Global Climate Change at Millennial Time Scales. P. U. Clark, R. S. Webb and L. D. Keigwin. Washington, American Geophysical Union. 112: 394.

Bouma, A. H., 1962. Sedimentology of some flysch deposits: a graphic approach to facies interpretation. Elsevier, Amsterdam,

Broecker, W., Bond, G., Klas, M., Clark, E. and **Mcmanus, J.,** 1992. Origin of the northern Atlantic's Heinrich events. Climate Dynamics, 6, 265-273.

Brownfield, M. E. and **Charpentier, R. R.,** 2003. Assesment of the Undiscovered Oil an Gas of the senegal Province, Mauretania, Senegal, the Gambia, and Guinea-Bissau, Northwest Africa. U.S. Geological Survey Bullletin, 2207, 1-26.

Calvert, S. E., 1976. The mineralogy and geochemistry of nearshore sediments. Treatise on Cemical Oceanoghraphy. J. P. Riley and R. Chester. San Diego, Academic Press. 6: 187-280.

Chappell, J., 2002. Sea level changes forced ice breakouts in the Last Glacial cycle: new results from coral terraces. Quaternary Science Review, 21, 1229-1240.

Clark, P. U., Alley, R. B. and **Pollard, D.,** 1999. Northern Hemisphere Ice-Sheet influences on global climate change. Science, 286, 1104-1111.

Claussen, M., Kubatzki, C., Brovkin, V., Gandopolski, A., Hoelzmann, P. and **Pachur, H.-J.,** 1999. Simulation of an abrupt change in Saharan vegetation in the mid-Holocene. Geophysical Research Letters, 26, 2037-2040.

Dansgaard, W., Johnsen, S. J., Clausen, H. B., Dahl-Jensen, D., Gundestrup, N. S., Hammer, C. U., Hvidberg, C. S., Steffensen, J. P., Sveinbjörnsdottir, A. E., Jouzel, J. and **Bond, G. C.,** 1993. Evidences for general instability of past climate from a 250-kyr ice.core record. Nature, 218-220.

Debenay, J.-P. and **Redois, F.,** 1997. Distribution of twenty seven dominant species of shelf benthic foraminifers on the continental shelf, north fo Dakar (Senegal). Marine Mircopaleontology, 29, 237-255.

deMenocal, P., Ortiz, J., Guilderson, T., Adkins, J., Sarnthein, M., Baker, L. and **Yarusinsky, M.,** 2000a. Abrupt onset and termination of the African Humid Period: rapid climate response to gradual insolation forcing. Quaternary Science Review, 19, 347-361.

deMenocal, P. B., Ortiz, J., Guilderson, T. and **Sarnthein, M.,** 2000b. Coherent High- and Low-Latitude Climate Variability during the Holocene Warm Period. Science, 288, 2198-2202.

deMenocal, P. B., Ruddiman, W. F. and **Pokras, E. M.,** 1993. Influences of high- and low-latitude processes on African terrestrial climate: Pleistocene eolian records from equatorial Atlantic Ocean Drilling Program Site 663. Paleoceanography, 8, 209-242.

Dietz, R. S. and **Knebel, H. J.,** 1971. Trou sans Fond submarine canyon: Ivory Coast, Africa. Deep-sea Research, 18, 441-447.

Dietz, R. S., Knebel, H. J. and **Somers, L. H.,** 1968. Cayar Submarine Canyon. GSA Bulletin, 79, 1821-1828.

Emery, D. and Myers, K. J. 1996. Sequence Stratigraphy. Oxford, U.K., Blackwell.

Eschard, R., Albouy, E., Deschamps, R., Euzen, T. and **Ayub, A.,** 2003. Downstream evolution of turbiditic channel complexes in the Pab Range outcrops (Maastrichtian, Pakistan). Marine and Petroleum Geology, 20, 691-710.

Fairbanks, R. G., 1989. A 17,000 year glacial eustatic sea level record: influence of glacial melting rates on the Younger Dryas event and deep ocean circulation. Nature, 342, 637-641.

Flood, R. D. and **Damuth, J. E.,** 1987. Quantitative characteristics of sinuous distributary channels on the Amazon Deep-Sea Fan. GSA Bulletin, 98, 728-738.

Foucault, A. and **Mèliéres, F.,** 2000. Palaeoclimatic cyclicity in central Mediterranean Pliocene sediments: the mineralogical signal. Palaeogeographgy, Palaeoclimatology, Palaeoecology, 158, 311-323.

Gasse, F., 2000. Hydrological changes in the African tropics since the Last Glacial Maximum. Quaternary Science Review, 19, 189-211.

Gasse, F., Lédée, V., Massault, M. and **Fontes, J.-C.,** 1989. Water-level fluctuations of Lake Tanganyika in phase with oceanic changes during the last glaciation and deglaciation. Nature, 342, 57-59.

Gasse, F. and **Van Campo, E.**, 1994. Abrupt post-glacial climate events in West Asia and North Africa monsoon domains. Earth and Planetary Science Letters, 126, 435-456.

Gingele, F. X., Müller, P. M. and **Schneider, R. R.**, 1998. Orbital forcing of freshwater input in the Zaire Fan area - clay mineral evidences from the lat 200 kyr. Palaeogeographgy, Palaeoclimatology, Palaeoecology, 138, 17-26.

Hagen, E., 2001. Northwest African upwelling scenario. Oceanologica, 24, 113-128.

Hanebuth, T., Stattergger, K. and **Grootes, P. M.,** 2000. Rapid flooding of the Sunda Shelf: a late-glacial sea-level record. Science, 288, 1033-1035.

Hasiotis, T., Papatheodorou, G. and **Ferentinos, G.,** 2005. A high resolution approach in the recent sedimentation processes at the head of Zakynthos Canyon, western Greece. Marine Geology, 214, 49 - 73.

Heinrich, H., 1988. Origin and Consequences of Cyclic Ice Rafting in the Northeast Atlantic Ocean during the past 130,000 years. Quaternary Research, 29, 142-152.

Henrich, R., Hanebuth, T. J. J., Krastel, S., Neubert, N. and **Wynn, R. B.,** 2008. Architecture and sediment dynamics of the Mauretania Slide Complex. Marine and Petroleum Geology, 25, 17-33.

Holz, C., Stuut, J.-B. and **Henrich, R.,** 2004. Terrigenous sedimentation processes along the continental margin off NW Africa: implications from grain-size analysis of seabed sediments. Sedimentology, 51, 1145-1154.

Holz, C., Stuut, J.-B. W., Henrich, R. and **Meggers, H.,** 2007. Variability in terrigenous sedimentation processes off northwest Africa and its relation to climate changes: Inferences from grain-size distribution of a Holocene marine sediment record. Sedimentary Geology, 202, 499-508.

Hooghiemstra, H., Lézine, A.-M., Leroy, S. A. G., Dupont, L. and **Marret, F.,** 2006. Late Quaternary palynology in marine sediments: A synthesis of the understanding of pollen distribution patterns in the NW African setting. Quaternary International, 148, 29-44.

Jacobi, R. D., 1976. Sediment slides on the northwestern continental margin of Africa. Marine Geology, 22, 157-173.

Jacobi, R. D. and **Hayes, D. E.** 1982. Bathymetry, mircophysography and reflectivity characteristics of the West African Margin between Sierra Leone and Mauritania. Geology of the Northwest African contiental margin. U. von Rad, K. Hinz, M. Sarnthein and E. Seibold. Berlin, Springer-Verlag: 182-210.

Jennerjahn, T., C., Ittekkot, V., Arz, H., W., Behling, H., Pätzold, J. and **Wefer, G.,** 2004. Asynchronous terrestrial and marine signals of climate change during Heinrich Events. Science, 306, 2236-2239.

Jullien, E., Grousset, F., Malaizé, B., Duprat, J., Sanchez-Goni, M. F., Eynaud, F., Charlier, K., Schneider, R., Bory, A., Bout, V. and **Flores, J. A.**, 2007. Low-latitude "dusty events" vs. high-latitude "icy Heinrich events". Quaternary Research, 68, 379-386.

Karageorgis, A. P., Anagnostou, C. L. and **Kaberi, H.,** 2005. Geochemistry and mineralogy of the NW Aegean Sea surface sediments: implications for river runoff and anthropogenic impact. Applied Geochemistry, 20, 69-88.

Klein, G. D., 1985. The frequency and periodicity of preserved turbidites in submarine fans as a quantitative record of tectonic uplift in collision zones. Tectonophysics, 119, 181-193.

Kleinhans, M. G., 2004. Sorting in grain flows at lee side of dunes. Earth-Science Reviews, 65, 75-102.

Kocurek, G., Havholm, K. G., Deynoux, M. and **Blakey, R. C.,** 1991. Amalgamated accumulations resulting from climatic and eustatic changes, Akchar Erg, Mauritania. Sedimentology, 38, 751-772.

Koopmann, B., 1981. Sedimentation von Saharastaub im subtropischen Nordaltantik während der letzten 25.000 Jahre. Meteor Forschungs-Ergebnisse, 35, 23-59.

Krastel, S., Hanebuth, T. J. J., Wynn, R. B., Antobreh, A. A., Henrich, R., Holz, C., Kölling, M., Schulz, H. D. and **Wien, K.,** 2004. Cap Timiris Canyon: A newly discovered channel-system off Mauritania. EOS Transactions, 45, 417-423.

Krastel, S., Wynn, R. B., Hanebuth, T., Henrich, R., Holz, C., Meggers, H., Kuhlmann, H., Georgiopoulou, A. and **Schulz, H. D.,** 2006. Mapping of seabed morphology and shallow sediment structure of the Mauritania continental margin, Northwest Africa: some implications for geohazard potential. Norwegian Journal od Geology, 86, 163-176.

Krastel and cruise participants (2006). Report and preliminary results of RV Meteor cruise M65/2, Dakar - Las Palmas, 04.07.-26.07.2005. Berichte aus dem Fachbereich Geowissenschaften der Universität Bremen. Bremen: 185.

Kuhlmann, H. (2003). Reconstruction of the sedimentary history offshore NW Africa: Application of core-logging tools. Faculty of Geoscience. Bremen, Bremen: 103.

Kuhlmann, H., Meggers, H., Freudenthal, T. and **Wefer, G.,** 2004. The transition of the monsoonal and the N Atlantic climate system off NW Africa during the Holocene. Geophysical Research Letters, 31,

Kutzbach, J. E. and **Liu, Z.,** 1997. Response of the African monsoon to orbital forcing and ocean feedbacks in the middle Holocene. Science, 278, 440-443.

Lambeck, K., Esat, T. M. and **Potter, E.-K.,** 2002. Links betwen climate and sea levels for the past three million years. Nature, 419, 199-206.

Lancaster, N., Kocurek, G., Singhvi, A., Pandey, V., Deynoux, M., Ghienne, J.-F. and **Lô, K.**, 2002. Late Pleistocene and Holocene dune activity and wind regimes in the western Sahara Desert of Mauritania. Geology, 30, 991-994.

Lange, H., 1982. Distribution of chlorite and kaolinite in eastern Atlantic sediments off North Africa. Sedimentology, 29, 427-431.

Lèzine, A.-M., 1991. West African paleoclimates during the last climatic cycle inferred from an Atlantic deep-sea pollen record. Quaternary International, 35, 456-463.

Lézine, A.-M., Duplessy, J.-C. and **Cazet, J.-P.,** 2005. West African monsoon variability during the last deglaciation and the Holocene: Evidence from fresh water algae, pollen and isotope datat from core KW31, Gulf of Guinea. Palaeogeographgy, Palaeoclimatology, Palaeoecology, 219, 255-237.

Lonsdale, P., 1982. Sediment drift of the Northeast Atlantic and thier relationship to the observerd abyssal currents. Bull. Inst. Geol. Bassin Aquitaine, 141-150.

Martinez, P., Bertrand, P., Shimmield, G. B., Cochrane, K., Jorissen, F. J. and **Dignan, M.,** 1999. Upwelling intensity and ocean productivity changes off Cape Blanc (nortwest Africa) during the last 70.000 years: geochemical and micropalaeontological evidence. Marine Geology, 158,

Martinson, D. G., Pisias, N. G., Hays, J. D., Imbrie, J. D., Moore, T. C. and **Shackleton, N. J.,** 1987. Age Dating and the orbital theory of the ice ages: development of a high-resolution 0 to 300,000-year chronostratigraphy. Quaternary Research, 27, 1-29.

Masson, D. G., Kenyon, N. H. and **Weaver, P. P. E.** 1996. Slides, Debris Flows, and Turbidity Currents. Oceanography. C. P. Summerhayes and S. A. Thorpe, Mason Publishing: 136-151.

Matthewson, A. P., Shimmield, G. B. and **Kroon, D.,** 1995. A 300 kyr high-resolution aridity record of the North African continent. Paleoceanography, 10, 677-692.

Mayall, M., Jones, E. and **Casey, M.,** 2006. Turbidite channel reservoirs - Key elements in facies prediction and effective development. Marine and Petroleum Geology, 23, 821-841.

McHugh, C. M. G., Damuth, J. E. and **Mountain, G. S.,** 2002. Cenozoic mass-transport facies and their correlation with relative sea level changes, New Jersey continental margin. Marine Geology, 184, 295-334.

McIntyre, A., Ruddiman, W. F., Karlin, K. and **Mix, A. C.,** 1989. Surface water response of the equatorial Atlantic Ocean to orbital forcing. Paleoceanography, 4, 19-55.

McMaster, R. L. and **Lachance, T. P.,** 1969. Northwestern African continental shelf sediments. Marine Geology, 7, 57-67.

Mittelstaedt, E., 1991. The ocean boundary along the North-west African coast: Circulation and oceanographic proberties at the sea surface. Progress in Oceanography, 26, 307-355.

Moreno, A., Targarona, J., Henderiks, J., Canals, M., Freudenthal, T. and **Meggers, H.,** 2001. Orbital forcing of dust supply to the North Canary Basin over the last 250kyr. Quaternary Science Review, 20, 1327-1339.

Moreno, E., Thouveny, N., Delanghe, D., McCave, I. N. and **Shackelton, N. J.,** 2002. Climatic and oceanographic changes in the Northeast Atlantic reflected by magnetic properties of sediments deposited on the Portuguese Margin during the last 340ka. Earth and Planetary Science Letters, 202, 465-480.

Mullenbach, B. L., Nittrouer, C. A., Puig, P. and **Orange, D. L.,** 2004. Sediment deposition in a modern submarine canyon: Eel Canyonn, northern California. Marine Geology, 211, 101-119.

Mutti, E. and **Normark, W. R.** 1991. An integrated approach to the study of turbidite systems. Seismic Facies and Sedimentary Processes of Submarine Fans and Turbidite Systems. P. Weimer and M. H. Link. New York, Springer: 75-106.

Nakajima, T., Satoh, M. and **Okamura, Y.,** 1998. Channel-levee complexes, terminal deep-sea fan and sediment wave fields associated with the Toyama Deep-Sea Channel system in the Japan Sea. Marine Geology, 147,

Nicholson, S. E., 2000. The nature of rainfall variability over Africa on time scales of decades to millenia. Global and Planetary Change, 26, 137-158.

Normark, W. R., Piper, D. J. W. and **Hiscott, R. N.,** 1998. Sea level controls on the textural characteristics and depositional architecture of the Hueneme and associated submarine fan systems, Santa Monica Basin, California. Sedimentology, 45, 53-70.

Pailler, D. and **Bard, E.,** 2002. High frequency palaeoceanographic changes during the past 140000yr recorded by the organic matter in sediments of the Iberian Margin. Palaeogeographgy, Palaeoclimatology, Palaeoecology, 181, 431-452.

Peltier, W. R. and **Fairbanks, R. G.,** 2006. Global glacial ice volume and Last Glacial Maximum duration from an extended Barbados sea level record. Quaternary Science Review, 25, 3322-3337.

Petschick, R., Kuhn, G. and **Gingele, F.,** 1996. Clay mineral distribution in surface sediments of the South Atlantic: sources, transport, and relation to oceanography. Marine Geology, 130, 203-229.

Pierau, R., Hanebuth, T., Krastel, S. and **Henrich, R.,** in review-a. Late Quaternary climatic events and sea level changes recorded by turbidite activity, Dakar Canyon, NW-Africa. Quaternary Research

Pierau, R., Henrich, R., Preiss-Daimler, I., Krastel, S. and **Geersen, J.,** in review-b. Sediment transport and turbidite architecture in the submarine Dakar Canyon off NW-Africa. Marine and Petroleum Geology,

Pierau, R., Krastel, S., Geersen, J., Hanebuth, T. J. J. and **Henrich, R., subm.** Trigger mechanisms of turbidity currents in two neighbouring submarine canyons at the Senegalese continentla margin: a comparison of the Diola and Dakar Canyon. Marine Geology,

Pokras, E. M., 1987. Diatom record of Late Quaternary climatic changes in the eastern Equatorial Atlantic and tropical Africa. Paleoceanography, 2, 273-286.

Pokras, E. M. and **Mix, A. C.,** 1985. Eolian evidence for spatial variability of Late Quarternary climates in tropical Africa. Quaternary Research, 24, 137-149.

Prins, M. A. and **Postma, G.,** 2000. Effects of climate, sea level, and tectonics unraveled for last deglaciation records of the Arabian Sea. Geology, 28, 375-378.

Prins, M. A., Postma, G., Cleveringa, J., Cramp, A. and **Kenyon, N. H.,** 2000. Controls on terrigenous sediment supply to the Arabian Sea during the late Quaternary: the Indus Fan. Marine Geology, 169, 327-349.

Prospero, J. M. 1996. The Atmospheric Transport of Particles to the Ocean. Particle Flux in the Ocean. V. Ittekkot, P. Schäfer, S. Honjo and P. J. Depetris, John Wiley & Sons Ltd: 19-52.

Prospero, J. M. and **Lamb, P. J.,** 2003. African Droughts and Dust Transport to the Caribbean: Climate Change Implications. Science, 302, 1024-1027.

Rea, D. K., 1994. The paleoclimatic record provided by eolian deposition in the deep sea: the geologic history of wind. Reviews of Geophysics, 32, 159-195.

Reading, H. G. and **Richards, M.,** 1994. Turbidite Systems in Deep-Water Basin Margins Classified by Grain Size and Feeder System. AAPG Bullletin, 78, 792-822.

Redois, F. and **Debenay, J.-P.,** 1999. Répartition des foraminifères benthiques actuels sur le plateau continental sénégalais au sud de Dakar. Oceanologica Acta, 22, 215-232.

Renssen, H., Brovkin, V., Fichefet, T. and **Grosse, H.,** 2006. Simulation of the Holocene climate evolution in Northern Afica: The termination of the African Humid Period. Quaternary International, 150, 95 - 102.

Rognon, P. and **Coudé-Gaussen, G.,** 1996. Paleoclimates off Northwest Africa (28°-35°N) about 18.00 yr B.P. based on Continental Eolian Deposits. Quaternary Research, 46, 118-126.

Rossignol-Strick, M., 1985. Mediterranean quarternary sapropels, an immediate response of the African monsoon to variation of insolation. Palaeogeographgy, Palaeoclimatology, Palaeoecology, 49, 237-263.

Salaheldin, T. M., Imran, J., Chaudhry, M. H. and **Reed, C.,** 2000. Role of fine-grained sediment in turbidity current flow dynamics and resulting deposits. Marine Geology, 171, 21-38.

Sarnthein, M., 1978. Sand deserts during glacial maximum and climate optimum. Nature, 272, 43-46.

Sarnthein, M. and **Diester-Haass, L.,** 1977. Eolian-Sand Turbidites. Journal of Sedimentary Petrology, 47, 868-890.

Sarnthein, M., Tetzlaff, G., Koopmann, B. and **Pflaumann, U.,** 1981. Glacial and interglacial wind regimes over the eastern subtropical Atlantic and North-West Africa. Nature, 293, 193-196.

Sarnthein, M., Thiede, J., Pflaumann, U., Erlenkeuser, H., Fütterer, D., Koopmann, B., Lange, H. and **Seibold, E.** (1982). Atmospheric and oceanic circulation patterns off Northwest Africa during the past 25 millon years. Geology of the Northwest African Continental Margin. U. von Rad, K. Hinz, M. Sarnthein and E. Seibold. Berlin, Springer: 545-604.

Satur, N., Hurst, A., Cronin, B. T., Kelling, G. and **Gürbüz, K.,** 2000. Sand body geometry in a sand-rich, deep-water clastic system, Miocene Cingöz Formation of southern Turkey. Marine and Petroleum Geology, 17, 239-252.

Satur, N., Kelling, G., Cronin, B. T., Hurst, A. and **Gürbüz, K.,** 2005. Sedimentary architecture of a canyon-style fairway feeding a deep-water clastic system, the Miocenen Cingöz Formation, southern Turkey: significance for reservoir characterisation and modelling. Sedimentary Geology, 173, 91-119.

Schütz, L. and **Sebert, M.,** 1987. Mineral aerosols and source identification. Journal of Aerosol Science, 18, 1-10.

Seibold, E. and **Fütterer, D.,** 1982. Sediment dynamics on the Northwest African continental margin. The Ocean Floor. R. A. Scrutton and M. Talwabi. Chichester, John Wiley & Sons: 147-163.

Shanahan, T., Overpeck, J. T., Wheeler, C. W., Beck, J. W., Pigati, J. S., Talbot, M. R., Scholz, C. A., Peck, J. and **King, J. W.,** 2006. Paleoclimatic variations in West Africa from a record of late Pleistocene and Holocene lake level stands of Lake Botsumtwi, Ghana. Palaeogeographgy, Palaeoclimatology, Palaeoecology, 242, 287-302.

Shanmugam, G., 2002. Ten turbidite myths. Earth-Science Reviews, 58, 311-341.

Shepard, F. P., 1972. Submarine Canyons. Earth-Science Reviews, 8, 1-12.

Siddall, M., Bard, E., Rohling, E. J. and **Hemleben, C.,** 2006. Sea-level reversal during Termination II. Geology, 34, 817-820.

Siddall, M., Rohling, E. J., Almogi-Labin, A., Hemleben, C., Meischer, D., Schmelzer, I. and **Smeed, D. A.,** 2003. Sea-level fluctuations during the last glacial cycle. Nature, 423, 853-858.

Stein, R., 1985. Rapid grain-size analyses of clay and silt fraction by SediGraph 5000D; comparison with Coulter counter and Atterberg methods. Journal of Sedimentary Petrology, 55, 590-593.

Stow, D. A. and **Mayall, M.,** 2000. Deep-water sedimentary systems: New models for the 21st century. Marine and Petroleum Geology, 17, 125-135.

Stow, D. A. V. and **Bowen, A. J.,** 1980. A physical model for the transport and sorting of fine grained sediment by turbidity currents. Sedimentology, 27, 31-46.

Stramma, L., Hüttl, S. and **Schafstall, J.,** 2005. Water masses and currents in the upper tropical northeast Atlantic off northwest Africa. Journal of Geophysical Reserarch, 110,

Stramma, L. and **Schott, F.,** 1999. The mean flow field of the tropical Altantic Ocean. Deep-Sea Research II, 46, 279-303.

Stuiver, M., Reimer, P. J., Bard, E., Beck, J. W., Burr, G. S., Hughen, K. A., Kromer, B., McCormac, G., Van der Plicht, J. and **Spurk, M.,** 1998. INTCAL98 Radiocarbon Age Calibration, 24.000 - 0 cal BP. Radiocarbon, 40, 1041-1084.

Stuut, J.-B., Zabel, M., Rathmeyer, V., Helmke, P., Schefuß, E., Lavik, G. and **Schneider, R.,** 2005. Provenace of present-day eolian dust collected off NW Africa. Journal of Geophysical Reserarch, 110,

Stuut, J.-B. W., Prins, M. A., Schneider, R. R., Weltje, G. J., Jansen, J. H. F. and **Postma, G.,** 2002. A 300-kyr record of aridity and wind strenght in southwest Africa: inferences from grain-size distributions of sediments on Walvis Ridge, SE Atlantic. Marine Geology, 180, 221-233.

Svensson, A., Andersen, K. K., Bigler, M., Clausen, H. B., Dahl-Jensen, D., Davies, S. M., Johnsen, S. J., Muscheler, R., Parrenin, F., Rasmussen, S. O., Röthlisberger, R., Seierstad, I., Steffensen, J. P. and **Vinther, B. M.,** 2008. A 60000 year Greenland stratigraphic ice core chronology. Climate of the Past, 4, 47-57.

Swap, R., Ulanski, S., Cobbett, M. and **Garstang, M.,** 1996. Temporal and spatial characteristics of Saharan dust outbreaks. Journal of Geophysical Reserarch, 101, 4205-4220.

Swezey, C., 2001. Eolian sediment response to late Quaternary climate changes: temporal and spatial patterns in the Sahara. Palaeogeographgy, Palaeoclimatology, Palaeoecology, 167, 119-155.

Talbot, M. R. and **Delibras, G.,** 1980. A new Pleistocene-Holocene water-level curve for Lake Bosumtwi, Ghana. Earth and Planetary Science Letters, 47, 336-344.

Talling, P. J., Wynn, R. B., Masson, D. G., Frenz, M., Cronin, B. T., Scheibel, R., Akhmetzhanov, A. M., Dallmeier-Tiessen, S., Benetti, S., Weaver, P. P. E., Georgiopoulou, A., Zühlsdorff, C. and **Amy, L. A.,** 2007. Onset of submarine debris flow deposition far from original giant landslide. Nature, 450, 541-544.

Thouveney, N., Moreno, E., Delanghe, D., Candon, L., Lancelot, Y. and **Shackelton, N. J.,** 2000. Rock magnetic detection of distal ice-rafted debris: clue for the identification of Heinrich events on the Portuguese margin. Earth and Planetary Science Letters, 180, 61-75.

Tiedemann, R., Sarnthein, M. and **Shackelton, N. J.,** 1994. Astronomic timescale for the Pliocene Atlantic $d^{18}O$ and dust flux records of the Ocean Drilling Progam site 659. Paleoceanography, 9, 619-638.

Tiessen, H., Hauffe, H.-K. and **Mermut, A. R.,** 1991. Deposition of Harmattan dust and its influence on base saturation of soils in northern Ghana. Geoderma, 49, 285-299.

Tjallingii, R. 2006. Application and quality of X-Ray Flourescence Core Scanning in reconstructing the Pleistocene NW African continental margin sedimentation patterns and paleoclimate variations. Faculty of Geoscience. Bremen, Bremen: 114.

Toucanne, S., Zaragosi, S., Bourillet, J. F., Naughton, F., Cremer, M., Eynaud, F. and **Dennielou, B.,** 2008. Activity of the turbidite levee of the Celtic-Amorican margin (Bay of Biscay) during the last 30,000 years: Imprints of the last European deglaciation and Heinrich events. Marine Geology, 247, 84-103.

Van Camp, L., Nykjær, L., Mittelstaedt, E. and **Schlittenhardt, P.,** 1991. Upwelling and boundary circulation off Northwest Africa as depicted by infrared and visible satellite observations. Progress in Oceanography, 26, 357-402.

van Kreveld, S. A., Knappertsbusch, M., Ottens, J., Ganssen, G. G. and **van Hinte, J.,** 1996. Biogenic carbonate and ice-rafted debris (Heinrich layer) accumulation in deep-sea sediments from a Northwest Atlantic piston core. Marine Geology, 131, 21-46.

Vidal, L., Labeyrie, L., Cortijo, E., Arnold, M., Duplessy, J. C., Michel, E., Becqué, S. and **van Weering, T. C. E.,** 1997. Evidence for changes in the North Atlantic Deep Water linked to meltwater surges during the Heinrich events. Earth and Planetary Science Letters, 146, 13-27.

Weaver, P. P. E., Wynn, R. B., Kenyon, N. H. and **Evans, J.,** 2000. Continental margin sedimentation, with special reference to the north-east Atlantic margin. Sedimentology, 47, 239-356.

Weber, M. E., Wiedicke-Hombach, M., Kudrass, H. R. and **Erlenkeuser, H.,** 2003. Bengal Fan sediment transport activity and response to climate forcing inferred from sediment physical properties. Sedimentary Geology, 155, 361-381.

Weimer, P. and **Slatt, R. M.,** 1999. Turbidite systems, Part 1: Sequence and seismic stratigraphy. Leading Edge, 19, 454-463.

Wissmann, G. 1982. Stratigraphy and Structural Features of the Continental Margin Basin of Senegal and Mauritania. Geology of the Northwest African contiental margin. U. von Rad, K. Hinz, M. Sarnthein and E. Seibold. Berlin, Springer-Verlag: 160-181.

Wynn, R. B., Cronin, B. T. and **Peakall, J.,** 2007. Sinuous deep-water channels: Genesis, geometry and architecture. Marine and Petroleum Geology, 24, 341-387.

Wynn, R. B., Masson, D. G., Stow, D. A. V. and **Weaver, P. P. E.,** 2000. The Northwest African slope apron: a modern analogue for deep-water systems with complex seafloor topography. Marine and Petroleum Geology, 17, 253-265.

Wynn, R. B., Weaver, P. P. E., Masson, D. G. and **Stow, D. A.,** 2002. Turbidite depositional architecture across three interconnected deep-water basins on the north-west African margin. Sedimentology, 49, 669-695.

Yokoyama, Y., Esat, T. M. and **Lambeck, K.,** 2001. Coupled climate and sea-level changes deduced from Huon Peninsula coral terraces of the last ice age. Earth and Planetary Science Letters, 193, 579-587.

Zabel, M., Schnneider, R. R., Wagner, T., Abegbie, A. T., Vries, U. d. and **Kolonic, S.,** 2001. Late Quaternary climate changes in Central Africa as inferred from terrigenous input of the Niger fan. Quaternary Research, 56, 207-217.

Zhao, M., Beveridge, N. A. S., Shackelton, N. J., Sarnthein, M. and **Eglinton, G.,** 1995. Molecular stratigraphy of cores off northwest Africa: Sea surface temperature history over the last 80 ka. Paleoceanography, 10, 661-675.

Zühlsdorff, C., Hanebuth, T. J. J. and **Henrich, R.,** 2007a. Persistent quasi-periodic turbidite activity of Saharan Africa and its comparability to orbital and climate cyclicities. Geo-Marine Letters,

Zühlsdorff, C., Wien, K., Stuut, J.-B. W. and **Henrich, R.,** 2007b. Late Quarternary sedimentation within a submarine channel-levee system offshore Cap Timiris, Mauritania. Marine Geology, 240, 217-234.

9 Acknowledgements

I would like to thank Prof. Dr. Rüdiger Henrich who gave me the opportunity to do this Ph.D. thesis which was embedded in the RCOM project C2. Furthermore I thank Prof. Dr. Sebastian Krastel for his spontaneous agreement and effort evaluating this thesis.

I acknowledge all my co-authors for the helpful suggestions and the support. Thanks to Till for pushing forward me for the first manuscript and all the discussion at the beginning of this project. Further, I thank Sebastian for providing the seismic and Parasound data as well as Jacob for data processing and illustrating. I'm grateful to Inga for the discussions about very small stuff and the introduction into the magic Matlab plots. I'm sincerely thankful to all of you!

I enjoy the work with Brit, Helga, and Susanne from the AWI and thank them for all their support in the laboratory. Without the support of Swantje, Florian, Holger, Gitte and Sissy during the time consuming sample preparation, I would stay until today in the dark Atterberg room. I thank all my colleagues Britta, Babette, Basti, Jean, Käthe, Meral, Kalle, Regina and Helge for their support during the thesis. Further, I would like to thank all colleagues at the Department and MARUM who supports me over the last years. I'm grateful to my former office mate Christine to introduce me in the turbidity stuff and for her support during my start-up in Bremen. I will miss the discussion with Helge, Kalle and Stefan about the weakly footie events. I thank the girl's room for post-lunch breaks and all the funny moments. I'm very grateful to Ulli. Thank you for the relaxed and productive atmosphere and all the fruitful discussions in our coop at the "Lidodeck". Thank you!

Many, many thanks to Janine for your moral support, for many discussions and for much more. Thank you so much! My family are deeply acknowledged for all kinds of support from the distance.